BRILLOUIN SCATTERING AND COHERENT PHONON GENERATION

by

Raymond Chiao

B. A. Princeton University

(1961)

submitted in partial fulfillment

of the requirements for the degree of

doctor of philosophy

at the

MASSACHUSETTS INSTITUTE OF TECHNOLOGY

June, 1965

Signature of Author. . . . . Signature Redacted
Department of Physics, May 27, 1965

Certified by . . . . . Thesis Supervisor

Accepted by . . . . . Signature Redacted
Chairman, Departmental Committee
te Students

Signature Redacted

BRILLOUIN SCATTERING AND COHERENT PHONON GENERATION

by

Raymond Chiao

Submitted to the Department of Physics on May 26, 1965

in partial fulfillment of the requirement for the

degree of doctor of philosophy

ABSTRACT

The scattering of light off sound waves, known as the (normal)Brillouin effect, has been previously used to investigate velocities of sound in the hypersonic range. Using a He-Ne red laser as the exciting source, one can improve such measurements easily by better than an order of magnitude in accuracy. More importantly, this technique has allowed us to detect for the first time a significant width to the Brillouin components in some liquids, allowing us to measure the attenuation of hypersonic waves.

With the advent of extremely high-power lasers it is now possible to generate hypersonic waves of great intensity from light waves, using the stimulated Brillouin effect. One can view this effect as the parametric generation of sound from intense light in a nonlinear (e. g. electrostrictive) medium. The sound waves so generated are, in solids, typically in the frequency range of 20 KMc and have a peak power of $\sim$ 1Kwatt of a duration of $\sim 3 \times 10^{-8}$ sec.

A theoretical study has also been made on the possibility of diffractionless propagation of light beams which undergo nonlinear (e. g. electrostrictive) interaction with the medium. Such a phenomenon may occur when the diffracted rays from a finite-aperture beam are confined by total internal reflection inside a dielectric waveguide which the light beam creates for itself.

Thesis Supervisor: Charles H. Townes
Title: Provost of M. I. T. and Professor of Physics

DEDICATION

I dedicate this thesis to my Saviour Jesus Christ, whose I am and whom I serve.

ACKNOWLEDGEMENTS

I am deeply grateful to my thesis advisor, Professor Charles H. Townes, for the wealth of ideas which are the basis of this thesis. I wish to thank Professor Boris Stoicheff for invaluable experimental help. Professors Ali Javan and Jacques Ducuing and Uno Ingard gave me much useful advice, for which I am grateful. I thank Professor Robert Newnham for X-ray identification of the axes of various crystals.

My thanks are especially extended to Elsa Garmire and Paul Fleury for collaboration in experiments and helpful discussions. To Dr. Abraham Szoke, Dr. Francesco DeMartini, Dr. George Flynn, Joel Parks, Ronald Cordover, Michael Feld, Howard Schlossberg, Lon Hocker, Mark Kovacs, John Murray, Richard Smith, Eugene Leonard, Richard Solomon and Eugene Pfitzer, I am grateful for illuminating discussions and for the loan of equipment.

Especial thanks are due to Mrs. Wanda Schwartz for typing my thesis.

I respectfully thank my parents for the many years of upbringing and encouragement they have given me.

BIOGRAPHICAL NOTE

The author was born in Hong Kong on October 9, 1940, and emigrated to America in 1947. He received an A. B. degree in physics from Princeton University in 1961 and is a member of Phi Beta Kappa (1960). His publications include "Angular Dependence of Maser-Stimulated Raman Radiation in Calcite" (Phys. Rev. Letters, 12, 290, 1964); "Stimulated Brillouin Scattering and Coherent Generation of Intense Hypersonic Waves" (Phys. Rev. Letters, 12, 392, 1964); "Self-Trapping of Optical Beams" (Phys. Rev. Letters, 13, 1479, 1964); "Brillouin Scattering in Liquids Excited by the He-Ne Maser" (J. Opt. Soc. Am., 54, 1286, 1964); "Raman and Phonon Masers" (Quantum Electronics and Coherent Light, Proc. of the International School of Physics "Enrico Fermi", 1963, P. Miles and C. H. Townes, eds., Academic Press, 1964, p. 326).

TABLE OF CONTENTS

TABLE OF FIGURES

TABLE OF FIGURES (con'd.)

Introduction

Radiation and matter can interact in a variety of ways. The lowest order process of interaction results in the familiar one-photon absorption and the associated dispersion of electromagnetic radiation. This process is linear because the polarization of the matter responsible for these effects is linear in electric field. One consequence of this linearity is that there is no alteration (except for transient effects) of the frequency of the interacting radiation. Stimulated emission associated with this lowest order process has led to the now familiar maser and laser action.

The next order process of interaction results in two-photon effects, such as the Raman and Brillouin scattering. These processes are nonlinear in the sense that the polarization of the matter varies nonlinearly with the electric field. Thus new frequencies can arise through nonlinear mixing and parametric processes. For example, in Brillouin scattering in which light is scattered off sound waves, the scattered light waves are shifted in frequency with respect to that of the incident light due to modulation by the scattering sound waves. As in the one-photon case, there are stimulated processes of emission and absorption associated with two-photon effects in addition to the normal effects (i. e. scattering from zero-point and thermal fluctuations). These lead to the stimulated Brillouin effect and phonon maser action.

In this thesis, nonlinear interactions of light and the collective motions of matter, in particular sound waves, will be investigated.

Chapter I. The Kinematics of Brillouin Scattering

One may view Brillouin scattering either classically or quantum mechanically, but both give the same answer as far as the kinematics of the process is concerned. First, classically one envisages light waves being diffracted by a grating of periodically varying index of refraction caused by the sound wave. The diffracted light will also suffer a Doppler shift since the grating is moving at the speed of sound. The Bragg law gives us (see fig. 1):

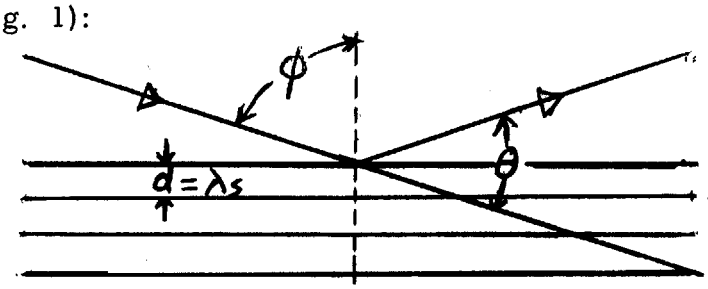

fig. 1: Classical Description of Brillouin Scattering

$$2d \cos \phi = m \frac{\lambda_p}{n_p} \qquad m = 1, 2, 3, \ldots \tag{1.1}$$

where ϕ is the incidence angle and λ_p is the incident wavelength and n_p is the index of refraction of the medium at λ_p. Since $\theta = \pi - 2\phi$:

$$2d \sin \frac{\theta}{2} = \frac{\lambda_p}{n_p} m$$

where θ is the scattering angle. Since $d = \lambda_s$, the wavelength of sound, and $\lambda_s \nu_s = v_s$:

$$m \nu_s = \left(\frac{v_s}{c}\right) 2 n_p \nu_p \sin \frac{\theta}{2}. \tag{1.2}$$

The Doppler shift suffered by the scattered light is (as is easily seen by transforming into an inertial frame moving along with the sound wave):

$$\frac{\Delta\nu}{\nu_p} = \pm 2\, n_p \left(\frac{v_s}{c}\right)\cos\phi = \pm 2\, n_p \left(\frac{v_s}{c}\right) \sin\frac{\theta}{2} \tag{1.3}$$

where $\Delta\nu$ is the Doppler shift. Since the sound wave is modulating the incident light at frequency ν_s, we require $\nu_s = \Delta\nu$ and hence m = 1 and we obtain the Brillouin shift formula[1] :

$$\nu_s = \Delta\nu = \pm 2\, n_p\, \nu_p \frac{v_s}{c} \sin\frac{\theta}{2}. \tag{1.4}$$

Of course, it must be pointed out that in the above analysis one makes the approximations that since $\frac{v}{c} \sim 10^{-5}$ the Doppler shift is small (and hence first order) and the wavelength of the shifted radiation is very nearly equal to the incident wavelength, thus allowing us to use (1.1).

Quantum mechanically, one envisages Brillouin scattering as a collision process in which a photon collides inelastically with a phonon and emerges as a photon of a different energy (see fig. 2).

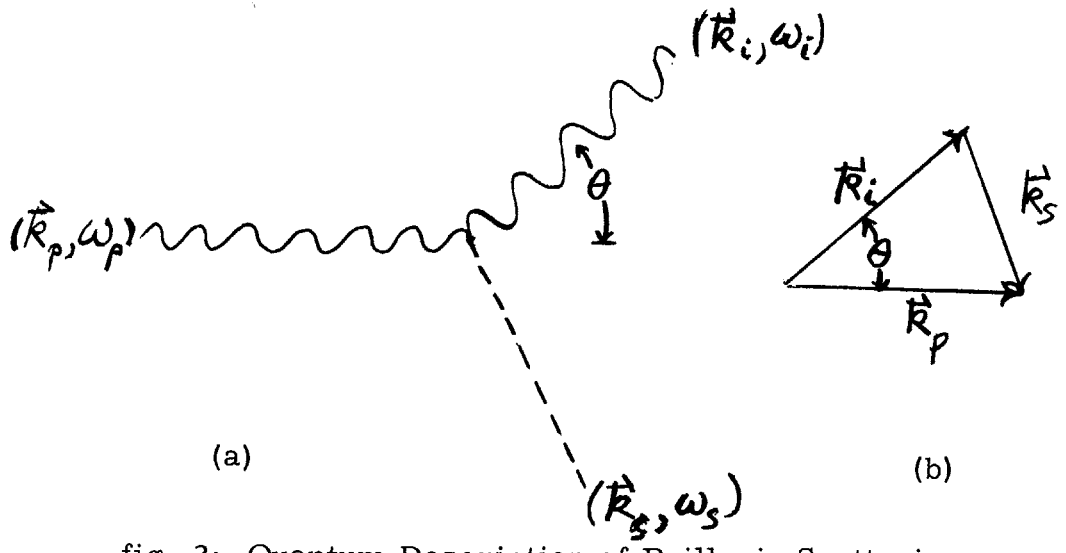

fig. 2: Quantum Description of Brillouin Scattering

Energy and momentum must be conserved in such a process, and since $\hbar\omega_{p,i,s}$ represent the energies and $\hbar\vec{k}_{p,i,s}$ represent the momenta of the incident, scattered photon and phonon respectively, we require:

(1.5) $$\omega_i = \omega_p \pm \omega_s$$

(1.6) $$\vec{k}_i = \vec{k}_p \pm \vec{k}_s$$

$\left.\begin{matrix} + \text{ "anti-Stokes"} \\ - \text{ "Stokes"} \end{matrix}\right\}$

where + is for the case of phonon annihilation and - is for phonon creation. Now the magnitude of the wave-vectors are related to frequencies by:

(1.7) $$|k_p| = \frac{\omega_p}{c} n_p \,, \quad |k_i| = \frac{\omega_i}{c} n_i \,, \quad |k_s| = \frac{\omega_s}{v_s} \,.$$

It is clear that conservation of momentum, represented by the wave-vector triangle in fig. 2(b), implies the $|k_p|$, $|k_i|$, $|k_s|$ must be of the same order of magnitude so long as θ is not small. Hence (1.7) implies that $\omega_s \sim \left(\frac{v_s}{c}\right) \omega_p$ is very small compared with ω_p. Thus from (1.5) $\omega_i = \omega_p$ to a part in 10^5 and we may therefore also set $n_i = n_p$, whence:

(1.8) $$|k_p| = |k_i|$$

implying that the triangle in fig. 2(b) is isosceles. Hence the sound wave always moves away from the scattered light wave (i.e. $\vec{k}_i \cdot \vec{k}_s < 0$). By geometry:

(1.9) $$|k_s| = 2 |k_p| \sin \frac{\theta}{2}$$

or, converting to frequencies using (1.7)

(1.10) $$\omega_s = \Delta\omega = 2n_p \omega_p \left(\frac{v_s}{c}\right) \sin \frac{\theta}{2}$$

which is identical to (1.4). Again it must be pointed out that this relationship was derived with the assumption that $\frac{v}{c}$ is small.

Let us investigate the case involving higher orders of $\frac{v}{c}$ so that relativistic effects will become significant. We will start with equations (1.5) and (1.6). (Clasically, the interpretation of these equations, as will

become evident in the next chapter, is that of phase matching in time and space of the interacting waves.) The law of cosines applied to the wave-vector triangle (fig. 2(b)) gives us:

$$k_s^2 = k_i^2 + k_p^2 - 2k_i k_p \cos\theta . \tag{1.11}$$

We assume $n_i = n_p$ temporarily. This is not a good assumption since it is typically in error by a part in 10^7 so that it must be taken into account in first order correction to the Brillouin shift. Nevertheless, for algebraic simplicity, we defer the discussion for the case $n_i \neq n_p$. Equations (1.11) and (1.5) imply the quadratic equation for ω_s ($n_i = n_p \equiv n$, $\beta \equiv \frac{v_s}{c}$):

$$\omega_s^2 (1 - n^2\beta^2) \mp \left[4 n^2\beta^2\omega_p \sin^2\frac{\theta}{2}\right] \omega_s - 4 n^2\beta^2\omega_p^2 \sin^2\frac{\theta}{2} = 0 \tag{1.12}$$

which has the solutions:

$$\omega_s = \frac{n\beta\omega_p}{1-n^2\beta^2}\left(\mp 2 n \beta \sin^2\frac{\theta}{2} + \sqrt{4\sin^2\frac{\theta}{2} - n^2\beta^2\sin^2\theta}\right) \tag{1.13}$$

where + is for the sound wave associated with the anti-Stokes (up-shifted in frequency, cf. (1.5)) component of scattered radiation and - for the Stokes (down-shifted in frequency) component. We have chosen the + sign in front of the square root since in the limit $\beta \to 0$, ω_s must be positive. Expanding in orders of β:

$$\omega_s = \frac{n\beta\omega_p}{1-n^2\beta^2}\left(2\sin\frac{\theta}{2} \mp 2n\beta\sin^2\frac{\theta}{2} - n^2\beta^2\sin\frac{\theta}{2}\cos^2\frac{\theta}{2} + O(\beta^4) + \ldots\right) \tag{1.14}$$

Thus both the Stokes and the anti-Stokes are shifted to the blue slightly, causing a $\sim \frac{v}{c}$ asymmetry in the Brillouin shifts[2].

In the case when $n_i \neq n_p$ the situation is complicated by the fact that (1.12) is no longer quadratic and becomes:

$$\omega_s^2 (1 - n_i^2\beta^2) \mp \omega_s (2\beta^2 \omega_p (n_i^2 - n_i n_p \cos\theta)) - \left[(n_i^2 + n_p^2) - 2n_i n_p \cos\theta\right] \beta^2\omega_p^2 = 0 \tag{1.15}$$

where $n_i = n(\omega_p \pm \omega_s) \cong n_p \pm \omega_s \frac{dn}{d\omega} + \frac{\omega_s^2}{2} \frac{d^2n}{d\omega^2} + \ldots$

We will solve (1.15) neglecting terms $O(\beta^4)$ and using $\omega_s = O(\beta)$. Then:

$$\omega_s = 2 n_p \beta\omega_p \sin\frac{\theta}{2} \pm 2\beta^2 n_p^2 \omega_p \sin^2\frac{\theta}{2} \left(1 + \frac{\omega_p}{n_p} \frac{dn}{d\omega}\right) + O(\beta^3). \tag{1.16}$$

Therefore, the net shift to the blue of both Brillouin components described above is enhanced in the case of normal dispersion ($\frac{dn}{d\omega} > 0$). For the case of fused quartz $\frac{\omega_p}{n_p} \frac{dn}{d\omega} = 1.3 \times 10^{-2}$.

We may also apply (1.15) to the case of anisotropic crystals if we let $n_{p,i}$ be the index of refraction along the incident and scattered directions respectively, with proper considerations of polarizations (same as from a dielectric boundary). Thus, neglecting dispersion:

$$\omega_s = \frac{\beta^2\omega_p}{1 - n_i^2\beta^2} \left(\pm (n_i^2 - n_i n_p \cos\theta) + \sqrt{n_i^2 n_p^2 \sin^2\theta + \frac{1}{\beta^2}((n_i^2 + n_p^2) - 2 n_i n_p \cos\theta)} \right) \tag{1.17}$$

or to lowest orders[3] :

$$(1.18) \qquad \omega_s = \beta(\theta)\omega_p \sqrt{(n_i^2 + n_p^2) - 2n_i n_p \cos\theta} \pm \beta^2(\theta)\omega_p(n_i^2 - n_i n_p \cos\theta) + O(\beta^3)$$

where β is in general a function of θ, being dependent also on crystal orientation, and is computed from a secular equation[4]:

$$(1.19) \qquad \left| \lambda_{iklm} k_k k_l - \rho \omega^2 \delta_{im} \right| = 0$$

where ρ is the density, λ_{iklm} are the adiabatic moduli of elasticity. The phase velocity along a propagation vector k is defined as $v_s = \frac{\omega}{k}$ where ω is an eigenfrequency of (1.19).

Chapter II. The Dynamics of Brillouin Scattering: Energy Considerations

Pictured clasically, the interaction of light with sound waves arises from reflection of the light off a grating of index of refraction caused by the sound waves. Hence there must exist a relationship between the index of refraction of the medium and its density in order for the coupling of light and sound to occur. Such a relationship arises from the phenomenon of electrostriction, which is the constriction of the material placed in an electric field. Let us examine this phenomenon on the basis of some elementary energy considerations. Consider a condenser immersed in a compressible fluid. When a voltage is applied, fluid flows into the region between the plates, compressing the fluid already there, because this lowers the free energy of the system due to an increase in dielectric constant. Thus an electrostrictive pressure arises, which can be calculated as follows (see fig.3):

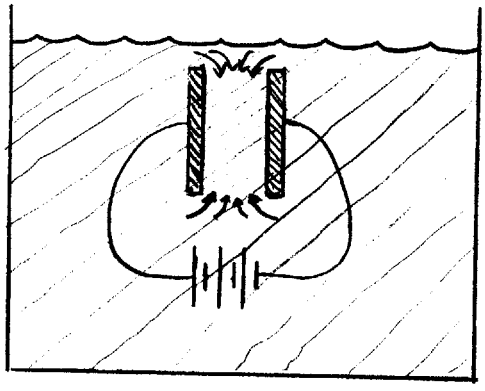

fig. 3: Condenser Immersed in a Fluid

$\delta W = \delta\epsilon \frac{E^2}{8\pi} V_o$, V_o = volume of condenser

$- P_{el} \delta V = \delta W$

(2.1) $$P_{el} = \gamma \frac{E^2}{8\pi}$$

where $\gamma \equiv \rho \frac{\partial \epsilon}{\partial \rho}$ is the electrostrictive constant. Note that the electrostrictive pressure P_{el} depends quadratically on the electric field causing it. This means that if we replace the battery by a sine wave generator, a sound wave of double the frequency will be generated. Furthermore, if two different frequency generators were placed in parallel, sound waves will be generated at the sum and difference frequencies.

Conversely, a change in the density of the material between the plates of the condenser will cause a change in the dielectric constant by an amount:

(2.2) $$\Delta \epsilon = \gamma \frac{\Delta \rho}{\rho_o} = -\gamma \frac{\Delta V}{V_o} = \gamma \frac{\Delta P}{B}$$, B = Bulk modulus

thus causing a polarization to develop ($\epsilon = 1 + 4\pi\chi$):

(2.3) $$\Delta P = (\Delta \chi) E = \frac{\Delta \epsilon}{4\pi} E = \frac{\gamma}{4\pi} \frac{\Delta P}{B} E .$$

Hence the presence of a sound wave will modulate a voltage signal to produce an oscillating dipole moment at sum and difference frequencies.

As a simple model of the interaction of a light wave and a sound wave, let us consider a delay line immersed in a fluid as shown in fig. 4:

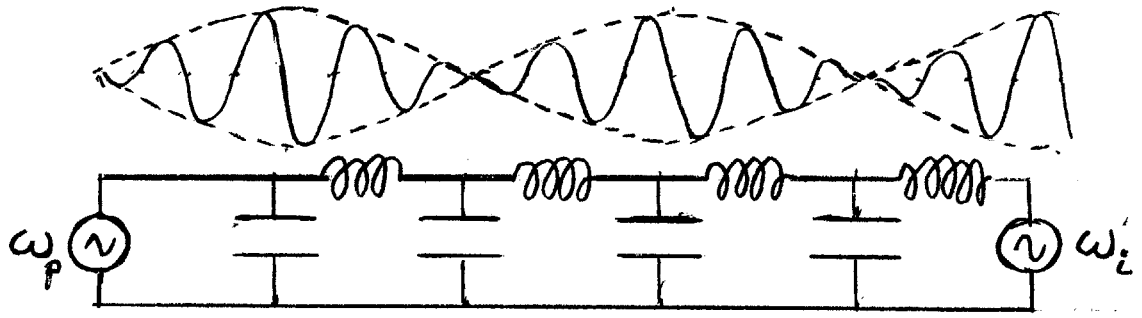

fig. 4: Delay-Line Immersed in a Fluid

Dashed line represents sound wave; solid line represents voltage wave.

The gaps of the condensers will behave as if they were pistons applying the electrostrictive pressure (2.1) to the fluid. If the delay line is driven by two signal generators at frequencies ω_p and ω_i, two waves with wave vectors k_p and k_i will travel down the delay line, causing a sound wave to be generated at a frequency $\omega_s = \omega_p - \omega_i$ and with a wave vector $k_s = k_p - k_i$ (see fig. 4), provided, of course, that $k_s = \frac{\omega_s}{v_s}$. Generally this requires the waves at ω_p and ω_i to travel in opposite directions, corresponding to the backward case of (1.1) ($\theta = \pi$). Conversely, in the presence of the wave at ω_p alone, a sound wave at frequency ω_s travelling across the gaps of the condensers will cause the generation of a voltage wave at ω_i. In normal Brillouin scattering the sound waves are present due to thermal excitation, and generate a small amount of ω_i (typically 10^{-6} as intense as the incident radiation at ω). In stimulated Brillouin scattering, a very intense signal at ω_p is catastrophically converted into large amounts of sound wave at ω_s and electromagnetic wave at ω_i. This occurs catastrophically because even only a very small noise-generated amount of sound wave will generate arbitrarily large amounts of the wave at ω_i, which in turn causes the sound wave to be amplified by large amounts, and thus the interaction of these waves will feed each other energy, leading to an instability. Of course, this catastrophic conversion can occur only if the power generated in these waves exceeds the power lost, due to absorption mechanisms, hence leading to a threshold condition. The intensity of sound and electromagnetic waves thus produced are much larger than in normal Brillouin scattering; the intensity at ω_i can be nearly equal to that of ω_p.

We shall proceed to derive the threshold condition using energy considerations. Let us calculate the energy interchange between an intense

"pump"[5] (laser) wave:

$$E_p(\vec{r}, t) = E_{po} \cos (\vec{k}_p \cdot \vec{r} - \omega_p t + \phi_p) \tag{2.4}$$

and an "idler" (frequency-shifted light) wave:

$$E_i(\vec{r}, t) = E_{io} \cos (\vec{k}_i \cdot \vec{r} - \omega_i t + \phi_i) \tag{2.5}$$

and a "signal" (sound) wave:

$$P_s(\vec{r}, t) = P_{so} \cos (\vec{k}_s \cdot \vec{r} - \omega_s t + \phi_s) \tag{2.6}$$

First, consider the power transferred by the pump and the idler to the sound wave. The process of electrostriction causes a local compression δV which in the presence of the local pressure P_s due to the sound wave does work of an amount:

$$\delta W = - P_s(\vec{r}, t)\, \delta V(\vec{r}, t). \tag{2.7}$$

Thus the average power transferred to the sound wave per unit volume will be:

$$\frac{d u_s}{dt} = - \int \frac{d^3 r}{V_o} \int_{-T/2}^{T/2} \frac{dt}{T} P_s(\vec{r}, t) \frac{\partial}{\partial t} V(\vec{r}, t) \tag{2.8}$$

where, using (2.1)

$$- \frac{\delta V(\vec{r}, t)}{V_o} = \frac{\delta P_{el}(\vec{r}, t)}{B} = \delta \left(\frac{\gamma}{8\pi B} \cdot 2 \vec{E}_p(\vec{r}, t) \cdot \vec{E}_i(\vec{r}, t) \right) \tag{2.9}$$

omitting nonresonant terms. This gives

$$(2.10)\qquad \frac{du_s}{dt} = \frac{\gamma}{4\pi B} P_{so} (\vec{E}_{po} \cdot \vec{E}_{io})\omega_s \cdot \frac{1}{4} \Big[\delta(\vec{k}_p - \vec{k}_i - \vec{k}_s)\delta(\omega_p - \omega_i - \omega_s) - \cos(2\phi_s)\delta(\vec{k}_p - \vec{k}_i - \vec{k}_s)\,\delta(\omega_p - \omega_i + \omega_s) \Big]$$

where we have chosen

$$(2.11)\qquad \phi_p - \phi_i - \phi_s = \frac{\pi}{2}.$$

The sum of Dirac delta functions contains the kinematical relations (1.5, 0.6) for the Stokes case and the anti-Stokes case respectively.

Second, consider the power transferred by the pump and the sound wave into the idler. The dipole moment $\delta\vec{\mu}$ arising from the local change in dielectric constant caused by the sound wave in the presence of the idler's local electric field E_i leads to an energy transfer of:

$$(2.12)\qquad \delta W = \vec{E}_i(\vec{r}, t) \cdot \delta\vec{\mu}(\vec{r}, t)$$

Thus the average power transferred to the idler wave per unit volume will be:

$$(2.13)\qquad \frac{du_i}{dt} = \int \frac{d^3r}{V_o} \int_{-T/2}^{T/2} \frac{dt}{T} \vec{E}_i(\vec{r}, t) \cdot \frac{\partial \vec{p}(\vec{r}, t)}{\partial t}$$

where, using (2.3):

$$(2.14)\qquad \delta\vec{p}(\vec{r}, t) = \delta\left(\frac{\gamma}{4\pi B} P_s(\vec{r}, t)\, \vec{E}_p(\vec{r}, t)\right)$$

again omitting nonresonant terms. This gives

$$(2.15)\qquad \frac{du_i}{dt} = \frac{\gamma}{4\pi B} P_{so}(\vec{E}_{po} \cdot \vec{E}_{io})\, \omega_i \frac{1}{4} \left[\delta(\vec{k}_p - \vec{k}_i - \vec{k}_s)\, \delta(\omega_p - \omega_i - \omega_s) + \cos(2\phi_s)\, \delta(\vec{k}_p - \vec{k}_i + \vec{k}_s)\, \delta(\omega_p - \omega_i + \omega_s)\right]$$

again choosing the phase condition (2.11). Note that the second terms of (2.10) and (2.15) always have opposite sign independent of the choice of phases, which implies that the anti-Stokes cannot build up simultaneously with the sound wave, so that parametric generation of the anti-Stokes cannot occur. Viewed quantum mechanically, the incident quantum can gain in energy (and increase in frequency) only if a phonon is destroyed in the process.

Hence if we choose the kinematical relations

$$(2.16)\qquad \vec{k}_p = \vec{k}_i + \vec{k}_s$$

$$\omega_p = \omega_i + \omega_s$$

$$\phi_p = \phi_i + \phi_s + \frac{\pi}{2}$$

we get:

$$(2.17)\qquad \begin{cases} \left(\frac{du_s}{dt}\right)_{gain} = \frac{\gamma \omega_s}{16\pi B} P_{so} E_{po} E_{io} \\ \left(\frac{du_i}{dt}\right)_{gain} = \frac{\gamma \omega_i}{16\pi B} P_{so} E_{po} E_{io} \end{cases}$$

where we have chosen the polarization of $\vec{E}_p$ and hence $\vec{E}_i$ to be perpendicular to the plane of scattering. The energy density of sound wave is[6] $u_s = \frac{P_{so}^2}{2B}$ and a loss mechanism will cause damping according to:

$$\frac{du_s}{dt}_{loss} = -\frac{u_s}{\tau_s} \quad .$$

Similarly, the energy density for the idler wave is $u_i = \epsilon_o \frac{E_{io}^2}{8\pi}$ (ϵ_o is the dielectric constant at the idler frequency) and the decay law is:

$$\frac{du_i}{dt}_{loss} = -\frac{u_i}{\tau_i} \quad .$$

We require that both the sound waves and the idler build up, implying:

$$(2.18) \quad \begin{cases} \frac{du_s}{dt}_{gain} + \frac{du_s}{dt}_{loss} \geq 0 \\ \frac{du_i}{dt}_{gain} + \frac{du_i}{dt}_{loss} \geq 0 \end{cases}$$

Hence

$$(2.19) \quad \frac{\gamma \omega_s}{16\pi B} P_{so} E_{po} E_{io} \geq \frac{1}{\tau_s} \frac{P_{so}^2}{2B}$$

$$(2.20) \quad \frac{\gamma \omega_i}{16\pi B} P_{so} E_{po} E_{io} \geq \frac{1}{\tau_i} \frac{E_{io}^2}{8\pi} \epsilon_o \quad .$$

Multiplying (2.19) and (2.20) together we get the threshold condition:

$$(2.21) \quad \frac{E_{po}^2}{8\pi} \geq \frac{1}{\omega_s \tau_s \omega_i \tau_i} \frac{2B \epsilon_o}{\gamma^2} \quad .$$

This states that in order to have catastrophic buildup of sound and idler waves, the pump must be sufficiently intense to overcome losses.

Perhaps a more transparent way of describing the above treatment

is that we are calculating the buildup in time of particular normal modes of the idler field and sound waves which can couple kinematically. (This way of picturing the interaction is best suited for the quantum mechanical approach to Brillouin scattering.)[7] Hence the above approach is appropriate for resonant cavities, the normal modes of which decay in a time:

$$(2.22)\quad \begin{cases} t_s = \dfrac{L_s}{v_s}\ \dfrac{1}{1-r_s} = \dfrac{Q}{\omega_s} \\ t_i = \dfrac{L_i}{c}\ \dfrac{1}{1-r_i} = \dfrac{Q}{\omega_i} \end{cases}$$

where L_s and L_i are the lengths of the sound and idler cavities, respectively and r_s and r_i are the reflectivities of the mirrors forming the cavities, and Q_s and Q_i are the quality factors of these cavities. In most cases, the sound wave is so highly attenuated that the cavity losses are negligible in which case:

$$(2.23)\quad \tau_s = \frac{1}{\alpha_s} = \frac{\ell_s}{v_s} = \frac{1}{v_s \mathcal{H}_s}$$

where ℓ_s is the attenuation length, α_s is the percentage loss of sound power per unit time and $\mathcal{H}_s$ is the percentage loss per unit length.

For the case of quartz, where $\tau_s = 5 \times 10^{-9}$ sec[8] and using an auxiliary cavity for the idler with length 10 cm and $r = 0.9$, so that $\tau_i \cong 3 \times 10^{-9}$ sec and where $\gamma = 0.6$[9] and the bulk modulus is 1×10^{12} dynes/cm^2, we get for the threshold:

$$(2.24)\quad \frac{E_{po}^2}{8\pi}\, n_p c \geq 10 \ \text{Mw/cm}^2 .$$

This power is easily attainable using present Q-switching techniques with the ruby laser. However, considerations concerning the rate of growth must accompany this figure for threshold; such considerations will be given in the next chapter.

Chapter III. The Coupled Wave Equations and Their Solutions

Maxwell's equations state that:

$$(3.1)\qquad \begin{cases} \nabla \times \vec{E} = -\frac{1}{c}\frac{\partial \vec{B}}{\partial t} & \nabla \cdot \vec{D} = 4\pi \rho_{true} \\ \nabla \times \vec{H} = \frac{1}{c}\frac{\partial \vec{D}}{\partial t} + 4\pi \vec{J} & \nabla \cdot \vec{B} = 0 \end{cases}$$

We consider the case where $J = 0$ and $\rho_{true} = 0$. The constitutive equations are:

$$(3.2)\qquad \begin{cases} \vec{D} = \epsilon_o \vec{E} + \epsilon_1 \vec{E} \\ \vec{B} = \vec{H} \end{cases}$$

where ϵ_1 arises from pressure fluctuations via electrostriction (cf. (2.2)):

$$(3.3)\qquad \epsilon_1 = \gamma \frac{P_s}{B} .$$

Deriving the wave equation from (3.1) we proceed as usual:

$$(3.4)\qquad \nabla \times (\nabla \times \vec{E}) = -\frac{1}{c^2}\ddot{\vec{D}} = \nabla(\nabla \cdot \vec{E}) - \nabla^2 E .$$

Now $\nabla \cdot (\epsilon_o + \epsilon_1)E = 0$ so that

$$(3.5) \qquad \epsilon_o \nabla \cdot E = - \nabla \cdot (\epsilon_1 E) = - \nabla \epsilon_1 \cdot \vec{E} - \epsilon_1 \nabla \cdot E .$$

Since $\epsilon_1 << \epsilon_o$

$$(3.6) \qquad (\epsilon_o + \epsilon_1) \nabla \cdot \vec{E} = - \nabla \epsilon_1 \cdot E \simeq \epsilon_o \nabla \cdot \vec{E} .$$

Therefore the electromagnetic wave equation becomes:

$$(3.7) \qquad \frac{1}{c_i^2} \ddot{\vec{E}} + \frac{\alpha_i}{c_i^2} \dot{\vec{E}} - \nabla^2 \vec{E} = \frac{\gamma}{B\epsilon_o} \left[\vec{\nabla} (\nabla P_s \cdot \vec{E}) - \frac{1}{c_i^2} \frac{\partial^2}{\partial t^2} (P_s \vec{E}) \right]$$

where the second term is a phenomenologically introduced loss, and where $c_i = \frac{c}{\sqrt{\epsilon_o}}$.

Next we derive the wave equation for sound. Newton's equation states:

$$(3.8) \qquad \rho_o \frac{\partial \vec{u}}{\partial t} = - \vec{\nabla} P + \vec{f}$$

where P is the pressure and $\vec{f}$ is an external force per unit volume on a small "particle" of fluid moving at a velocity $\vec{u}$ and ρ_o is its density. The continuity equation states:

$$(3.9) \qquad \frac{\partial \rho}{\partial t} + \nabla \cdot (\rho \vec{u}) = 0 .$$

If we let $\rho = \rho_o + \rho_s$ where $\rho_s << \rho_o$, (3.9) becomes:

$$\frac{\partial \rho_s}{\partial t} = -\rho_o \nabla \cdot u - \vec{u} \cdot \nabla \rho_s \tag{3.10}$$

where the seond term is negligible since $\rho_s << \rho_o$. Using $\frac{\rho_s}{\rho_o} = \frac{P_s}{B}$,[10] (3.10)becomes:

$$\frac{1}{B} \frac{\partial P_s}{\partial t} = -\nabla \cdot u . \tag{3.11}$$

Taking the $\vec{\nabla}\cdot$ of (3. 8) and $\frac{\partial}{\partial t}$ of (3.11)we get:

$$\frac{\partial^2 P_s}{\partial t^2} = \frac{B}{\rho_o} \nabla^2 P_s + \frac{B}{\rho_o} \nabla \cdot \vec{f} = v_s^2 \nabla^2 P_s + v_s^2 \nabla \cdot \vec{f} \tag{3.12}$$

where in our case $\vec{f}$ is due to electrostriction. We derive $\vec{f}$ more rigorously as follows[11]: Conservation of energy tells us that in the interaction of matter and radiation:

$$\frac{d W_{em}}{dt} = -\frac{d W_{mat}}{dt} , \tag{3.13}$$

W_{mat} and W_{em} being the energy in matter and radiation respectively:

$$\frac{d W_{mat}}{dt} = -\int \vec{f} \cdot \vec{u} \, dv , \tag{3.14}$$

and

$$\frac{d W_{em}}{dt} = \frac{1}{8\pi} \int \frac{\partial}{\partial t} (E \cdot D) \, dv = \frac{1}{8\pi} \int E^2 \frac{\partial \epsilon}{\partial t} \, dv . \tag{3.15}$$

Now $\epsilon = \epsilon(\rho(\vec{r}, t))$.[12] Hence, using the chain rule and (3. 9):

$$(3.16)\qquad \frac{\partial \epsilon}{\partial t} + \vec{u}\cdot\nabla\epsilon = \frac{d\epsilon}{d\rho}\left(\frac{\partial \rho}{\partial t} + \vec{u}\cdot\nabla\rho\right) = \frac{d\epsilon}{d\rho}\left(-\rho_o \vec{\nabla}\cdot\vec{u}\right)$$

$$(3.17)\qquad \frac{\partial \epsilon}{\partial t} = -\rho_o \frac{d\epsilon}{d\rho}\nabla\cdot\vec{u} - \vec{u}\cdot\vec{\nabla}\epsilon$$

$$(3.18)\qquad \frac{dW_{em}}{dt} = -\frac{1}{8\pi}\int\left(\gamma E^2\nabla\cdot u + E^2\nabla\epsilon\cdot\vec{u}\right)dv\,.$$

Integrating by parts the first term and eliminating the surface term since $\vec{u} = 0$ at the surface:

$$(3.19)\qquad \frac{dW_{em}}{dt} = -\frac{1}{8\pi}\int\left[-\nabla(\gamma E^2) + E^2\nabla\epsilon\right]\cdot\vec{u}\,dv\,.$$

Since $\vec{u}$ is arbitrary, (3.13) and (3.14) and (3.19) imply

$$(3.20)\qquad \vec{f} = -\frac{1}{8\pi}\nabla(\gamma E^2) + \frac{1}{8\pi}E^2\nabla\epsilon\,.$$

The first term corresponds to electrostriction and since $\vec{f} = -\vec{\nabla}P_{el}$, we have:

$$(3.21)\qquad P_{el} = \frac{\gamma}{8\pi}E^2\,.$$

The second term of (3.20) corresponds to the force which causes a fluid level to rise into the gap between a pair of capacitor plates. We now can calculate the source term in (3.12) using (3.3):

$$(3.22)\qquad -\nabla\cdot\vec{f} = \frac{1}{8\pi}\gamma\left(\nabla^2E^2 - \nabla E^2\cdot\nabla\frac{P_s}{B} - E^2\nabla^2\frac{P_s}{B}\right).$$

The last term is a small modification of the velocity of sound by an amount

$\frac{2\delta v_s}{v_s} = \frac{E^2}{8\pi}\frac{\gamma}{B} \approx 10^{-2}$ assuming $\gamma \simeq 0.6$, $B \simeq 10^{10}$ (values for quartz) and $E \sim 10^5$ esu $(3 \times 10^7$ volts/cm$)$[13]. In any case both the second and last terms are negligible because $P_s << B$. Thus the wave equation for the sound wave is:

$$\ddot{P}_s + \alpha_s \dot{P}_s - v_s^2 \nabla^2 P_s = -v_s^2 \gamma \nabla^2 \frac{E^2}{8\pi} \tag{3.23}$$

where we again introduce phenomenologically the loss term.

The solutions will be assumed to have the form

$$\begin{cases} \vec{E}_p = \vec{E}_{po}\, e^{i(\omega_p t - \vec{k}_p \cdot \vec{r} + \phi_p)} \\ \vec{E}_i = \vec{E}_{io}\, e^{i(\omega_i t - \vec{k}_i \cdot \vec{r} + \phi_i)} \\ \vec{P}_s = \vec{P}_{so}\, e^{i(\omega_s t - \vec{k}_s \cdot \vec{r} + \phi_s)} \end{cases} \tag{3.24}$$

where E_{po}, E_{io}, P_{so} are slowly varying functions of $\vec{r}$ and t. We assume that E_{po} is very large and E_{io} and P_{so} very small. Taking the time and space averages of waves equations (3.7) and (3.23) with (3.24) substituted into them (which we can do if $\frac{1}{E_{io}}\frac{\partial E_{io}}{\partial t} << \omega_i$, etc.) we see that the wave equations will become, since only resonant terms remain:

$$\ddot{P}_s + \alpha_s \dot{P}_s - v_s^2 \nabla^2 P_s = -v_s^2 \nabla^2 \frac{\gamma}{8\pi} \frac{(2\vec{E}_i^* \cdot \vec{E}_p)}{2} \tag{3.25}$$

$$\ddot{\vec{E}}_i + \alpha_i \dot{\vec{E}}_i - c_i^2 \nabla^2 \vec{E}_i = \frac{\gamma c_i^2}{B \epsilon_o} \left[\vec{\nabla} \frac{(\vec{\nabla} P_s^* \cdot \vec{E}_p)}{2} - \frac{1}{c_i^2} \frac{\partial^2}{\partial t^2} \frac{(P_s^* \cdot \vec{E}_p)}{2} \right] \tag{3.26}$$

$$(3.27)\qquad \ddot{\vec{E}}_p + \alpha_p \dot{\vec{E}}_p - c_p^2 \nabla^2 \vec{E}_p = \frac{\gamma c_p^2}{B \epsilon_o}\left[\vec{\nabla}\frac{(\vec{\nabla} P_s^* \cdot \vec{E}_i)}{2} - \frac{1}{c_p^2}\frac{\partial^2}{\partial t^2}\frac{(P_s^* \cdot \vec{E}_i)}{2}\right].$$

Equation (3.27) immediately tells us that we can consider E_{po} a constant, i.e. independent of space and time, since its source term is a product of two small quantities. In other words, the percentage rate of decay of E_{po} is small compared with the percentage rates of growth of E_{io} and P_{so}. The first of the source terms in (3.26) is a vector parallel to $\vec{k}_i$, which makes the idler slightly nontransverse, and arises from polarization charge, as one sees from (3.6). This nontransverse component of the idler will not propagate outside of the medium, where one makes observations, and we shall omit it. In any case, to reduce (3.25-27) to scalar equations we choose $\vec{k}_s \cdot \vec{E}_p = 0$. Thus (3.25) and (3.26) reduce to, assuming E_{io}, P_{so} are small and slowly varying and keeping lowest order terms only:

$$(3.28)\qquad (2 i \omega_s \dot{P}_{so} + i \alpha_s \omega_s P_{so} + 2 i v_s^2 \vec{k}_s \cdot \vec{\nabla} P_{so}) = + \frac{\gamma}{8\pi} v_s^2 k_s^2 i E_{io} E_{po}$$

$$(3.29)\qquad (2 i \omega_i \dot{E}_{io} + i\alpha_i \omega_i E_{io} + 2 i c_i^2 \vec{k}_i \cdot \vec{\nabla} E_{io}) = \frac{\gamma}{2 B \epsilon_o} \omega_i^2 i P_{so} E_{po}$$

where the factor i in the source terms arises from the choice of phase

$\phi_p = \phi_i + \phi_s + \pi/2$. One notices that had one chosen the anti-Stokes equation in place of (3.29), the source terms would have opposite signs, independent of the choice of phases, again proving that the anti-Stokes idler cannot build up simultaneously with the sound wave. Simplifying we get:

$$\dot{P}_{so} + \frac{\alpha_s}{2} P_{so} + v_s \hat{k}_s \cdot \nabla P_{so} = \Gamma_s E_{io} E_{po} \tag{3.30}$$

$$\dot{E}_{io} + \frac{\alpha_i}{2} E_{io} + c_i \cdot \hat{k}_i \cdot \nabla E_{io} = \Gamma_i P_{so} E_{po} \tag{3.31}$$

where $\hat{k}_s$ and $\hat{k}_i$ are the unit vectors along the directions of sound and idler waves and

$$\Gamma_s = \frac{\gamma}{16\pi} \omega_s \tag{3.32}$$

$$\Gamma_i = \frac{\gamma}{4 B \epsilon_o} \omega_i \ . \tag{3.33}$$

Since (3.30) and (3.31) are linear, we solve by separation of variables. Let

$$\begin{cases} P_{so} = R_s(\vec{r})\, T_s(t) \\ E_{io} = R_i(\vec{r})\, T_i(t) \end{cases} \tag{3.34}$$

Multiplying (3.30) and (3.31) together and dividing by $P_{so} E_{io}$:

$$\left(\frac{\dot{T}_s}{T_s} + \frac{\alpha_s}{2} + v_s \hat{k}_s \cdot \frac{\nabla R_s}{R_s} \right) \left(\frac{\dot{T}_i}{T_i} + \frac{\alpha_i}{2} + c_i \hat{k}_i \cdot \frac{\nabla R_i}{R_i} \right) = \Gamma_i \Gamma_s E^2_{po} \ . \tag{3.35}$$

Since the right side is independent of $(\vec{r},\ t)$, so must the left, implying:

$$(3.36)\qquad \begin{cases} \dot{T}_s = \beta_s T_s \\ v_s \hat{k}_s \cdot \nabla R_s = v_s (\hat{k}_s \cdot \vec{q}_s) R_s \end{cases}$$

$$(3.37)\qquad \begin{cases} \dot{T}_i = \beta_i T_i \\ c_i \cdot \hat{k}_i \cdot \nabla R_i = c_i (\hat{k}_i \cdot \vec{q}_i) R_i \end{cases}$$

so that exponential solutions (which are complete) result. Substituting these solutions back into (3. 30) and (3. 31) we see that $\beta_s = \beta_i \equiv \beta$ and $\vec{q}_s = \vec{q}_i \equiv \vec{q}$. Since kinematics imply that $\hat{k}_s \cdot \hat{k}_i \angle 0$ (i. e. the idler and sound waves are always travelling in opposing directions), this means that if we choose q real (travelling wave case) then it would seem that one wave will always rob power from another. However, we must superpose solutions to fit boundary conditions to get the correct solution.

Let us first consider the boundary value problem of a resonant cavity for either idler or sound wave. Since we shall demand that $R_{i,s}$ be zero at the boundary, it is clear that $\vec{q}$ must be imaginary to give us the necessary oscillatory solutions. Let us choose to resonate the idler; then $\vec{q} = i\,\Delta\vec{k}$ points in the direction $\hat{k}_i$ (this corresponds to a slight shift in wavelength in order to couple to a mode of the resonator). We get from (3. 35):

$$(3.38)\qquad \left(\beta + \frac{\alpha_s}{2} + i\,\Delta k'\, v_s\right)\left(\beta + \frac{\alpha_i}{2} + i\,\Delta k\, c_i\right) = \Gamma_i \Gamma_s E_{po}^2$$

where $\Delta k' = \Delta k\,(\hat{k}_i \cdot \hat{k}_s)$. At threshold $\beta = \Delta k = 0$ and using (2. 23):

$$(3.39) \qquad \frac{E_T^2}{8\pi} = \frac{2 B \epsilon_o}{\gamma^2} \frac{1}{\omega_i \tau_\pi \omega_s \tau_s}$$

in agreement with (2.21). Solving β in general we obtain ($c_i >> v_s$):

$$(3.40) \qquad \beta = -\left(\frac{\alpha_i + \alpha_s}{4} + \frac{i\Delta k}{2} c_i\right) \pm \frac{1}{2}\sqrt{\left(\frac{\alpha_s - \alpha_i}{2} - i\Delta k c_i\right)^2 + 4 E_{po}^2 \Gamma_i \Gamma_s} .$$

Above threshold, only the (+) solution corresponds to a growing wave, and β, near threshold, is:

$$(3.41) \qquad \beta = \frac{\left[\left(\left(\frac{E_{po}}{E_T}\right)^2 - 1\right)\alpha_i \alpha_s - 2 i \Delta k \left(c_i \alpha_s + v_s' \alpha_i\right)\right]}{2\left[\left(\alpha_i + \alpha_s\right) + 2 i \Delta k c_i\right]}$$

where $v_s' = v_s \hat{k}_s \cdot \hat{k}_i$. Therefore the real part β, representing growth, is:

$$(3.42) \qquad 2 \mathrm{Re}\,\beta = \frac{\left[\left(\frac{E_{po}}{E_T}\right)^2 - 1\right] \cdot \left(\frac{\alpha_i \alpha_s}{\alpha_i + \alpha_s}\right) - 4\left(\frac{\Delta k c_i}{\alpha_i + \alpha_s}\right)^2 \left(1 + \frac{v_s'}{c} \frac{\alpha_i}{\alpha_s}\right)}{1 + 4\left(\frac{\Delta k c_i}{\alpha_i + \alpha_s}\right)^2}$$

which is clearly a maximum when $\Delta k = 0$. The imaginary part of β, representing "pulling", is:

$$(3.43) \qquad \operatorname{Im}\beta = -\Delta k\, c_i \left(\frac{\left[\left(\frac{E_{po}}{E_T} \right)^2 - 1 \right] \frac{\alpha_i \alpha_s}{(\alpha_i + \alpha_s)^2} + \left(\frac{\alpha_s + \frac{v_s'}{c} \alpha_i}{\alpha_s + \alpha_i} \right)}{1 + 4 \left(\frac{\Delta k\, c_i}{\alpha_i + \alpha_s} \right)^2} \right)$$

which is zero if $\Delta k = 0$. From (3.42) it must be concluded that the rate of growth is less than the lowest loss in the system near threshold. Thus for $\alpha_s \gg \alpha_i$, $2 \operatorname{Re}\beta = \left(\frac{E_{po}^2}{E_T^2} - 1 \right) \alpha_i$, the first factor being smaller than unity around threshold. For the case of quartz considered in the previous chapter, $\alpha_s \tilde{=} 2 \times 10^8$ sec^{-1} and $\alpha_i \tilde{=} 3 \times 10^8$ sec^{-1} are about equal, and thus $2 \operatorname{Re}\beta \tilde{=} 1.2 \times 10^8$ sec^{-1} when we are twice above threshold, giving us an e-folding time of 0.8×10^{-8} sec^{-1}. Since the laser pulse lasts only $\sim 2 \times 10^{-8}$ sec^{-1}, this means the signal will only be a factor of ten above the initial noise.

Larger rates of growth can be obtained by raising the power of the pump or by decreasing α_i and thereby decreasing the threshold. In either case, when we far exceed the threshold

$$(3.44) \qquad \beta = \frac{E_{po}}{\sqrt{\pi B \epsilon_o}} \cdot \sqrt{\omega_i \omega_s} \cdot \frac{\gamma}{8} \equiv \frac{1}{T} \quad .$$

For a pulse of 100MW/cm^2 (unfocussed laser beam), $E_{po} = 1 \times 10^3$ esu so that $\beta \cong .7 \times 10^9$ sec^{-1} for quartz, meaning a gain of e^{14} in 2×10^{-8} sec.

Taking the ratio of (3.30) and (3.31) will tell us the ratio of signal to idler:

$$(3.45) \qquad \frac{\left(\beta + \frac{\alpha_s}{2} + i\, v_s\, \Delta k' \right)}{\left(\beta + \frac{\alpha_i}{2} + i\, c_i\, \Delta k \right)} = \frac{\Gamma_s}{\Gamma_i} \left(\frac{E_{io}}{P_{so}} \right)^2$$

In the limit β and Δk small, the ratio of energy densities is:

$$\frac{u_s}{u_i} = \frac{\omega_s}{\omega_i} \cdot \frac{\alpha_i}{\alpha_s} = \frac{\omega_s \tau_s}{\omega_i \tau_i} . \tag{3.46}$$

When far above threshold (β large):

$$\frac{u_s}{u_i} = \frac{\omega_s}{\omega_i} . \tag{3.47}$$

This is a statement of the Manley-Rowe relations. Quantum mechanically stated, each photon of the idler is produced in association with a phonon of the signal. The energy of the photon is $\hbar \omega_i$, whereas the energy of the phonon is $\hbar \omega_s$, whence (3.47). Clearly, at maximum conversion by energy conservation the idler becomes very nearly equal in intensity to the pump. From (3.47) and since $\frac{d u_s}{dt} = 2 \beta u_s$ and $\frac{d u_s}{dt} = 2 \beta u_i$, we then see that maximum power in the sound wave is $\sim$0.6 kilowatt/cm^2 from a 10 megawatt/cm^2 laser beam. This corresponds quantum mechanically to converting every single pump photon into an idler photon and a signal phonon.

For the travelling wave case involving a general scattering angle θ, the geometrical shape of the region of interaction between pump, idler, and sound is usually quite complicated, especially when the pump beam is circular in cross section. On the one side of the boundary of the region of interaction in which the idler or the pump originates, the amplitude of the idler or the pump is zero everywhere. On the other side of the boundary from which the amplified idler or pump leaves, the uncoupled propagating wave solutions are projected back onto the boundary to give us boundary conditions for the other side. The procedure is then

to superpose exponential solutions to solve (3. 30) and (3. 31) with these given boundary conditions. This is in general a complicated problem except in the collinear case where $\hat{k}_i \cdot \hat{k}_s = -1$.

In the collinear case[14] let us choose the boundary conditions for (3. 30) and (3. 31) as follows (see fig. 5):

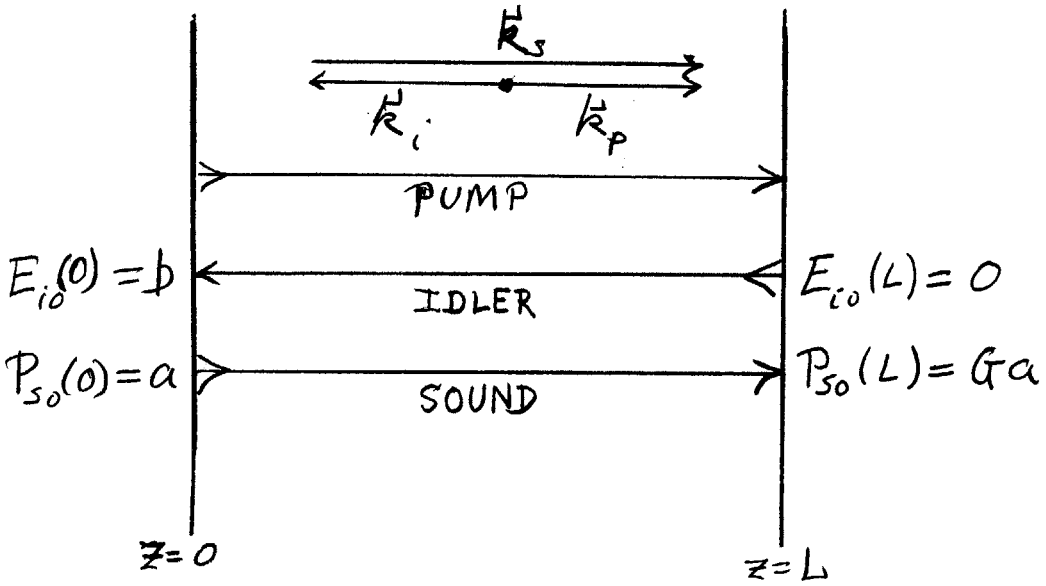

fig. 5: Boundary Conditions for Backward Wave Amplifier

(3. 48) $\qquad E_{io}(L) = 0 \quad \text{and} \quad P_s(0) = a.$

The slab of material is assumed to have no Fresnel reflections at the boundaries (no feedback). One may visualize these boundary conditions as those for a slab of "active" material ($\gamma \neq 0$) imbedded in a "passive" medium ($\gamma = 0$), with all other properties (i. e. c_i and v_s) the same. Now (3. 35) becomes ($\hat{k}_i \cdot \hat{k}_s = -1$ and $\vec{q} \cdot \hat{k}_s = +q$):

(3. 49) $$\left(\beta + \frac{\alpha_s}{2} + v_s q\right)\left(\beta + \frac{\alpha_i}{2} - c_i q\right) = \Gamma_i \Gamma_s E_{po}^2$$

which has as solutions, assuming $v_s \ll c_i$ and defining

$$\mathcal{H}_i = \frac{\alpha_i}{c_i} = \frac{1}{\ell_i}, \quad \mathcal{H}_s = \frac{\alpha_s}{v_s} = \frac{1}{\ell_s}$$

$$(3.50) \qquad 2q = -\left(\frac{\mathcal{H}_s - \mathcal{H}_i}{2} + \frac{\beta}{v_s}\right) \pm \sqrt{\left(\frac{\mathcal{H}_s + \mathcal{H}_i}{2} + \frac{\beta}{v_s}\right)^2 - \frac{\gamma^2}{16\pi B \epsilon_o} k_i k_s E_{po}^2} .$$

When E_{po}^2 is sufficiently large, q has an imaginary component. This has a quantum mechanical analogue in the splitting of degenerate states by a "mixing" perturbation by which these states can interact. In the present case the phase velocities of the normal mode of sound wave and the idler wave are split from their uncoupled propagation values by their interaction via the presence of the electrostriction and a large pump wave.[15] Let us define:

$$(3.51) \begin{cases} \xi = + \dfrac{\mathcal{H}_s - \mathcal{H}_i}{2} + \dfrac{\beta}{v_s}, \\ D = \sqrt{\dfrac{\gamma^2}{16\pi B \epsilon_o} k_i k_s E_{po}^2 - \left(\dfrac{\mathcal{H}_s + \mathcal{H}_i}{2} + \dfrac{\beta}{v_s}\right)^2} \\ 2q = -\xi + iD, \qquad 2q' = -\xi - iD \end{cases}$$

Now let us solve the boundary value problem as described in fig. 5. We have solutions of the form $P_{so} = P e^{q z} + P' e^{q' z}$ and $E_{io} = E e^{q z} + E' e^{q' z}$ with:

$$(3.52) \begin{cases} a = P + P' \\ 0 = E e^{qL} + E' e^{q' L} \end{cases}$$

We define as the amplitude gain of the sound wave:

$$(3.53) \qquad G = \frac{P\, e^{q L} + P'\, e^{q' L}}{P + P'} \quad .$$

The ratio of (3.30) with the two exponential solutions relates P's to the E's:

$$(3.54) \qquad \frac{\left(\frac{\beta}{v_s} + \frac{\mathcal{H}_s}{2} + q\right) P}{\left(\frac{\beta}{v_s} + \frac{\mathcal{H}_s}{2} + q'\right) P'} = \frac{E}{E'} = - \frac{e^{q' L}}{e^{q L}} \quad .$$

Hence we have for the amplitude gain:

$$(3.55) \qquad G = \frac{(q' - q)}{\left(\frac{\beta}{v_s} + \frac{\mathcal{H}_s}{2} + q'\right) e^{-q L} - \left(\frac{\beta}{v_s} + \frac{\mathcal{H}_s}{2} + q\right) e^{-q' L}}$$

$$= \frac{e^{-\xi/2\, L}}{\cos \frac{D L}{2} + \left(\frac{\beta}{v_s} + \frac{\mathcal{H}_s + \mathcal{H}_i}{2}\right) \frac{}{D} \sin \frac{D L}{2}} \quad .$$

This gain can become infinite if D is real because the denominator may then vanish, corresponding to a situation in which $P_s(0) = 0$, i.e. both idler and sound waves break into oscillation. The condition that D is real implies:

$$(3.56) \qquad \frac{E_{po}^2}{8\pi} \geq \frac{2 B \epsilon_o}{\gamma^2} \frac{1}{k_i k_s} \frac{1}{4} \left(\frac{1}{\ell_s} + \frac{1}{\ell_i}\right)^2 \quad .$$

For quartz this is about 1.5×10^5 Megawatts/cm^2. Strictly speaking (3.56) is for the case of infinite L, as we shall see shortly. For finite L and $D > 0$, there always exists a real β so that the denominator vanishes; we get the transcendental equation for β [16]:

$$\tan \frac{D L}{2} = - \frac{D}{\left(\frac{\beta}{v_s} + \frac{\mathcal{K}_s + \mathcal{K}_i}{2} \right)} . \tag{3.57}$$

The choice of a pure real β corresponds physically to the fact that the amplifier represented by fig. 5 becomes unstable for $D > 0$ and any arbitrary $L > L_c$, some critical value to be determined shortly, and starts to oscillate. Thus the solution will start growing exponentially in time, just like the case of the resonant cavity. But unlike the resonator case, there is also exponential spatial behavior; the solutions are, for the unstable case:

$$E_{io} = \frac{\mathcal{E}}{D} \left[\left(\frac{\beta}{v_s} + \frac{\mathcal{K}_s + \mathcal{K}_i}{2} \right) \sin \frac{D z}{2} + D \cos \frac{D z}{2} \right] e^{\beta t - \left(\frac{\beta}{v_s} + \frac{\mathcal{K}_s - \mathcal{K}_i}{2} \right) \frac{z}{2}} \tag{3.58}$$

$$P_{so} = \frac{\mathcal{E} E_{po}}{D} \frac{\gamma k_s}{16\pi} \sin \frac{D z}{2} e^{\beta t - \left(\frac{\beta}{v_s} + \frac{\mathcal{K}_s - \mathcal{K}_i}{2} \right) \frac{z}{2}}$$

Note the large spatial gain for the idler and the correspondingly large spatial decay of the sound wave. This occurs because the sound wave travels at such a slow speed that the idler can readily rob its power.

$\mathcal{E}$ is not determined uniquely from the boundary conditions $P_{so}(0) = 0$ and $E_{io}(L) = 0$, but like any oscillator problem, will be determined by initial noise. Of course, the maximum amount of power transferred to the idler and sound waves is still limited by the Manley-Rowe relations (cf. (3.45) and (3.47)) and the final steady-state level of oscillation will be determined by nonlinear saturation effects.

Solutions to (3.57) are obtainable by a graphical method, as illustrated by fig. 6:

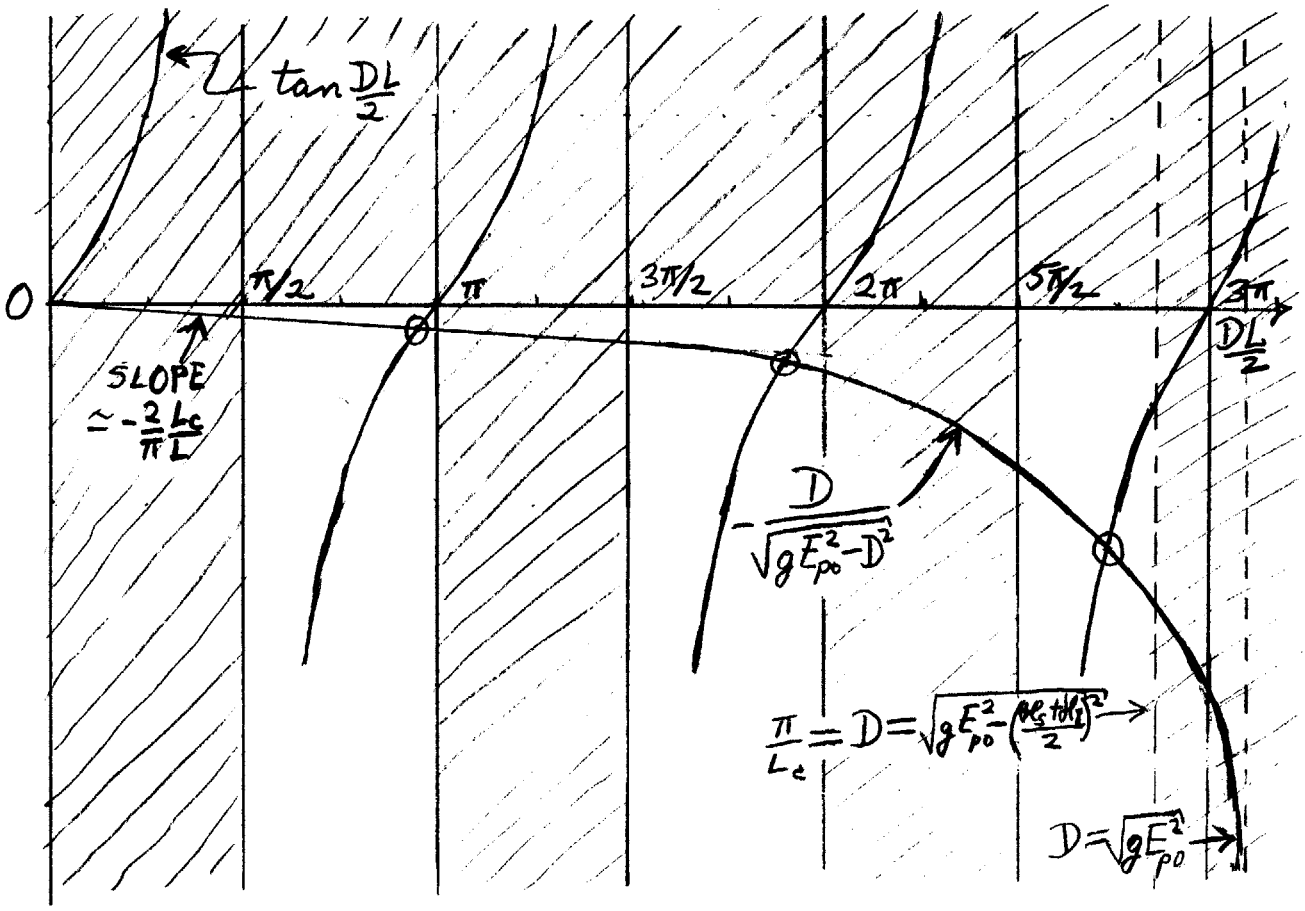

fig. 6: Graphical Solution for D

Unshaded areas denote regions where oscillation can build up. The circled intersections give solutions to (3.57). β is determined from D by

$$\beta = \sqrt{g E_{po}^2 - D^2} - \frac{\mathcal{H}_s + \mathcal{H}_i}{2} .$$

It is obvious on inspection of fig. 6 that near threshold, when $D \to 0$, it is necessary that $L \to \infty$ so that $\frac{D\,L}{2} \to \pi/2$ in order to be in the first region of instability. Indeed it is necessary that $L \geq L_c$ where:

$$(3.59) \qquad L_c = \frac{\pi}{\sqrt{g\,E_{po}^2 - \left(\frac{\mathcal{H}_s + \mathcal{H}_i}{2}\right)^2}}$$

where $g = \frac{\gamma^2 k_i\, k_s}{16\pi\, B \epsilon_o}$. Hence $L_c \to \infty$ as we approach the threshold (3.56). For $L \gg L_c$ and small n, inspection of fig. 6 shows that the roots become:

$$(3.60) \qquad \frac{D_n L}{2} \simeq n\pi \simeq \frac{2\pi L}{\lambda_n}$$

so that from (3.51) the rate of growth of the n^{th} mode is:

$$(3.61) \qquad \frac{\beta_n}{v_s} \simeq \sqrt{g\,E_{po}^2 - \frac{n^2\pi^2}{L^2}} - \frac{\mathcal{H}_s + \mathcal{H}_i}{2} \,.$$

The number of modes that will be excited will be:

$$(3.62) \qquad N \simeq \frac{1}{2}\,\frac{L}{L_c} \,.$$

The wavelength of the highest mode will be:

$$(3.63) \qquad \lambda_N = \frac{2\,L}{N} \simeq 4\,L_c$$

so that another physical significance of L_c is that it is one fourth the shortest wavelength excitable at a given power level. When we are far above threshold $\left(g E_{po}^2 \gg \left(\frac{\mathcal{H}_s + \mathcal{H}_i}{2} \right)^2 \right)$ and when $L \gg L_c$, all the lower modes grow at the same rate:[17]

$$\frac{\beta_n}{v_s} \simeq \frac{\pi}{L_c} \simeq \sqrt{\frac{\gamma^2}{16\pi B \epsilon_o} k_i k_s E_{po}^2} \tag{3.64}$$

so that still another physical significance of L_c is that it gives the spatial rate of growth of the idler and decay of the sound wave and also the temporal rate of growth of both waves for the lower modes when far above threshold. Notice that this growth rate is smaller than that of the resonator case (3.44) by a factor of $2\sqrt{\frac{v_s}{c_i}} \sim 9 \times 10^{-3}$. Physically this results because when we resonate the idler, feedback occurs at the speed of light, whereas in the backward travelling wave case, the slow-moving sound wave is an essential link in the feedback process, and hence will slow down the rate of buildup.

Numerically, let us examine the conditions which we obtain experimentally when a 10MW laser beam emitted from a ruby of diameter $2a = 1$ cm is focussed down by a lens withfocal length $f = 5$ cm into a piece of quartz, inside which the cylindrical focal region has a diffraction-limited radius of $1.22 \lambda \left(\frac{f}{2a}\right) = 4.3 \times 10^{-4}$ cm. and a diffraction-limited length $L_a = n \left(\frac{f}{a}\right)^2 \lambda = 1.1 \times 10^{-2}$ cm.[18] The energy flux in the focal region is 10^7 MW/cm^2, or $E_{po} \simeq 3 \times 10^5$ esu, which far exceeds the threshold (3.56), so that we use (3.64) to give us $\beta \simeq 2 \times 10^9$ sec^{-1}, meaning a gain of e^{40} in 2×10^{-8} sec. Also, from (3.64) we see[19] $L_c = 1 \times 10^{-3}$ cm. $\ll L_a = 1.1 \times 10^{-2}$ cm., the effective length of "active" material, so that the rate of growth of the lowest modes is independent of L_a and hence independent of the exact nature of the

boundary conditions, which in the focal region are clearly not as sharp as those used in the above analysis (cf. fig. 5). The number of modes which oscillate is calculated from (3.62) to be $N \simeq 7$. These modes (solutions given in (3.58) if D is replaced by D_n and β by β_n) have nearly the same rates of buildup in time and are identical in frequency so that spectroscopically they will appear indistinguishable. In space, however, they behave quite differently, with the n^{th} mode having a wavelength $\lambda_n = \frac{4 L_a}{(2n+1)}$. Hence we may superpose these modes to produce arbitrarily shaped mode patterns (which, however, cannot vary rapidly in a distance λ_N).

Indeed we should be able to solve the problem in which E_{po} varies slowly, such as in the case of the focal region, by superposing solutions of the case when $L \to \infty$. These solutions are:

$$(3.65) \qquad E_i(n) = L \frac{\mathcal{E}(n)}{2n\pi} \left(\left(\frac{\beta}{v_s} + \frac{\mathcal{H}_s + \mathcal{H}_i}{2} \right) \sin \frac{n\pi}{L} z \right) e^{\beta t - \left(\frac{\beta}{v_s} + \frac{\mathcal{H}_s + \mathcal{H}_i}{2} \right) \frac{z}{2}}$$

$$\equiv A_n u_n(z)\, g(z, t)$$

$$(3.66) \qquad P_s(n) = L \frac{\mathcal{E}(n)}{2n\pi} E_{po} \frac{\gamma k_s}{16\pi} \sin \frac{n\pi}{L} z \; e^{\beta t - \left(\frac{\beta}{v_s} + \frac{\mathcal{H}_s - \mathcal{H}_i}{2} \right) \frac{z}{2}}$$

$$\equiv B_n u_n(z)\, g(z, t)$$

where $g(z, t) = e^{\beta t - \left(\frac{\beta}{v_s} + \frac{\mathcal{H}_s - \mathcal{H}_i}{2} \right) \frac{z}{2}}$ is independent of n in the limit $L_c \to 0$; $u_n(z) = \sqrt{\frac{2}{L}} \sin \frac{n\pi}{L} a$; $A_n = \frac{L^{3/2}}{\sqrt{2}} \cdot \frac{\mathcal{E}(n)}{2n\pi} \left(\frac{\beta}{v_s} + \frac{\mathcal{H}_s + \mathcal{H}_i}{2} \right)$

and $B_n = \frac{L^{3/2}}{\sqrt{2}} \cdot \frac{\mathcal{E}(n)}{2n\pi} E_{po} \frac{\gamma k_s}{16\pi}$; and let $r = \frac{A_n}{B_n} = \frac{1}{16\pi} \cdot \frac{\frac{\beta}{v_s} + \frac{\varkappa_s + \varkappa_i}{2}}{E_{po}\, \gamma k_s}$

which also is independent of n. The equations (3.30) and (3.31) become for the focal region:

$$\dot{P}_{so} + \frac{\alpha_s}{2} P_{so} + v_s \frac{\partial P_{so}}{\partial z} = \Gamma_s E_{io} E_{po}(z) \tag{3.67}$$

$$\dot{E}_{io} + \frac{\alpha_i}{2} E_{io} - c_i \frac{\partial E_{io}}{\partial z} = \Gamma_i P_{so} E_{po}(z) \tag{3.68}$$

where $E_{po}(z) = E'_{po} \frac{\sin F^2 k_p (z - L/2)}{F^2 k_p (z - L/2)}$ ^{20} where $F^2 = \left(\frac{f}{2a}\right)^2 \equiv \frac{K}{k_p}$.

Let

$$\begin{cases} E_{io} = \left(\sum_n a_n u_n(z)\right) g(z, t) = U(z)\, g(z, t) \\ P_{so} = \left(\sum_n b_n u_n(z)\right) g(z, t) = U(z)\, g(z, t) \end{cases} \tag{3.69}$$

be trial solutions of (3.67) and (3.68). We then get conditions on a_n and b_n using the orthogonality of $u_n(z)$:

$$a_n = \frac{1}{E_{po}} r \sum_\ell b_{n-\ell}\, c_\ell \tag{3.70}$$

$$b_n = \frac{1}{E_{po}} \frac{1}{r} \sum_{\ell'} a_{n-\ell'}\, c_{\ell'} \tag{3.71}$$

where $c_n = \sqrt{\frac{2}{L}} \int_0^L \cos \frac{n\pi}{L} z\, E_{po}(z)\, dz$ and $c_n = c_{-n}$. Hence

$$(3.72) \qquad a_n = \frac{1}{E_{po}^2} \sum_{\ell\ell'} a_{n-\ell-\ell'} c_\ell c_{\ell'}$$

In the limit $L \to \infty$, these Fourier series become Fourier integrals so that (3.72) becomes:

$$(3.73) \qquad a(k) = \frac{1}{E_{po}^2} \int_{-\infty}^{\infty} dk'\, a(k')\, K(k, k')$$

$$(3.74) \qquad K(k, k') = \int_{-\infty}^{\infty} dk''\, c(k - k' - k'')\, c(k'') = c * c(k - k') .$$

This is a singular homogenous Fredholm equation of the second kind, with eigenvalue $\frac{1}{E_{po}^2}$ [21]. The kernel is real and symmetric. Generally the eigenvalue spectrum is continuous, with certain conditions depending on the kernel, so that we can superpose the eigenfunctions to form arbitrarily shaped solutions, just like Fourier integrals. For the field distribution in the focal region:

$$(3.75) \qquad c(k) = \frac{1}{2\pi} \int_{-\infty}^{\infty} dz \cos k z \cdot E'_{po} \frac{\sin K z}{K z}$$

$$= E'_{po} \frac{1}{4K} \left[\epsilon\left(\frac{k}{K} + 1\right) - \epsilon\left(\frac{k}{K} - 1\right) \right]$$

where $\epsilon(x) = \begin{cases} 1 & x > 0 \\ 0 & x = 0 \\ -1 & x < 0 \end{cases}$. Hence c (k) looks like fig. 7 (a):

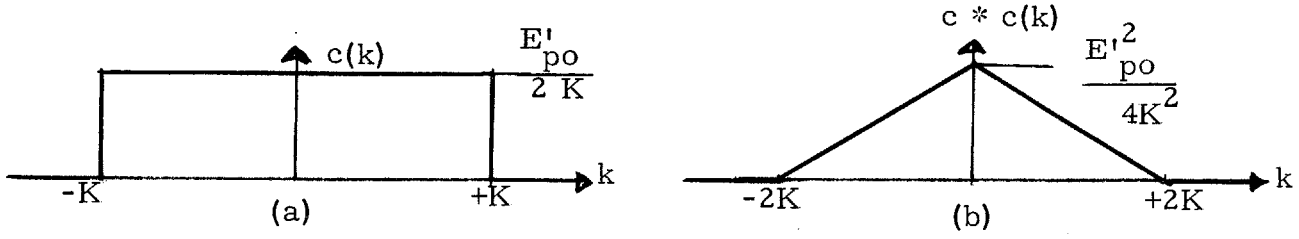

fig. 7: The Fourier Transform of the Field in the Focal Region c (k) and its Self-Convolution c * c (k).

Clearly $c(k) \rightarrow \delta(k)$ as $K \rightarrow 0$ and $E'_{po} \rightarrow E_{po}$, which is a trivial reduction to the previous problem. The kernel of the focal region is therefore (fig. 7 (b)):

$$(3.76) \qquad c * c(k) = \frac{E'^2_{po}}{4K^2} (2K - |k|) H(2K - |k|)$$

where H is the Heaviside function. Hence (3.73) becomes:

$$(3.77) \qquad a(k) = \frac{E'^2_{po}}{E^2_{po}} \frac{1}{4K^2} \int_{k-2K}^{k+2K} dk' \, a(k') (2K - |k - k'|) .$$

Upon differentiating twice, this becomes the differential equation:

$$(3.78) \qquad \frac{d^2a}{dk^2} = \frac{E'^2_{po}}{E^2_{po}} \frac{1}{4K^2} \left[a(k + 2K) - 2a(k) + a(k - 2K) \right].$$

Solutions will be of the form $a = a_o e^{\pm i k z_o}$ or $U(z) = \delta(z - z_o)$, where the transcendental equation

$$(3.79) \qquad z_o = \frac{E'_{po}}{E_{po}} \frac{1}{K} \sin K z_o$$

is the eigenvalue condition. Since $\sqrt{g} E_{po} = \frac{\beta}{v_s} \pm \frac{\mathcal{H}_i + \mathcal{H}_s}{2}$, (3.79) determines how quickly the mode z_o will grow. In order for there to be a solution to (3.79), clearly $E_{po} < E'_{po}$ must obtain. For $z_o \ll \frac{1}{K}$, $E_{po} \simeq E'_{po}$ is independent of z_o, implying modes localized in the focal region grow at the same rate as expected from the plane wave solutions. Modes with $z_o > \frac{1}{K}$ (located away from the focal region) grow more

slowly, with the modes localized near the nodes $\xi_o = \frac{n\pi}{K}$ not growing at all. One should note that we have assumed the growth factor g (ξ, t) is independent of k, which breaks down when k $\rightarrow \infty$. Indeed there will be a cutoff to the spectrum at $k_c = \frac{\pi}{2 L_c}$, corresponding to the highest mode excitable. Hence U (z) is smeared out by an amount $\Delta L \sim L_c$ from an exact Dirac delta function.

Again a_o is determined only by noise, with nonlinear saturation effects ultimately limiting its steady state value. The problem of exactly how oscillations build up from noise can become important under certain conditions. For instance, if the laser pulse is of such a short duration that the sound wave does not have sufficient time to propagate a long enough distance to establish the feedback necessary for the onset of oscillation, transient solutions arising from the noise will dominate the behavior of the waves. The criterion for this to happen is that $L_t = v_s \tau$, where τ is the pulse duration, is less than L_c, the shortest length of oscillator that will still make it unstable. For a laser pulse of $\tau = 2 \times 10^{-8}$ sec, the sound wave travels a distance $L_t = 1.2 \times 10^{-2}$ cm $>> L_c = 1 \times 10^{-3}$ cm for the focal region, so that instability will occur for most of the plane wave modes. However, since the effective length of the "active" region $L_a = 1.1 \times 10^{-2}$ cm is comparable with L_t, transient effects may be important for the lowest modes. Transient effects will probably also be important when the laser beam is weakly focussed or unfocussed.[22] We can introduce the effect of noise by inserting a term $\frac{a_o}{\xi^2/4 + k^2} \frac{1}{\beta}$ into (3.73), corresponding to a uniform excitation of all modes k (true at high temperatures). This makes the integral equation inhomogeneous and unique solutions are then possible[23].

Kroll has treated this problem in another way in the case when the laser field is constant[14]. He starts with (3.30) and (3.31) without transformation. Let us extend his method to allow for focal-region variations in field intensity. Let

$$(3.80)\qquad \begin{cases} u = z - v_s t & u' = z - c_i t \\ w = z + v_s t & w' = z + c_i t \end{cases}$$

By the chain rule of differentiation $\frac{1}{v_s}\frac{\partial}{\partial t} + \frac{\partial}{\partial z} = 2\frac{\partial}{\partial w}$ and $\frac{1}{c_i}\frac{\partial}{\partial t} - \frac{\partial}{\partial z} = -2\frac{\partial}{\partial u'}$ so that (3.30) and (3.31) become:

$$(3.81)\qquad 2 v_s \frac{\partial}{\partial w} P_{so} + \frac{\alpha_s}{2} P_{so} = \Gamma_s E_{io} E_{po}$$

$$(3.82)\qquad -2 c_i \frac{\partial}{\partial u'} E_{io} + \frac{\alpha_i}{2} E_{io} = \Gamma_i P_{so} E_{po} .$$

Let us obtain the Green's function for (3.81):

$$(3.83)\qquad 2 v_s \frac{\partial}{\partial w} G_s + \frac{\alpha_s}{2} G_s = \delta(w - w_o)$$

$$(3.84)\qquad \int_{w_o - \epsilon}^{w_o + \epsilon} dw \left(2 v_s \frac{\partial G_s}{\partial w} + \frac{\alpha_s}{2} G_s\right) \cong G_s \Big|_{w_o - \epsilon}^{w_o + \epsilon} 2 v_s = G_{so}\, 2 v_s = 1 .$$

Hence

$$(3.85)\qquad G_s = \frac{1}{2 v_s} e^{-\frac{\alpha_s}{4 v_s}(w - w_o)} H(w - w_o) .$$

Superposition gives:

$$(3.86) \qquad P_{so}(u, w) = \frac{1}{2 v_s} \int_{-\infty}^{w} dw_o \, \Gamma_s \, E_{io}(u, w_o) \, E_{po}(u, w_o) e^{-\frac{\alpha_s}{4 v_s}(w - w_o)}.$$

Changing the variables and using $z - v_s t = u = z_o - v_s t_o$:

$$(3.87) \qquad P_{so}(z, t)$$

$$= \frac{\Gamma_s}{2 v_s} \int_{-\infty}^{z} dz_o \, E_{io}(z_o, t - \frac{1}{v_s}(z - z_o)) \, E_{po}(z_o, t - \frac{1}{v_s}(z - z_o)) e^{-\frac{\mathcal{H}_s}{4}(z - z_o)}.$$

Similarly for E_{io} we get:

$$(3.88) \qquad E_{io}(z, t)$$

$$= -\frac{\Gamma_i}{2 c_i} \int_{-\infty}^{z} dz_o \, P_{so}(z_o, t + \frac{1}{c_i}(z - z_o)) \, E_{po}(z_o, t + \frac{1}{c_i}(z - z_o)) e^{+\frac{\mathcal{H}_i}{4}(z - z_o)}.$$

Physically, this says that the solution is a superposition of properly retarded sources originating from the coupling of the waves. We restrict ourselves to the case of a finite medium which has a boundary (without Fresnel reflection) at $z = 0$. The other boundary is not important if $L \to \infty$. Hence we replace the lower limits of integration of (3.87) and (3.88) by $z_o = 0$. We introduce noise sources by adding $B_o e^{-\frac{\alpha_s}{2} t}$ to (3.87) and $A_o e^{-\frac{\alpha_i}{2} t}$ to (3.88). Substituting (3.87) into (3.88) we then get:

$$(3.89) \qquad E_{io}(z, t) = A_o e^{-\frac{\alpha_i}{2} t} + B_o e^{-\frac{\alpha_s}{2} t} \; z$$

$$-\frac{\Gamma_i \Gamma_s}{4 c_i c_v} \int_0^{z} dz_1 \int_0^{z_1} dz_o \, E_{io}(z_1, t + \frac{1}{c_i}(z-z_1) - \frac{1}{v_s}(z-z_o)) \cdot$$

$$E_{po}(z_1, t + \frac{1}{c_i}(z-z_1) - \frac{1}{v_s}(z_1-z_o)) \, e^{+\frac{\mathcal{H}_i}{4}(z-z_1) - \frac{\mathcal{H}_s}{4}(z_1-z_o)} .$$

Kroll has solved this for the case $\frac{v}{c} \to 0$ and $\mathcal{H}_i \to 0$ by iteration[14]. His results indicate that for $z \gg \frac{t}{v_s}$, the growth factor is

$\exp \; 2\left(\sqrt{z \frac{t}{v_s}} \; \frac{1}{L_c}\right)$ instead of the usual $\exp\left(\frac{\pi}{L_c} \frac{t}{v_s} - \frac{\pi}{L_c} \frac{z}{2}\right)$

(see (3.58) and (3.64)). The growth factor can be measured by studying the intensity of stimulated Brillouin scattered light from long liquid cells using an unfocussed laser beam as a function of length of the cell.[50]

Chapter IV. Experimental Observations of the Stimulated Brillouin Effect

Experimental detection of the stimulated Brillouin effect can be accomplished by monitoring either the generated sound wave or idler wave. Since the hypersonic waves expected to be generated by the process are highly attenuated at room temperature, their detection would only be feasible near liquid Helium temperatures. Even then, when non-piezoelectric materials are used as the generating medium, detecting transducers for the hypersonic frequency range involves difficult bonding techniques and accompanying impedance-matching problems[24]. Also, detection of the microwave signal thereby generated is not trivial. Nevertheless, one should note that materials with very large Brillouin shifts may yield significant amounts of sub-millimeter radiation.[25]

The much simpler alternative is to detect the back-scattered light wave. Its frequency shift, which is the signature of the scattering process, is very small, necessitating the use of a high resolution spectroscopic technique or an optical heterodyne technique to measure it. (The pulsed laser is an intrinsically narrow line source, with theoretically a width of $\frac{1}{2\pi t} \simeq 10$ mc, where $t \simeq 20$ nsec is the pulse duration, so that very small shifts can be measured.) The latter technique is especially useful in examining near-forward scattering, where the frequency shift to be measured is sufficiently low to use standard electronic techniques[26]. But frequency shifts for large angle scattering are typically $\sim \frac{v_s}{c} \nu_p$ which is ~ 1 cm^{-1} for solids and ~ 0.1 cm^{-1} for liquids, which is large enough to make heterodyne techniques difficult

and spectroscopic ones easy, by the same token. And of all the high-resolution spectroscopic instruments, the highest in resolution, the easiest to calibrate, the simplest to align, and the most compact to incorporate into the apparatus is the Fabry-Perot interferometer[27]. Indeed, for the solids, the shifts are so large that an unconventionally small spacer had to be used to prevent overlapping orders. This was achieved by using three precision $\frac{1}{16}$" ball bearings as spacers, giving us an interorder spacing of 3.15 cm^{-1}.

From the previous chapter, we see that there are two main categories of methods for generating stimulated Brillouin scattering. One involves a resonator and the other involves a travelling-wave oscillator. Since the threshold (2.21) seemed so low for the resonator case, this was the first method attempted experimentally. A sketch of the experimental arrangement is shown in fig. 8:

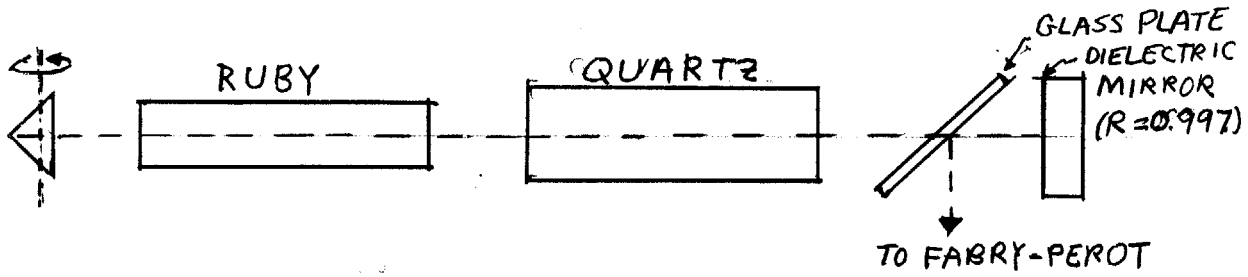

fig. 8: Experimental Arrangement for Observing Stimulated Brillouin Effect Inside the Cavity of a Laser

A Q-switched laser system[28], consisting of a 0.6 cm diameter and 8 cm long ruby at room temperature, placed inside a resonator system of a 99.7% dielectric mirror and a rotating prism, generated coherent light at 6943 Å with a power of ~3 Megawatts inside this cavity. Also placed inside this cavity was a rod of quartz 1.5 cm in diameter and

10 cm long and a thin piece of glass for coupling out a small amount of radiation to be examined spectroscopically using a Fabry-Perot interferometer. With the quartz piece removed, the output of the ruby spectroscopically consisted sometimes of a single mode and sometimes of a double mode with spacing 0.5 cm^{-1}. With the quartz placed inside the cavity, the backwards Brillouin-scattered radiation should be resonated by this same cavity since the frequency shift is very small, so that a new frequency component should have been observed with a (Stokes) shift of $\sim$1 cm^{-1} down from the laser component and almost as intense as the laser radiation if the stimulated Brillouin effect occurs intensely (3.47), so that we should have been able to detect it easily. However, the effect did not show up conclusively in a large number of trials. There are several explanations for this negative result. Firstly, γ was calculated from static values and may possibly be lower at hypersonic frequencies due to some relaxation phenomenon. Also, there is experimental evidence that γ may be smaller at higher frequencies, which will be discussed shortly. Since γ enters quadratically into the threshold and linearly into the rate of growth β (3.44), its effect will be large. Secondly, the threshold was calculated on the basis of 10% loss for 10 cm cavity length. The length actually used in the experiment was $\sim$100 cm, which lowers the threshold by a factor of 10. However, if the shift were so large that the Brillouin light fell on an absorptive portion of the ruby line, this could cause an increase in the threshold. Again there is some experimental evidence that this may be so, which we shall discuss later. Thirdly, and most importantly, the rate of growth (3.44) is independent of the threshold, as long as we far exceed it, and depends only on the square

root of intensity of the pump. For 10MW/cm^2 this means a gain of e^4 in 2 x 10^{-8} sec. The amount of normal Brillouin scattering in all directions for quartz is $\sim 10^{-7}$ x the incident power per scattering length in cm, so that for a solid angle of 10^{-6} the amplified signal will only be 10^{-11} of the laser intensity, which under our experimental conditions would have been difficult to detect. Another resonator type of experimental method was used by Dennis and Tannenwald[29] and Takuma and Jennings[30] in observations of the stimulated Brillouin effect. In the following we shall discuss the experiment of Takuma and Jennings.

Instead of using the laser cavity for resonating the idler, they used an auxiliary resonator external to the laser resonator and tilted at an angle θ, with respect to it. (cf. fig. 9)

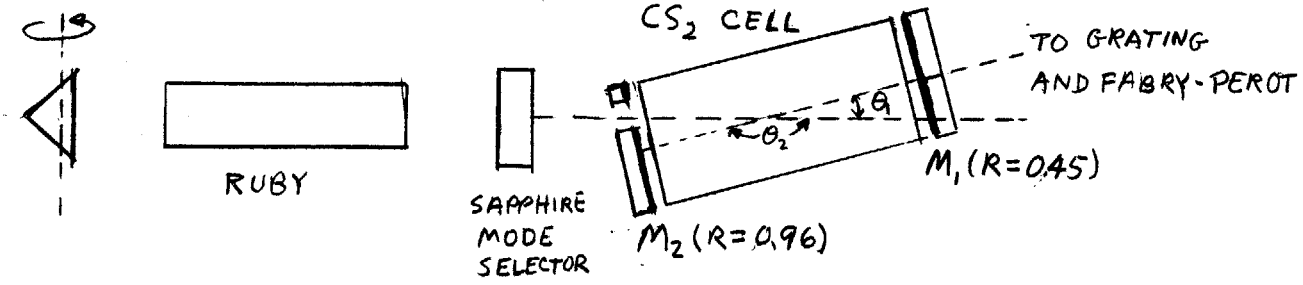

fig. 9: Experimental Arrangement used by Takuma and Jennings[30]

The substance they placed inside this off-axis resonator was CS_2. In any such a resonator configuration, it is clear that Brillouin scattering at both θ_1 and θ_2 can occur (see fig. 10) where $\theta_1 + \theta_2 = \pi$. Thus by comparing the thresholds for the onset of the θ_1 and θ_2 components, from (3. 39) we see that

$$(4.1) \qquad \frac{E_T^2(\theta_1)}{E_T^2(\theta_2)} = \frac{\gamma_2^2 \omega_2 \tau_2}{\gamma_1^2 \omega_1 \tau_1} = \frac{\gamma_2^2 \mu_1}{\gamma_1^2 \mu_2}$$

where $\omega_{1,2} \equiv \omega_s(\theta_{1,2})$ is given by (1.3) and $\gamma_{1,2} \equiv \gamma(\omega_{1,2})$ and $\tau_{1,2} \equiv \tau(\omega_{1,2})$ and $\mu \equiv \mathcal{H}_s \lambda_s$. Using the single relaxation theory of liquids, which we have verified to be valid in the Kmc region using the normal scattering technique (see Chap. V.):

$$(4.2) \qquad \frac{\mu_1}{\mu_2} = \frac{\omega_1}{1+\omega_1^2\tau_2^2} \quad \frac{1+\omega_2^2\tau^2}{\omega_2} = 46.5$$

where $\tau = 2.0 \times 10^{-9}$ sec is the relaxation time[31] and where $\omega_s(\theta_1) = 124$ mc and $\omega_s(\theta_2) = 5.8$ Kmc for $\theta_1 = 0.0433$ rad. which was used in their experiment. This would imply that $\frac{E_T^2(\theta_1)}{E_T^2(\theta_2)} = 46.5$ if γ were independent of frequency. In fact they observed experimentally that $\frac{E_T^2(\theta_1)}{E_T^2(\theta_2)} < 1$, so that this must mean:[32]

$$(4.3) \qquad \frac{\gamma(124 \text{ mc})}{\gamma(5800 \text{ mc})} > 6.8.$$

Hence in the case of quartz, perhaps γ is also smaller at hypersonic frequencies, supporting the first of the reasons listed above why we did not see the stimulated Brillouin effect in quartz using the resonator technique. However, the reasons why Takuma and Jennings saw it in CS_2 may simply be that they used larger power (50 Megawatts/cm^2) and that the threshold is lower and the rate of growth larger for CS_2 than for quartz. It goes without saying that their technique is very

useful if $\mu(\omega)$ is known since by varying θ_1 one can map out $\gamma(\omega_s)$.

Despite its higher threshold, the travelling-wave oscillator method was the means by which stimulated Brillouin scattering was first observed[33]. Because of the large field intensities in the focal region, much larger rates of growth can be obtained, in spite of the factor $2\sqrt{\frac{v_s}{c_i}}$ ((3.64) et seq.), than in the resonator case, once the threshold (3.56) is much exceeded, which, as seen in the previous chapter, is indeed the case at the reasonable unfocussed laser power levels of .1 0 Megawatt/cm^2, although practical considerations of beam divergence of the laser beam and aberrations in the focussing lens will make this figure higher. To get more power for this focal region experiment, we changed rubies; the new ruby had a diameter of 1.3 cm and length of 10 cm and generated a power of 50 Megawatts/cm^2 with an aperture of 1 cm and beam divergence of $\sim 3 \times 10^{-3}$ rad.[34] Furthermore, in contrast to the resonator techniques, all that is required experimentally is the simple procedure of focussing the laser beam into the material, obviating the alignment difficulties associated with the resonator. Collection of the backward-going idler light was accomplished by the same lens used to concentrate the laser beam (fig. 10). A glass plate placed in the path of the thus collimated[35] backward-scattered Brillouin light coupled a fraction of this light to the Fabry-Perot for analysis without deflecting away much of the forward-going laser beam. For the purpose of analysis $\sim$10% of this deflected laser beam was reflected by the mirror M_2 to be combined with the Brillouin scattered light for comparison in Fabry-Perot B. However, since the laser sometimes discharges in two modes of frequency separation 0.53 cm^{-1} [36], to be able to distinguish the Brillouin light from

fig. 10: Schematic of Experimental Apparatus Used to Observe Stimulated Brillouin Scattering in the Backward Direction. A travelling-wave oscillator is produced in the focal region.

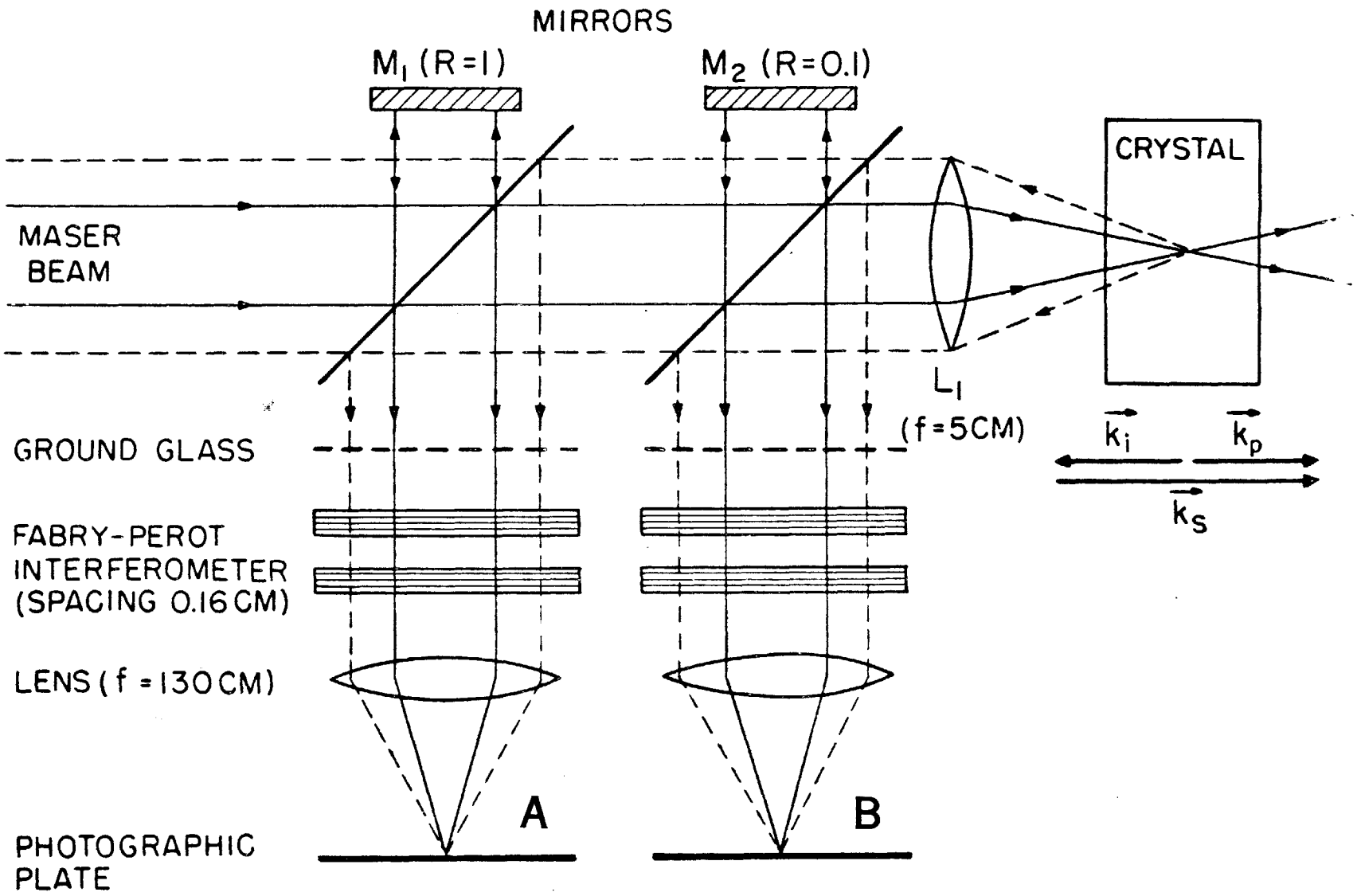
MIRRORS
M1 (R=1)
M2 (R=0.1)
CRYSTAL
MASER
BEAM
L1
(f=5CM)
ki
kp
ks
GROUND GLASS
FABRY-PEROT
INTERFEROMETER
(SPACING 0.16CM)
LENS (f=130CM)
A
B
PHOTOGRAPHIC
PLATE

fig. 11: Comparison of Fabry-Perot Interferograms of Laser and Stimulated Brillouin Effect. Both pairs (a) and (b) were taken simultaneously with experimental arrangement shown in fig. 10. Rings identified as laser radiation are labeled L; rings identified as stimulated Brillouin scattered light are labeled by B. In (a) the laser output consists of a single mode; in (b), a double mode. The laser was directed along the X-axis of the quartz and polarized along the Y-axis.

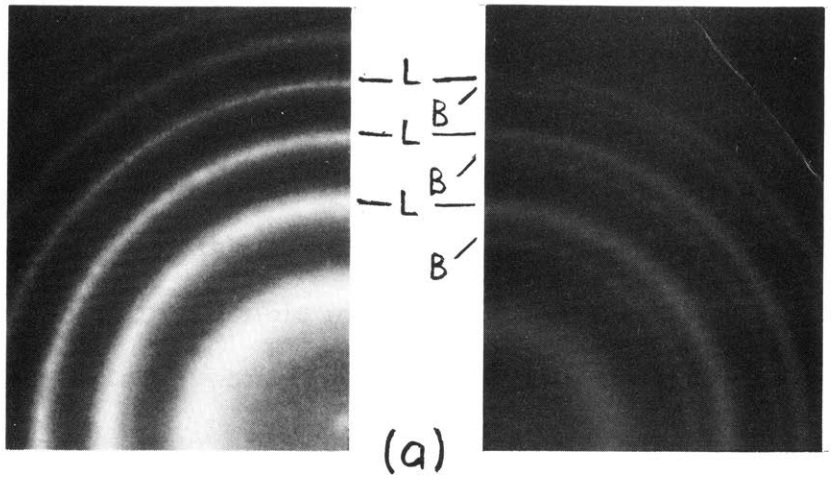

(a)

A B

(b)

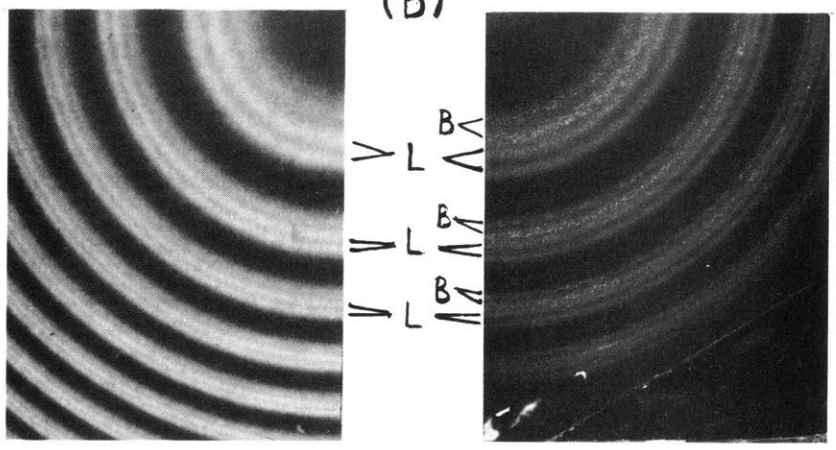

these modes another Fabry-Perot (labeled A in fig. 10) was introduced with an associated glass beam-splitter and a mirror M_1 of $\sim$100% reflectivity. The forward-going laser radiation can then be identified as those frequency components which are stronger in A than they are in B and the Brillouin components as those which are weaker in comparison[37].

Two such pairs of simultaneous shots at A and B are shown in fig. 11; pair (a) was taken when the laser going in a single mode, pair (b) when going in a double mode. The material used for these pictures was quartz at room temperature, with the laser beam entering it as an ordinary ray along the X-axis.[38] The rings labeled B are identified by the procedure described above as stimulated Brillouin components. Since the B pictures, taken using mirror M_2 of 10% to reduce the laser intensity in comparison with that of the Brillouin components, show the laser and the Brillouin components nearly equal in intensity, these must actually be $\sim$10 times weaker than the laser. That the effect observed is stimulated is clearly proved by the three following observations: (i) There is a threshold below which the rings labeled B disappear and above which they appear consistently and reproducibly; (ii) Only the Stokes component appears, which is clear from the fact that the Brillouin components (labeled B) are smaller in radius than the corresponding laser components (labeled L), whereas the normal effect at room temperature produces Stokes and anti-Stokes with equal intensity (see Chap. V); (iii) The intensity of the Brillouin components is $\sim 10^{-1}$ that of the laser, whereas in the normal effect we would expect less than 10^{-7} of the laser intensity. When the effect is generated even more strongly, the Brillouin rings

taken with Fabry-Perot B will appear more intense than the laser rings, as exemplified by fig. 12(a) and (b), but of course they cannot actually exceed the laser in intensity, as pictures taken with Fabry-Perot A showed, in which they were nearly equal in intensity. This means that the Manley-Rowe relations have been fulfilled and that there is an acoustic power of $\sim$1 Kilowatt in the focal region. Therefore, nearly all of the laser beam has been reflected as a Brillouin-shifted wave by the quartz, as if there were a dielectric mirror moving at velocity v_s in the focal region. Indeed, under such conditions, when attempts were made to analyze the forward going laser radiation which had passed through the crystal, its intensity was found to be much reduced.

To verify that we were actually generating sound waves and not some other excitation of the individual molecules or of the lattice, we need to measure the shifts and compare with those calculated from (1. 3) using ultrasonic values of the sound velocity. This is done in the table accompanying fig. 12, from which it is clear that we are exciting the longitudinal sound waves, as expected[39]. Stimulated Brillouin scattering was observed not only in the backward direction, but also at $\theta = \pi/2$, as shown in fig. 12(c), but much more weakly, with the idler $\sim 10^{-3}$ the intensity of the laser, and with the sound wave thus generated no longer purely longitudinal. The reason why the backward direction predominates in intensity of scattering over all other directions is a geometrical one, namely, that the "active" length L_a, which enters in the exponent in the growth factor, is much longer along the axis of the focal region than transverse to it. Figure 12(d) shows evidence for stimulated Brillouin scattering in sapphire in the backward direction, but it has a higher threshold than quartz and the

fig. 12: Stimulated Brillouin Spectra of Solids Taken with Fabry-Perot B. These interferograms have an interorder spacing of 3.15 cm^{-1}. They yield frequency shifts which compared with values calculated from ultrasonic data and from hypersonic data obtained by normal Brillouin scattering as follows:

	crystal	scattering angle	laser incident along	idler scattered along	laser polarized along	observed shift (cm^{-1})	shift calculated from ultrasonics* (cm^{-1})	shift calculated from hypersonics** (cm^{-1})
(a)	Quartz	180^{o}	Z	-Z	X	0.99	0.97^{u}	0.96
(b)	Quartz	180^{o}	X	-X	Z	0.85	0.88^{v}	0.90
(c)	Quartz	90^{o}	Z	$\pm$Y	X	0.73	0.70 ± 0.05^{w}	0.75 ± 0.03
(d)	Sapphire	180^{o}	Z	-Z	X	2.07	2.01^{u}	1.32

*Calculated from elastic constants given by H. B. Huntington, Solid State Phys., 1, 213 (1958).

$^{u}\ \rho v_L^2 = c_{33}$

$^{v}\ \rho v_L^2 = c_{11}$

$^{w}\ \rho v_L^2 = \frac{1}{4}\ (c_{11} + c_{33} + 4c_{44} + 2c_{13} \pm 4c_{14})$

**Calculated from data given by R. S. Krishnan, Proc. Indian Acad. Sci., A41, 91 (1955).

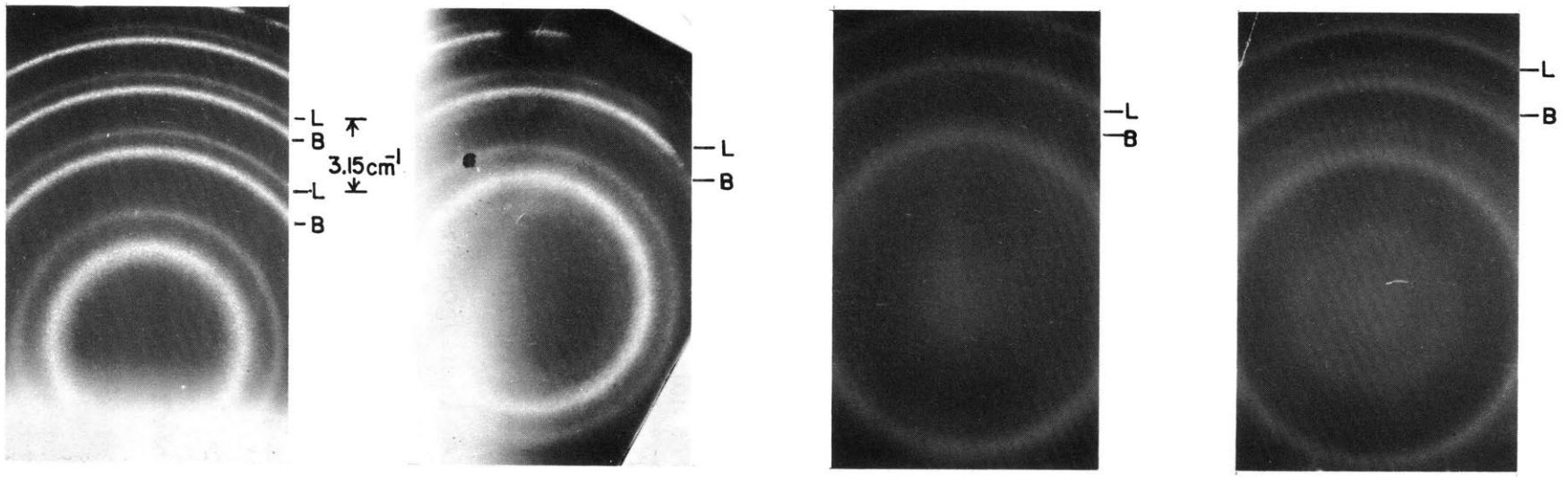

(a) (b) (c) (d)

effect does not occur very strongly at our power levels. That the stimulated Brillouin effect has been observed in sapphire, which is a nonpiezoelectric material and in quartz along its Z-axis (fig. 12(a)), where the piezoelectric coefficient vanishes due to symmetry[40], proves that electrostriction, and not piezoelectricity, is the phenomenon responsible for the coupling of the three waves involved in the stimulated scattering process. The shifts were measured using the method of fractional orders[41], giving accuracies of 3% for fig. 12 (a), (b) and (d) and 10% for fig. 12(c). Our data is also consistent with that obtained by Krishnan using normal Brillouin scattering[42].

The materials were badly damaged and produced accompanying ionization near the focal region during these experiments. In quartz the damage occurred reproducibly with an X-shaped cross-section when the laser was directed along the X-axis of the quartz, much as if two cleavage planes emanated from the focal region with an intersection angle of 53^{o} (which is unexpected since quartz does not cleave naturally). It is not clear that the stimulated Brillouin effect is the primary cause of this effect, since it occurred even when the Brillouin components were absent in the interferograms. Also, substances which did not exhibit stimulated Brillouin scattering, such as lithium fluoride, were badly damaged. Nevertheless, since the sound wave, once produced, will generate pressures of 10^{3} atmospheres and will raise the temperature 10^{4} ^{o}C due to its large attenuation, large local stresses will build up, cracking the crystal. Even without the sound wave (i. e. below the threshold of the stimulated Brillouin effect) one might conjecture that electrostrictive pressure $P_{e\ell} = \gamma \frac{E_{po}^{2}}{8\pi}$ alone may break the crystal, which perhaps may explain the above observations. However, if breakage is actually due to electrostriction alone,

we can compare its onset with that of stimulated Brillouin scattering, as follows. For from (3.56):

$$(4.4) \qquad \frac{E_T^2}{8\pi} = \frac{2B\epsilon_o}{\gamma^2} \frac{1}{k_i k_s} \frac{1}{4\ell_s^2}$$

assuming $\ell_s \ll \ell_i$. If b is the breakage coefficient defined by $P_B = bB$ where B is the Bulk modulus and P_B is the tensile strength of the material,

$$(4.5) \qquad \frac{E_B^2}{8\pi} = \frac{1}{\gamma} P_B = \frac{bB}{\gamma}$$

is then the critical field for fracture. Then

$$(4.6) \qquad \left(\frac{E_T}{E_B}\right)^2 = \frac{\epsilon_o}{b\gamma} \frac{1}{(4\pi)^2} \left(\frac{\lambda_p}{\ell_s}\right)^2 .$$

For quartz, $b \simeq 10^{-3}$, and hence we estimate $E_B^2 \cong 10^2 E_T^2$, so that this explanation of the occurrence damage is probably also invalid except in the cases where $\ell_s \simeq \lambda_p$ or when b is smaller. The correct explanation probably involves plasma formation in the focal region[43].

The stimulated Brillouin effect has also been seen to occur in various glasses by Atwood et al.[44], in association with damage track production. They introduced an ingenious experimental technique which greatly simplified the identification of forward-going laser radiation and backward-going stimulated Brillouin radiation, eliminating the introduction of Fabry-Perot A in fig. 10 for this purpose. Their technique is sketched in fig. 13.

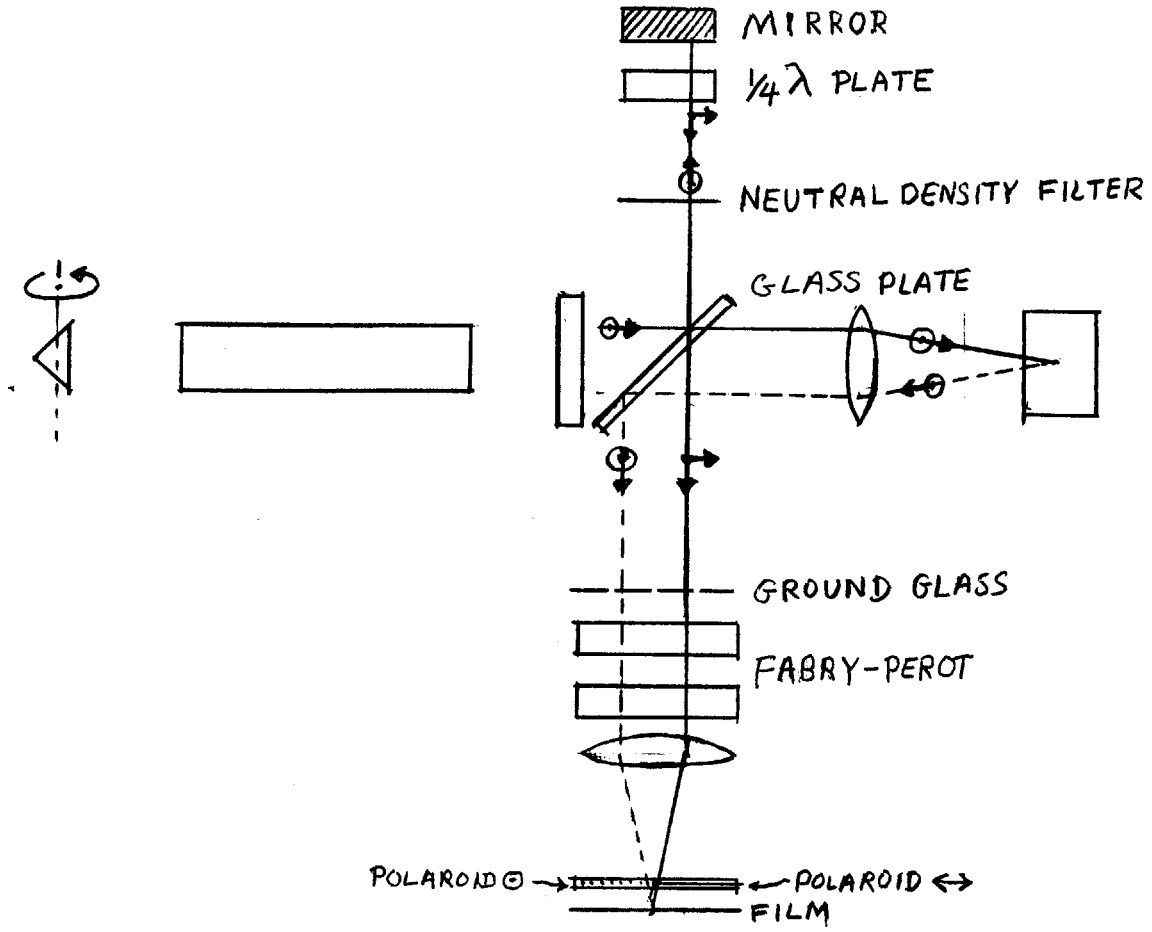

fig. 13: Simplified Apparatus for Detection of Stimulated Brillouin Scattering

The use of the quarter-wave plate as shown in fig. 13 makes mutually perpendicular the polarizations of forward-going and backward-going radiation reaching the Fabry-Perot.[45] Hence by placing immediately in front of the film a filter composed of two perpendicularly oriented polaroids placed side by side, one can immediately separate the frequency components present due to laser from those due to stimulated Brillouin scattering. Using this technique, De Martini[46] has seen the stimulated Brillouin effect in rutile, Rochelle salt and triglycine sulfate.

The stimulated Brillouin effect has also been seen in many liquids using the travelling-wave oscillator method by Brewer and Rieckhoff[47] and Garmire and Townes[48]. Liquids generally have lower thresholds than solids because they are much more compressible (cf. (3.56) and (3.64)), as evidenced by their smaller velocities of sound. Indeed, Brillouin shifts are ~ 10 times smaller in the liquids than in the solids. Because of this, a novel feature appears in the observation of the effect in the liquids which was absent in the case of the solids. As is apparent from examination of fig. 14 (we shall describe the work of Garmire and Townes), if the shift is so small that the Brillouin component lies within the amplification bandwidth of the ruby, the back-scattered Brillouin light will be amplified upon re-entry into the ruby and reflected by the prism back into the liquid cell, after further amplification, so that if it has been sufficiently intensified, it will generate its own Brillouin component. This iterative process can generate multiple orders of Brillouin shifts, as shown in fig. 15. That amplification has actually occurred is proved experimentally by the fact that the pictures of fig. 15, which were taken at site A of fig. 14, are orders of magnitude more intense than those taken at site B. Only Stokes shifts seem to be present in fig. 15(e) and (f), where the inner rings get progressively weaker, indicating that the outermost ring is from the original laser pulse. This is the situation when the laser excitation is weak and amplification of the Brillouin components is not strong. That the multiple shifts do not occur inside the liquid itself due to intrinsic higher order Brillouin scatterings, in which the first back-scattering wave undergoes stimulated Brillouin scattering to produce a forward-going doubly shifted (second-order Stokes) wave and a backward-going

fig. 14: Experimental Arrangement used by Garmire and Townes[48] for Observation of Stimulated Brillouin Effect in Liquids

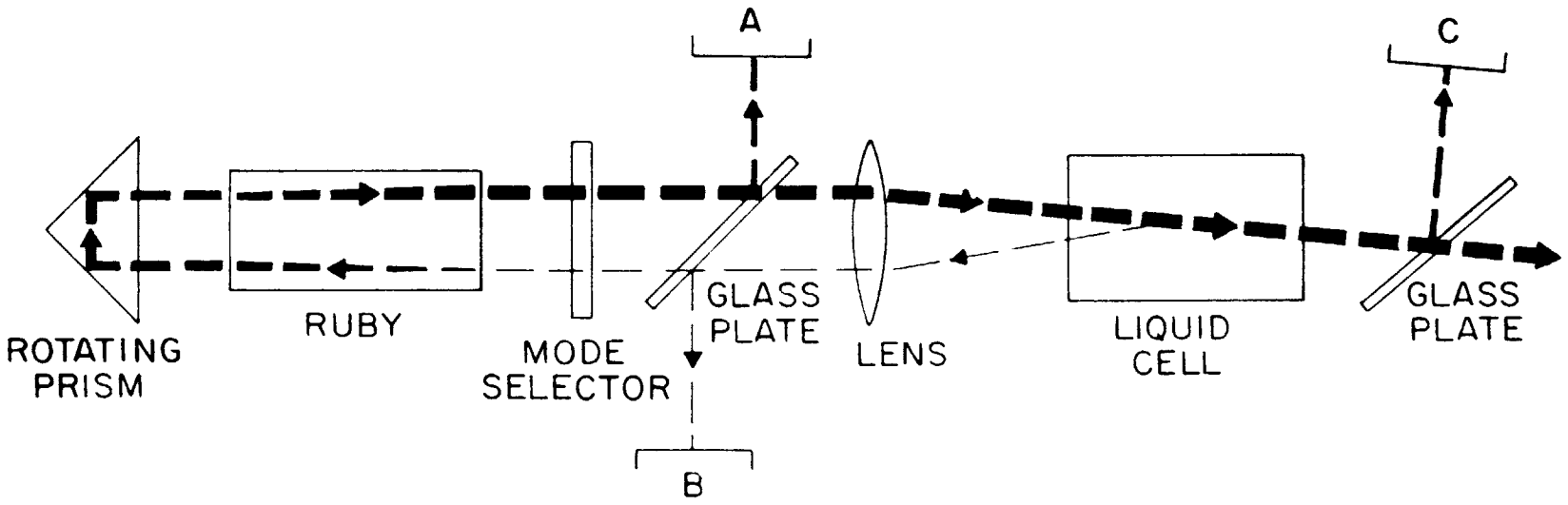
A
C
ROTATING
PRISM
RUBY
MODE
SELECTOR
GLASS
PLATE
LENS
LIQUID
CELL
GLASS
PLATE
B

fig. 15: Stimulated Brillouin Spectra of Liquids. These were taken with Fabry-Perot at position B shown in fig. 14. The interorder spacing is 0.701 cm^{-1}. Rings corresponding to Brillouin scatterings are labeled B_n; n = order of iterative generation. They yielded hypersonic velocities which compared with ultrasonic values as follows:

	Liquid	Brillouin Shift (cm^{-1})	Calculated Hypersonic Velocity (m/sec)	Ultrasonic* Velocity (m/sec)
(a)	Maser without any liquid target			
(b)	CCl_4	0.141	1007 ± 7	1040 ± 27
(c)	Methanol	0.139	1100 ± 11	
(d)	Acetone	0.153	1174 ± 7	1190 ± 40
(e)	CS_2	0.192_5	1242 ± 6	1265 ± 22
(f)	H_2O	0.188_5	1471 ± 8	1509 ± 25
(g)	Aniline	0.257_5	1699 ± 8	

*Acoustic velocities given by K. F. Herzfeld and T. A. Litovitz, Absorption and Dispersion of Ultrasonic Waves, New York, Academic Press (1959), p. 362.

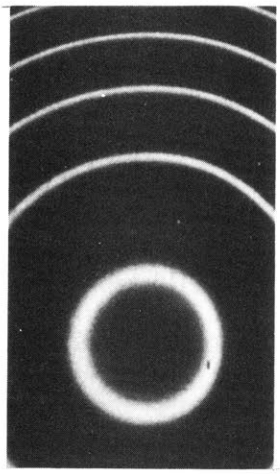
0.701 cm^{-1}

(a)

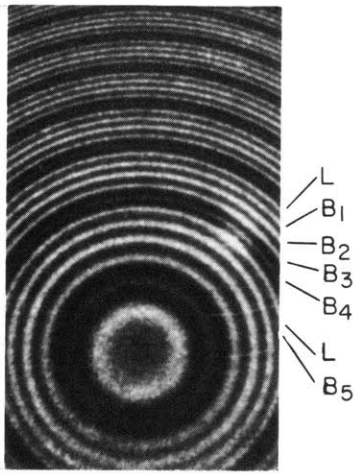
L
B1
B2
B3
B4
L
B5

(b)

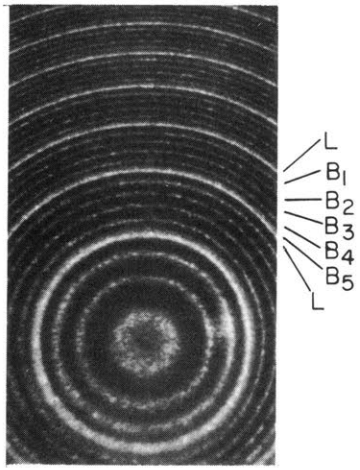
L
B1
B2
B3
B4
B5
L

(c)

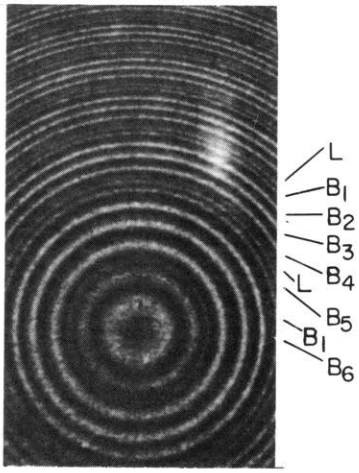
L
B1
B2
B3
B4
L
B5
B1
B6

(d)

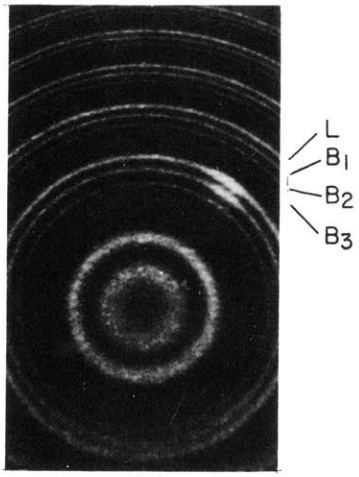
L
B1
B2
B3

(e)

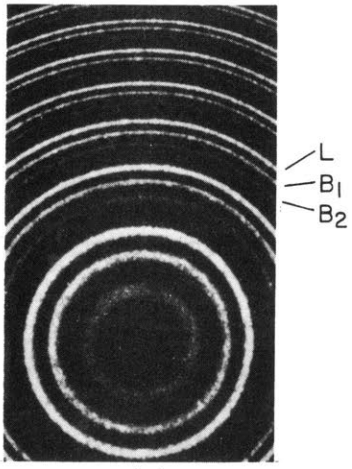
L
B1
B2

(f)

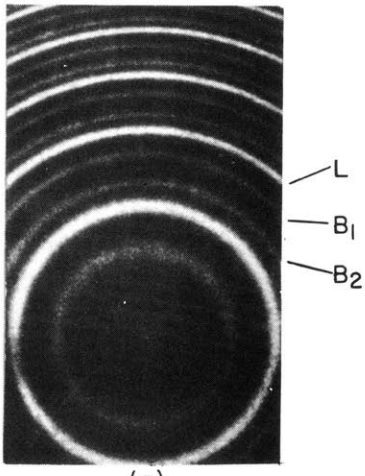
L
B1
B2

(g)

sound wave, and further iterations of this process, is shown by the fact that alternate Stokes orders are not absent, which such intrinsic scatterings in the liquid would imply. Under higher laser excitations this simple monotonic intensity profile of shifts became more complicated, as shown in fig. 15(b) and (d) and there appears to be anti-Stokes components if one identifies the most intense component (e. g. B_3 in fig. 15(b)) as the laser. However, the correct explanation of this intensity profile is that first few orders of Brillouin shifts are generated so strongly and amplified so much that they become more intense than the initial laser pulse itself. Of course, when the order of the shift becomes so large that the Brillouin radiation is near the edge of the amplification bandwidth of the ruby, they will become more and more attenuated. Although the process of intrinsic scatterings described above might give the first order anti-Stokes (since a backward-going sound wave is produced in the second order), it cannot give a backward-going second order anti-Stokes, which would be there according to 15(b) and (d). Hence the extrinsic iteration process, which involves amplication by the ruby, seems to dominate over any intrinsic iteration process.

This conclusion was verified experimentally by three observations by Brewer[49]. Firstly, a simple comparison of the output spectrum of the laser (properly temperature-controlled to avoid frequency drifts on successive shots) with and without a liquid target showed that, independent of the intensity profile of Brillouin components, the highest frequency component was indeed that of the laser and all the Brillouin shifts were to the Stokes side. Secondly, when an optical isolator (analyzer and 1/4 λ plate in series) was placed between the

laser and the liquid target, so that backward-going radiation could not have re-entered the laser[45], only one Brillouin Stokes component was seen, just as in the solids. Thirdly, by removing the liquid target far away from the laser, each step involved in the extrinsic iteration process could be time resolved, and successive pulses in time were identified as successively higher order Stokes shifts. By varying the distance of laser to target it may be possible to measure hypersonic phonon lifetimes[49]. In more recent developments, Brewer[50] has observed stimulated Brillouin scattering using an unfocussed laser beam, allowing experimental tests for Kroll's transcients theory (see previous chapter); he has also observed acoustical second harmonic generation, by using the second harmonic of the laser as a probe and observing back-scattering of this probe.

The largest number of shifts due to the extrinsic iteration process seen in the liquids is $\sim$10. This indicates the amplification bandwidth of the laser to be $\sim$1 cm^{-1}. Thus shifts in the solid are generally too large to be amplified and thereby undergo extrinsic iterative generation. Also, experiments inside the laser cavity using solids, as described earlier, may not be feasibly due to the possible quenching of the Brillouin shifted wave. However, Tannenwald[51] has recently observed multiple Brillouin scattering in solids. If the iterative process is extrinsic, this implies a broader amplification bandwidth for the ruby and excitation system used in his experiments, than those used previously.

Chapter V: Normal Brillouin Scattering

In the previous chapters, we have dealt with stimulated Brillouin scattering, which could only be observed with the advent of extremely powerful laser beams. The resulting generation of intense hypersonic waves will provide an important tool for physical acoustics, especially in investigations of acoustical nonlinearities. Nevertheless, some useful information may still be obtained from physical acoustics in the linear region, i. e. from studies of absorption and dispersion of hypersonic waves. For such studies it is not necessary to use the material-shattering intensities generated by the stimulated Brillouin effect. However, generation and detection of hypersonic waves by extension of conventional ultrasonic methods is very difficult. Fortunately, as was realized many years ago, these waves are generated, although weakly, simply by thermal excitation; examination of light scattered off these waves will yield their velocities and absorption[52]. This process of light scattering, which we shall call normal or thermal Brillouin scattering, to distinguish it from the previously discussed stimulated process, was observed previously using an incoherent Hg line source. But because of the large width of the exciting line, the Brillouin components of liquids were barely resolved from the central component and their intrinsic widths were undetectable.

With the advent of the continuous laser, it was realized by various workers[53] that it was ideally suited as a source for normal Brillouin scattering. Because of its intensity, exposure times are reduced from hours to seconds; because of its extremely narrow line-

width, the Brillouin components are resolved much better[54], and, for the first time, their widths are measurable[55]; because of its coherence, optical heterodyning with the scattered light is possible[56]; because of its almost perfect collimation, the scattering angle, even when it is small, can be precisely defined and varied[57]; because of its complete polarization, precise measurements of the depolarization of the Brillouin components can be made[58].

To calculate how much scattering we expect from thermally excited sound waves, let us first employ the energy-considerations method used in chapter II. There is present in the scattering medium the well-known black body distribution of sonic power; since $k\,T \gg \hbar\,\omega_s$, the energy per normal mode is by equipartition:

$$\frac{P_{so}^{2}}{2B}\,V \cong k\,T \tag{5.1}$$

where V is the volume of the target scattering medium, which for simplicity we assume to have the shape of a rectangular parallelepiped of dimensions d x d x ℓ (see fig. 16) oriented so that the scattered radiation is emitted along its long axis.

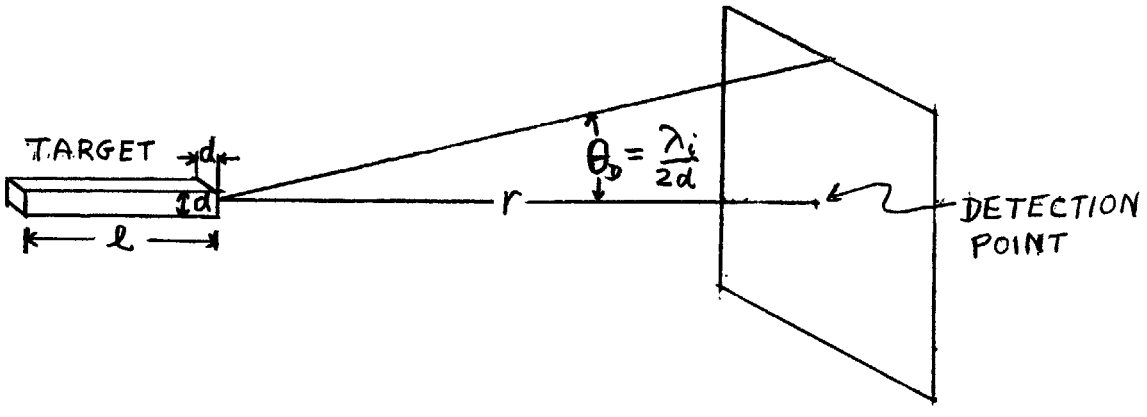

fig. 16: Normal Brillouin Scattering Diffracting from Rectangular Parallelepiped Target

The thermal sound waves will modulate the incident laser beam to generate an idler or scattered light wave with a power per unit volume of:

$$(5.2) \qquad \frac{d u_i}{d t}_{gain} = \frac{\gamma \omega_i}{16\pi B} P_{so} E_{po} E_{io}$$

which we calculated in chapter II (2.17b). However, in the present case $\omega_i = \omega_p \pm \omega_s$, $\vec{k}_i = \vec{k}_p \pm \vec{k}_s$; i.e. we must allow anti-Stokes as well as Stokes generation, since we no longer need concern ourselves with the converse process in which the sound wave is amplified, as was necessary in parametric generation. Since we are not interested in transient effects, in the steady-state the generated power in the idler will be radiated:

$$(5.3) \qquad \frac{d u_i}{d t}_{gain} \cdot V = \frac{c}{8\pi} E_{io}^2 A$$

where $A = d^2$. Hence the scattered amplitude is:

$$(5.4) \qquad E_{io} = \frac{\gamma \omega_i}{2Bc} P_{so} E_{po} \ell$$

and the intensity is:

$$(5.5) \qquad I_i = \frac{c}{8\pi} E_{io}^2 = \frac{\gamma^2 \omega_i^2}{32\pi B^2 c} P_{so}^2 E_{po}^2 \ell^2 .$$

To convert this into a formula for scattering cross-section, let us remove the detection apparatus a distance $r \gg \ell$ far away from the target. Let I(r) be the intensity which will be received at r. Diffraction and energy conservation imply (see fig. 16):

$$(5.6) \qquad I(r)\left(\frac{\lambda_i}{d}\right)^2 r^2 = I_i\, d^2 .$$

Hence

$$(5.7) \qquad r^2\, I(r) = \frac{\omega_i^4}{c^4}\ \frac{1}{16\pi^2}\left(\frac{\gamma P_{so}}{B}\right)^2 V^2\, I_o$$

$$= \frac{\omega_i^4}{c^4}\ \frac{1}{16\pi^2}\ (\Delta\epsilon)^2\, V^2\, I_o$$

where $\Delta\epsilon = \frac{\gamma P_{so}}{B}$ is the maximum change in dielectric constant due to the sound wave and where $I_o = \frac{c}{8\pi} E_{po}^2$ is the laser intensity. The scattering is highly directional for a given sound wave direction; the differential cross-section is zero unless the angle of observation is kinematically correct, in which case:

$$(5.8) \qquad d\sigma = r^2\, d\Omega \cdot \frac{I(r)}{I_o} = \frac{\pi^2}{\lambda_i^4}\ (\Delta\epsilon)^2\, V^2\, d\Omega$$

$$= \frac{2\pi^2}{\lambda_i^4}\ \frac{\gamma^2}{B}\ k\, T\, V\, d\Omega$$

where $d\Omega$ = solid angle of detection system and where $\lambda_i = \frac{2\pi c}{\omega_i}$. But <u>thermal</u> sound waves exist in <u>all</u> directions so that the total cross-section is:

$$(5.9) \qquad \sigma = 4\pi r^2\, \frac{I(r)}{I_o} = \frac{4\pi^3}{\lambda^4}\ (\Delta\epsilon)^2\, V^2 = \frac{8\pi^3}{\lambda_i^3}\ \frac{\gamma^2}{B}\, k\, T\, V.$$

Another quantity commonly used is the extinction coefficient, otherwise known as the total scattering coefficient[59]

$$(5.10) \qquad R = \frac{4\pi\, I(r)\, r^2}{(I_o A)\cdot \ell} = \frac{\sigma}{V} = \frac{8\pi^3}{\lambda_i^4}\,\frac{\gamma^2}{B}\,kT\,.$$

This quantity has the dimensions of cm^{-1} and tells us how much of the laser power is scattered per unit length of travel through the scattering medium. Both (5.9) and (5.10) are a factor 3 too large due to the neglect of polarization considerations, as we shall see shortly. The typical order of magnitude of R for liquids is $\sim 10^{-5}\ cm^{-1}$ and for solids $\sim 10^{-7}\ cm^{-1}$.

A more rigorous method of deriving these results starts from the wave equation (3.7). Because its source is oscillatory at the idler frequency, we proceed to solve it using temporal Fourier analysis:

$$(5.11) \qquad \vec{E}_i(\vec{r}, t) = \int_{-\infty}^{\infty} e^{i\omega_i t}\, \vec{E}_i(\vec{r}, \omega_i)\, d\omega_i\,.$$

The source term of the wave equation is ($\vec{P}$ = polarization):

$$(5.12) \qquad -\frac{1}{c_i^2}\ddot{\vec{P}} = -\frac{\gamma}{B}\int_{-\infty}^{\infty} \frac{\omega_i^2}{c^2}\, e^{i\omega_i t}\, \vec{g}(\vec{r}, \omega_i)\, d\omega_i$$

where

$$(5.13) \qquad \vec{g}(\vec{r}, \omega_i) = \frac{1}{2\pi}\int_{-\infty}^{\infty} e^{-i\omega_i t}\, P_s(\vec{r}, t)\, \vec{E}_p(\vec{r}, t)\, dt.$$

The wave equation then reduces to the Helmholtz equation, which has a Green's function[60] $G(r) = \frac{1}{4\pi r}\, e^{\pm i k_i r}$, so that the solution by superposition is:

$$(5.14) \qquad \vec{E}_i(\vec{r}, \omega_i) = \frac{1}{4\pi} \frac{\gamma}{B} \frac{\omega_i^2}{c^2} \int \vec{g}(\vec{r}', \omega_i) \frac{e^{i k_i (\vec{r} - \vec{r}')}}{|\vec{r} - \vec{r}'|} d^3 r'$$

where we have chosen (+) for the exponent since we detect outgoing waves. When we are far away from the target, i.e. $r \gg r'$, we use the approximation (see fig. 17):

$$(5.15) \qquad |\vec{r} - \vec{r}'| \cong r - \hat{k}_i \cdot \vec{r}'$$

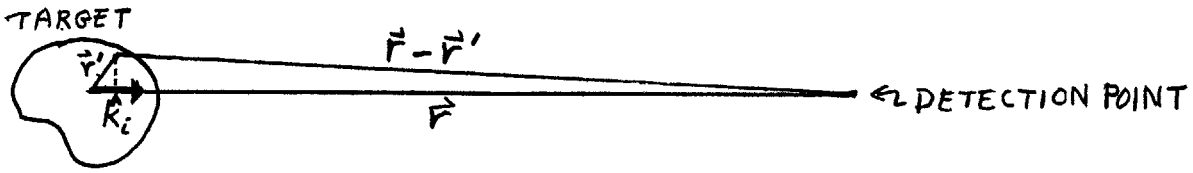

fig. 17: Radiation from an Extended Source. Cross-section is calculated with the approximation $r \gg r'$.

Hence (5.14) becomes:

$$(5.16) \qquad \vec{E}_i(\vec{r}, \omega_i) \cong \frac{\gamma}{B} \frac{\omega_i^2}{c^2} \frac{e^{i k_i r}}{4\pi r} \int \vec{g}(\vec{r}', \omega_i) e^{-i \vec{k}_i \cdot \vec{r}'} d^3 r'.$$

The latter integral is called the form factor. Using the spatial Fourier analysis of $P_s(\vec{r}, t)$ (i.e. plane wave decomposition) and remembering that $\vec{E}_p = \vec{E}_{po} \cos(\vec{k}_p \vec{r} - \omega_p t + \phi_p)$ this form factor reduces to $V \delta(\vec{k}_p \pm \vec{k}_s - \vec{k}_i)$ which states the kinematics of the process. If the sound wave has an infinite lifetime, (5.16) becomes:

$$(5.17) \qquad \vec{E}_i(\vec{r}, \omega_i) \cong \frac{\omega_i^2}{c^2} \frac{e^{i k_i r}}{4\pi r} \left(\frac{\gamma P_{so}}{B}\right) \frac{\vec{E}_{po}}{2} V.$$

From this we can calculate intensity of the scattered wave by squaring, as we did before in (5. 7) et seq. , and obtain the scattering cross-section:

$$(5.18) \qquad \sigma = \frac{8\pi^3}{3} \frac{\gamma^2}{B} \, k\,T\,V \frac{1}{\lambda_i^4} \, .$$

This is smaller than (5. 9) by a factor of $\frac{1}{3}$. The reason for the difference is that actually only the transverse component of the polarization source (5. 12) radiates, so that we replace $\vec{g}(\vec{r}', \omega_i)$ in (5. 16) by $\hat{k}_i \times (\hat{k}_i \times \vec{g}(\vec{r}', \omega_i))$. This introduces a factor of $\hat{E}_p \cdot \hat{E}_i = \sin \Psi$ into the scattering amplitude (5. 17). By geometry, $\hat{E}_p \cdot \hat{k}_i = \cos \Psi = \sin \theta \cos \phi$, where θ = scattering angle and ϕ = azimuthal angle of k_i relative to $\vec{E}_p$ [61]. Integrating $\sin^2 \Psi$ over solid angle gives us $\frac{4\pi}{3}$ in the total cross section (5. 18).

If the sound wave has a finite lifetime τ_s, then we expect that there should be a smear in its frequency $\delta\omega_s \sim \frac{1}{\tau_s}$. Nevertheless, when we observe scattering precisely at an angle θ, we are picking out a plane wave of an exact wave vector $\vec{k}_s$ (therefore of infinite spatial extent) for observation, as is clear from the Bragg picture of the scattering process. However, because of the uncertainty $\delta\omega_s$ of the frequency ω_s (and hence the velocity) of this wave due to its finite lifetime, we will observe a corresponding smear in the frequency of the scattering light wave equal to $\delta\omega_s$, as is clear from the Doppler picture of the scattering process. Another experimental procedure for measuring the lifetime of the sound wave is to use at infinitely sharp frequency filter centered at some frequency ω_i in the detection of the scattered light and to vary the scattering angle θ, and thereby measuring the smear $\delta k_s \sim \frac{v_s}{\tau}$ in k_s for a given

frequency ω_s[62]. However, it is easier to fix θ and observe the spectrum of the scattered light. These conclusions can also be drawn more rigorously using (5.13). For if $P_s = P_{so}\, e^{-t/2\tau} \exp i\,(\vec{k}_s \cdot \vec{r} - \omega_s t + \phi_s)$[63] then

$$\vec{g}(\vec{r}, \omega_i) = \frac{e^{i\left(\frac{\pi}{2} + \phi_s + \beta\right)}}{\left((\Delta\omega)^2 + \frac{\tau^{-2}}{4}\right)^{1/2}} e^{i\vec{k}_i \cdot \vec{r}}\, P_{so}\, E_{po} \tag{5.19}$$

where $\Delta\omega = \omega_i - \omega_p \pm \omega_s$. The spatial factor $e^{i\vec{k}_i \cdot \vec{r}}$ enters into the form factor in (5.16) to give as scattering only in the observation direction. The Lorentzian factor in $\vec{g}(\vec{r}, \omega_i)$ gives the spectral distribution of the scattered light (5.16), which we see has a full-width at half-height $\delta\nu_B = \frac{1}{2\pi\tau}$ where t = lifetime of the sound wave.[64] Similarly, if we put in $P_s = P_{so}\, e^{\frac{-\vec{q}\cdot\vec{r}}{2}} \cdot e^{i(\vec{k}_s \cdot \vec{r} - \omega_s t + \phi_s)}$, with $q = \frac{v_s}{\tau}$, we would obtain a Lorentzian smearing of the scattered light around the kinematically exact scattering angle θ, as one can see by evaluating the form factor. Which Lorentzian factor comes into the observations depends on whether we vary ω_i or θ.

Hence it is clear that we can measure not only the velocity of a sound wave involved in the scattering process by measuring the shift in frequency of the Brillouin components, but also its absorption or lifetime by measuring the widths of these components. It should be noted that nothing more than the kinematics of the scattering process is actually involved in deducing the velocity and absorption of this sound wave, so that these quantities are as reliably measured as in experiments where the sound wave is directly detected. The dynamics of the scattering process, which deals with the intensity

of the scattered radiation, is unessential as far as the properties of the sound wave is concerned. Nevertheless, dynamical considerations related to the cross-section (5.18) can yield useful information about some other properties of the scattering medium.

Firstly, if we know the temperature of the target, by measuring the total amount of light scattered relative to the power of the laser beam for a given length of target (i.e. by measuring R) we can calculate γ. Furthermore, by measuring the intensity of the Brillouin components as a function of angle of scattering (i.e. by measuring $\frac{d\sigma}{d\Omega}(\theta)$), we can obtain γ as a function of the frequency ω_s of the sound wave (cf. Takuma and Jennings experiment of chapter IV).

Secondly, at extremely low temperatures, the principle of detailed balancing will show that the ratio of intensities of anti-Stokes to Stokes Brillouin components is $e^{-\hbar\omega_s/kT}$, thus enabling us to determine the temperature of the target[65]. However, since most experiments are done around room temperature, the Stokes and the anti-Stokes are to an extremely good approximation equal in intensity, so that this method of temperature measurement is not feasible. Physically this arises because at high temperatures there are a very large number of phonons per mode (we can treat the sound wave classically) so that spontaneous emission is completely swamped by stimulated emission of the scattered light, and since there are as many thermal sound waves travelling in a direction toward the incident beam as there are away, Doppler shifts upward in the frequency of the scattered radiation are as intense as Doppler shifts downward.

Thirdly, there exist in the scattering medium entropy fluctuations[66] due to thermal excitation, as well as pressure fluctuations, since in general $\epsilon = \epsilon(P, s)$ and:

$$\Delta\epsilon = \left(\left(\frac{\partial \epsilon}{\partial P}\right)_s \Delta P + \left(\frac{\partial \epsilon}{\partial s}\right)_p \Delta s\right). \tag{5.20}$$

We have already considered the effect of the first term on light scattering. As we have seen, since the pressure fluctuations propagate according to the wave equation for sound, the scattered light will suffer a Doppler shift proportional to the velocity of propagation of the fluctuation. However, since entropy fluctuations propagate according according to the diffusion equation (since $\Delta s\big|_p = \rho C_p \frac{\Delta T\big|_p}{T}$):[67]

$$\nabla^2 s - D \frac{\partial s}{\partial t} = 0 \tag{5.21}$$

where $D = \frac{\rho C_p}{K}$, ρ = density, C_p = specific heat capacity at constant pressure, K = thermal conductivity of the scattering medium, the scattered light from these fluctuations will suffer no Doppler shift because the velocity of propagation of entropy waves is zero. More rigorously, plane wave solutions of (5.21) have the form $s = s_{so} e^{-t/2\tau} \cos(\vec{k}_s \cdot \vec{r})$ where $\tau = \frac{\rho C_p}{2k_s^2 K}$. Substituting this into the form factor (see (5.16)) gives the usual kinematical condition $\vec{k}_i = \vec{k}_p \pm \vec{k}_s$, whence $k_s = 2k_p \sin\frac{\theta}{2}$, but the spectral distribution is now a Lorentzian centered around $\omega_i = \omega_p$ with a width[68] $\delta\nu_R = \frac{1}{2\pi} \frac{k_s^2 K}{\rho C_p}$, as can be seen by evaluating (5.13). Hence

we expect there to be light scattered at an unshifted frequency (the Rayleigh component) in addition to the Brillouin components. The width of this Rayleigh component will be a measure of the thermal conductivity of the medium; measurements of width as a function of scattering angle gives $K(k_s)$.

Fourthly, if the dielectric constant is a function of the density of scattering medium alone and is independent of the temperature, then:

$$\Delta \epsilon = \left(\frac{\partial \epsilon}{\partial P}\right)_T \Delta P \tag{5.21}$$

is another way of expressing (5.20). In other words, the total amount of scattering, Brillouin plus Rayleigh, can be calculated starting with (5.21) (assuming $\overline{\Delta P \Delta s} = 0$). Hence if we do not measure the spectral characteristics of the scattered light (and since the frequencies of the various components differ very little from the frequency of the incident radiation), the total cross-section for Rayleigh and Brillouin components taken together, calculated using the same method as for (5.18) is:

$$\sigma_{R+B} = \frac{8\pi^3}{3} \frac{\gamma_T^2}{B_T} kT \, V \frac{1}{\lambda_p^4} \tag{5.22}$$

where $\gamma_T = \rho\left(\frac{\partial \epsilon}{\partial \rho}\right)_T$ and B_T are isothermal values, whereas:

$$\sigma_B = \frac{8\pi^3}{3} \frac{\gamma_s^2}{B_s} kT \, V \frac{1}{\lambda_i^4} \tag{5.18}$$

where $\gamma_s = \rho\left(\frac{\partial \epsilon}{\partial \rho}\right)_s$ and B_s are adiabatic values, is the

Brillouin components cross-section derived previously (5.18). Since $\frac{B_s}{B_T} = \frac{C_p}{C_V}$ [69] and since $\gamma_s = \gamma_T$ when $\left(\frac{\partial \epsilon}{\partial T}\right)_\rho = 0$: [70]

$$\frac{\sigma_B}{\sigma_{R+B}} = \frac{C_v}{C_p} \quad . \tag{5.23}$$

This enables us to measure the ratio of specific heats of the medium.

Fifthly, not only are there pressure and entropy fluctuations in the medium, but there are also anisotropy fluctuations. In solids, these give rise to light scattering off transverse sound waves; in liquids these give rise to a depolarized continuous background around the Rayleigh component.[71] Furthermore, there is scattering from the rotational states of the molecules, which, due to their interactions, usually is so smeared out that light scattered off them will add to the continuous background around the Rayleigh component [71]. This background, sometimes called the "Rayleigh wings", extends typically 10 cm^{-1}. Scattering off rotational states is an example of Raman scattering, which arises from the individual molecules rather than from collective notions of the media.

There are two main categories of experimental methods for detecting normal Brillouin scattering. The first involves optical heterodyning, the second, high-resolution spectroscopic techniques. Although the first method is by far the higher in resolution, it requires a very intense scattering source and careful alignment procedures in order to utilize the coherence of the laser beam[72]. So far this technique has been successfully used only for detection of critical scattering[73]. The second method involves use of either a

high-resolution grating spectrograph or a Fabry-Perot. Using these means various workers have detected normal Brillouin scattering using the He-Ne red laser as a source. Fabelinskii et al.[74] saw widths in carbon tetrachloride and benzene by photographing the Fabry-Perot rings; Benedek et al.[75] measured the velocities of sound of various solids and liquids using a grating spectrograph; Stoicheff et al.[76] used the pressure-scanning Fabry-Perot system to measure velocities in various liquids and obtained a width measurement of the Brillouin components of acetic acid. Although the Fabry-Perot is a much higher resolution instrument than the grating spectrograph, its light-gathering power is usually inferior unless proper experimental procedures are adopted. As we shall see later, this is because the Fabry-Perot selects light from a very small portion of the scattering path, whereas by orienting this path parallel to the slit of a grating instrument, light from the entire length of the path can be collected.

We describe the experimental arrangement for 90° scattering of Stoicheff et al. in fig. 18. The output of a He-Ne red laser whose power ranged from 4 milliwatts (and linewidth 660 Mc) to 20 milliwatts (and linewidth 810 Mc) was directed on a liquid sample placed inside a second cavity external to the laser. Light scattered at $\sim 90^{\circ}$ is collected by a f/10 lens and passed through a dielectrically coated (R = 0.90) Fabry-Perot interferometer with a 2.9992 cm spacer, which gave an inter-order spacing of 0.1667 cm^{-1}. The resulting ring pattern was either photographed using a 1.3 m focal length lens or, using a 36 cm focal lens, pressure-scanned through a pinhole centered on the pattern for photoelectric recording[77] (an RCA 6199 photomultiplier was used for this purpose). For scattering in the

fig. 18: The Experimental Arrangement Used by Chiao and Stoicheff for Observations of Normal Brillouin Scattering in Liquids at $\theta \cong 90^{o}$. Brewster angle windows are shown rotated through 90^{o}.

FIG. 1: CHIAO & STOICHEFF

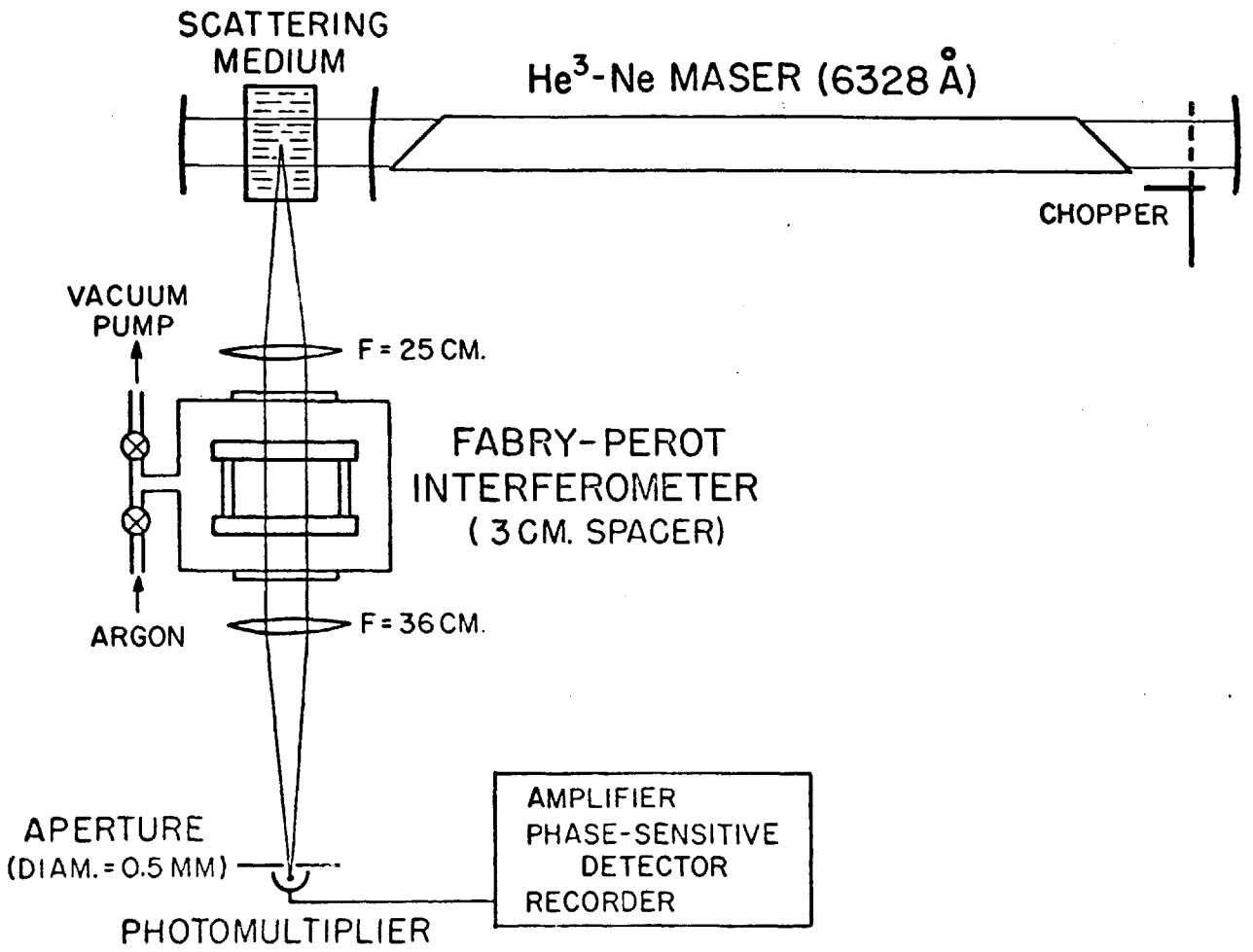

near-backward direction, the laser beam was focussed into the sample and the scattered light deflected into the interferometer with a mirror.

Examples of Brillouin spectra obtained by pressure-scanning of the interferometer are shown in fig. 19. The traces are noisy due to the poor quality of the photomultiplier. However, the Brillouin components were so intense that they were easily visible to the eye and were photographed in seconds. Unfortunately, since the exact angle at which the $\theta \cong 90^{o}$ data was obtained was unmeasured, the calculated velocities were unreliable to $\sim 5\%$, although the standard deviation of the frequency shifts was $\sim 0.1\%$. In the near backward direction the angle was measured crudely to $\pm 5^{o}$ by measuring the length of the image of the scattering path at the pinhole knowing the length of the cell and the magnification of the lens system. In any case, the velocity is not a very sensitive function of angle near the backward direction, and the following values were obtained at $\theta = 165^{o}$: in toluene, v_s (6.45 KMc) = 1380 m/sec; in CS_2, v_s (6.36 KMc) = 1253 m/sec; in water, v_s (6.15 KMc) = 1470 m/sec. The accuracy of these velocities is $\sim 0.5\%$.

The width of the Brillouin components in acetic acid is quite noticeable in fig. 19(b) in comparison with those of ether ethyl at 14.0 ^{o}C in fig. 19(a). However, the zero level, determined by blocking the scattered light, shown in fig. 19(b) should not be used as the base line for determining the widths of the components, since there is a sizeable amount of background scattering (the "Rayleigh wings") which forms the real base line. This implies that a larger free spectral range than that used in this experiment is needed for an accurate

fig. 19: Recorder Traces of Brillouin Spectra Taken with Experimental Arrangement as Shown in fig. 18.

a) Spectra of ethyl ether showing the effect of temperature on the Brillouin shift.

b) Observed spectrum of acetic acid and its analysis into the central (Rayleigh) and Brillouin components. (The large noise spikes in the central component are due to scattering by dust particles.)

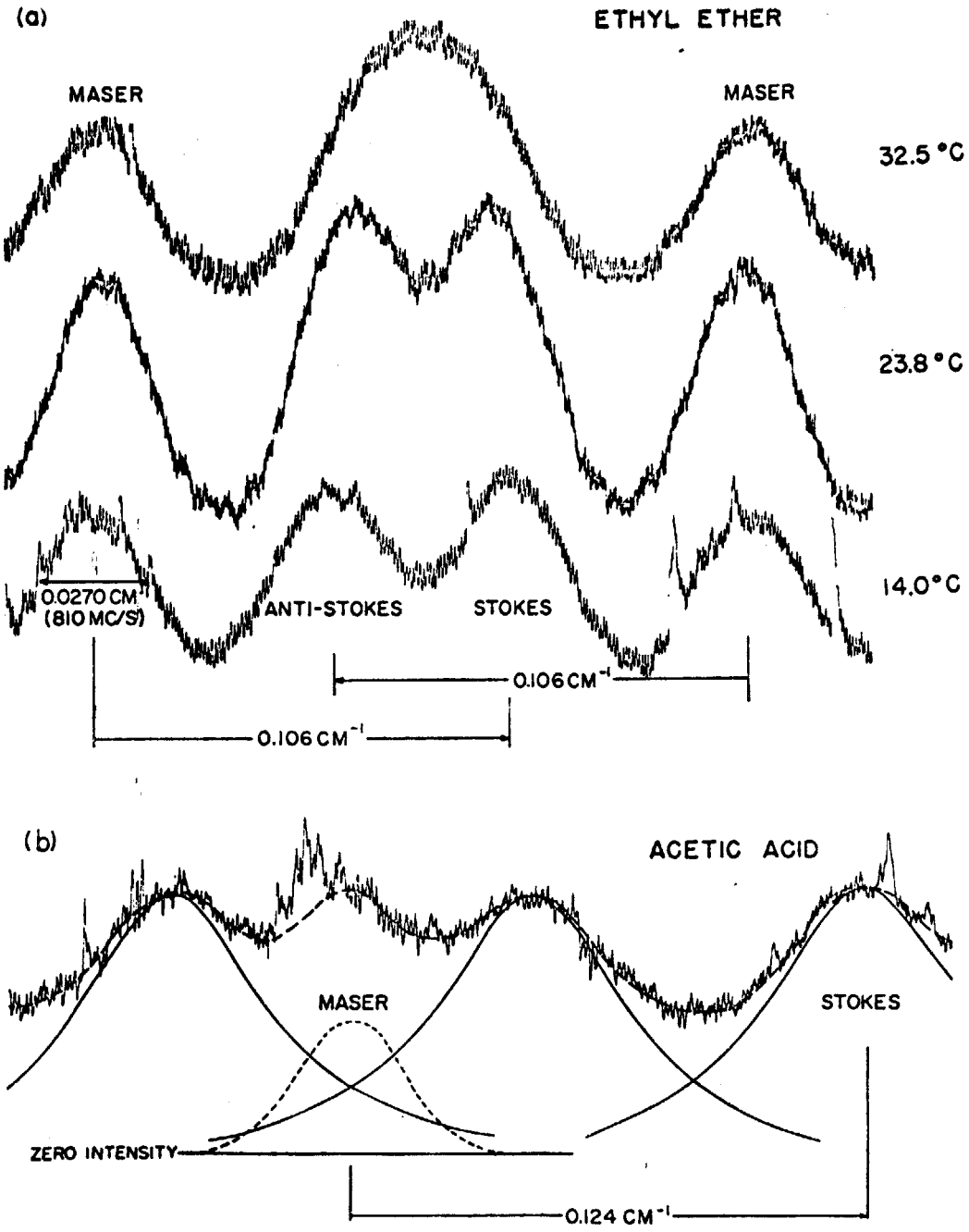

FIG. 2: CHIAO & STOICHEFF

determination of this base line. A later measurement[78] of the width of acetic acid at $\theta = 90^{o}$ showed it to be 190 Mc, so that the broadening evident in fig. 19(b) is $\sim$25% of the maser linewidth. It should be noted that the linewidth of the maser is not real, but is simply due to the fact that many modes of the laser, which were separated by $\sim$60 Mc, could not be resolved by the analyzing system.

As is apparent by inspection of the Brillouin formula (1.4), by varying the angle of scattering it is possible to vary the frequency of the sound wave whose velocity and absorption we are measuring. It is thus possible to do acoustical spectroscopy, i.e. investigate the absorption and velocity of hypersonic waves as a function of frequency. Thus we can extend the study of relaxation processes to hypersonic frequencies[78,79]. Also, if acoustical waves can interact resonantly with molecules, atoms, or nuclei or with other collective modes of the medium (e.g. through spin-phonon coupling[80] and magneto-acoustic coupling[81]), the properties of such resonances can give interesting spectroscopic information about the low-lying levels of the medium, especially when selection rules forbid coupling to microwaves.[78,79] One way of picturing this coupling is that if the acoustical branch of the ω vs k curve intersects a low-lying optical branch and if interaction occurs, the crossing levels are repelled from each other (see fig. 20(b) below), giving rise to anomalous dispersion of the acoustical phase velocity (which is the velocity which enters into the kinematics of Brillouin scattering) and absorption of the acoustical wave. More rigorously, let us start with the coupled wave equations[82]:

$$v^2 \nabla^2 P + a \dot{P} - \frac{\partial^2}{\partial t^2} P = c_1 v^2 \nabla^2 F \qquad (5.24)$$

$$(5.25) \qquad u^2 \nabla^2 F + b \dot{F} - \frac{\partial^2}{\partial t^2} F - \omega_o^2 F = u^2 c_2 \nabla^2 P .$$

(5.24) represents a sound wave; (5.25) represents an optical branch, which, when uncoupled with the sound wave and when b = 0, has the dispersion relation:

$$(5.26) \qquad \omega^2 = \omega_o^2 + u^2 k^2 .$$

This optical phonon has an effective mass $m^* = \frac{\hbar \omega_o}{u^2}$ near k = 0. These equations differ from the coupled equations (3.7) and (3.23) used for the stimulated Brillouin effect in that they are linear and therefore can be solved exactly using exponential solutions $P = P_o e^{i(k z - \omega t)}$ and $F = F_o e^{i(kz - \omega t)}$ where P_o and F_o are now constants. Substituting these solutions into the coupled equations, we get the dispersion relation:

$$(5.27) \qquad (- v^2 k^2 + i a \omega + \omega^2) (- u^2 k^2 + i b \omega + (\omega^2 - \omega_o^2)) = c_1 c_2 v^2 u^2 k^2$$

which is quartic in ω. If a = b = 0 we can solve (5.27):

$$(5.28) \qquad v(k)^2 = \left(\frac{\omega}{k}\right)^2 = \frac{1}{2} \left(\frac{\omega_o^2}{k^2} + u^2 + v^2 \right) \pm \frac{1}{2} \sqrt{\left(\frac{\omega_o^2}{k^2} + u^2 - v^2 \right)^2 + 4u^2 v^2 c_1 c_2} .$$

When $u^2 \ll v^2$ and $c_1 c_2$ is small:

$$(5.29) \qquad v(k) = v_{\pm} \pm \frac{1}{2} \frac{4u^2 v^2}{\frac{\omega_o^2}{k^2} - v^2} \frac{c_1 c_2}{v_{\pm}}$$

where $v_+ = \frac{\omega_o}{k}$ and $v_- = v$. Choosing the (-) branch (that of the sound wave), we see that $v_-(k)$ looks like fig. 20(a),

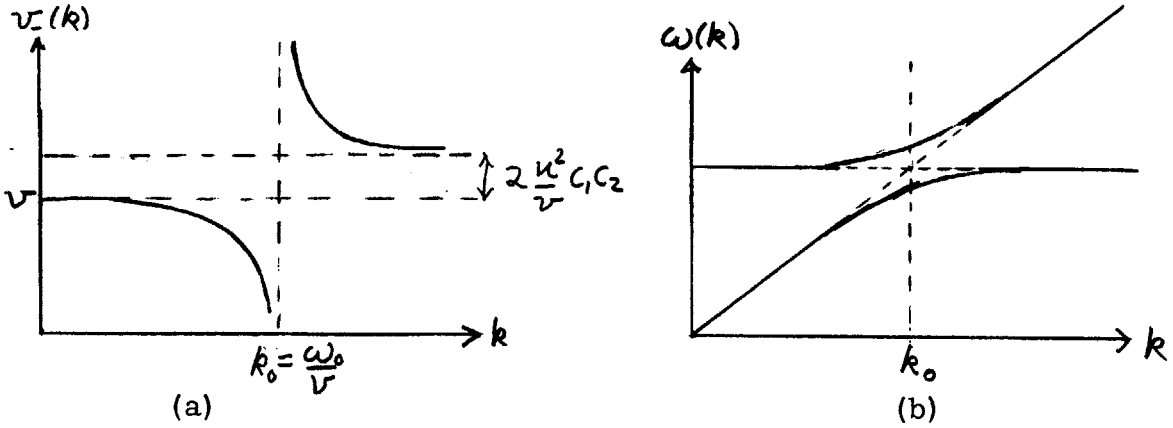

fig. 20: Dispersion of Lossless Sound Waves Near Resonance

which is analogous to the optical case. For the case when $a \neq 0$ and $b \neq 0$, let us solve (5.27) near $k = k_o = \frac{\omega_o}{v}$. We will let $k = k_o + q$, where $q \ll k_o$ is real, be the independent variable and $\omega = \omega_o + \Omega$, where $\Omega \ll \omega_o$ is complex, be the dependent variable. Keeping the largest terms, we get:

$$(5.30) \qquad \Omega = \frac{1}{2\omega_o} \left[\left(-2v^2 k_o q + i(a+b)\omega_o \right) \pm \sqrt{\left(-2v^2 k_o q + i(a-b)\omega_o \right)^2 + 4c_1 c_2 u^2 v^2 k_o^4} \right].$$

Expanding near k_o we get:

$$(5.31) \qquad \Omega = \Omega_{\pm} \pm \Delta\Omega$$

where $\Omega_+ = v\,q + \frac{ia}{2}$ and $\Omega_- = i\,b$ and where

(5.32) $$\text{Im}\ \Delta\Omega = -\frac{c_1 c_2 \left(\frac{u}{v}\right)^2}{4} \frac{(a-b)\,k_o^2}{\left(q^2 + \frac{(a-b)^2}{4}\frac{1}{v^2}\right)}$$

(5.33) $$\text{Re}\ \Delta\Omega = -\frac{c_1 c_2 \left(\frac{u}{v}\right)^2}{4} \frac{2q\,v\,k_o^2}{q^2 + \frac{(a-b)^2}{4}\frac{1}{v^2}}$$

which imply a Lorentzian shape to the resonance. The maximum absorption of the sound wave above background, which occurs at $k = k_o$, and the minimum dip in velocity, which occurs at $k = k_o - \frac{(a-b)}{2}\frac{1}{v}$, are[83]:

(5.34) $$\alpha_{max} = -c_1 c_2 \left(\frac{u}{v}\right)^2 \frac{2\omega_o^2}{a-b}$$

(5.35) $$\Delta v_{min} = +c_1 c_2 \left(\frac{u}{v}\right)^2 \frac{2\omega_o\,v}{a-b}$$

(5.36) $$\frac{\Delta v_{min}}{v} = \frac{1}{\omega_o}\alpha_{max}$$

and the width of the resonance is $\delta\nu = \frac{|a-b|}{v}$. Notice that α_{max} may be negative if $a > b$, so that there is a <u>decrease</u> in the sound wave attenuation. This arises physically from the transfer of energy from the optical mode to the acoustical mode when the former is less lossy.

The almost perfect collimation of the laser beam makes it very easy experimentally to study normal Brillouin scattering as a

function of scattering angle. In fig. 21, we show the experimental arrangement used by Chiao and Fleury[78]. The scattering angle θ was varied by a combination of rotation of the adjustable mirror and translation along the precision optical rail in such a way that the reflected laser beam passed through the center of the cylindrical cell. The mirror was mounted on a spectroscopic table with a vernier angular scale for measuring θ. With a proper centering of the lens which collects the scattered light, $\theta = 0^{o}$ was established as the direction normal to the Fabry-Perot plates. With similar centering alignments to prevent deflection of the laser beam, a lens with focal length f = 10 cm[84] was used to focus the incident beam into the cylindrical cell, and the scattered beam was collected and analyzed by a pressure-scanning Fabry-Perot system similar to that shown in fig. 18. The use of a high-quality photomultiplier (RCA 7326) eliminated the lock-in detection system used previously. Its anode output, loaded with a $\sim$ 1 Megohm resistor and d. c. biased to eliminate dark current, was put directly into a voltage recorder. Typically a couple of millivolts of peak signal from the Brillouin components was obtained.

Examples of Brillouin spectra thus obtained are shown in fig. 22, where liquid toluene was the scattering medium. In (a) the scattering angle was $70.0^{o} \pm 0.3^{o}$; the temperature was $22.8\ ^{o}C$. In (b) the scattering angle was $30.0^{o} \pm 0.3^{o}$; the temperature was $22.4\ ^{o}C$. Again, the linewidth of the maser is not real, since the Fabry-Perot (interorder spacing 15 Kmc and finesse 50) could not resolve the 60 Mc cavity modes of the laser. In these interferograms the maser power was 10 milliwatts and its apparent width was 540 Mc,

fig. 21: Experimental Arrangement for Observing Normal Brillouin Scattering as a Function of Angle. The scattering angle θ was varied by a combination of rotation of the adjustable mirror and translation along the precision optical rail. The mirror was mounted on a spectroscopic table with a vernier angular scale for measuring θ.

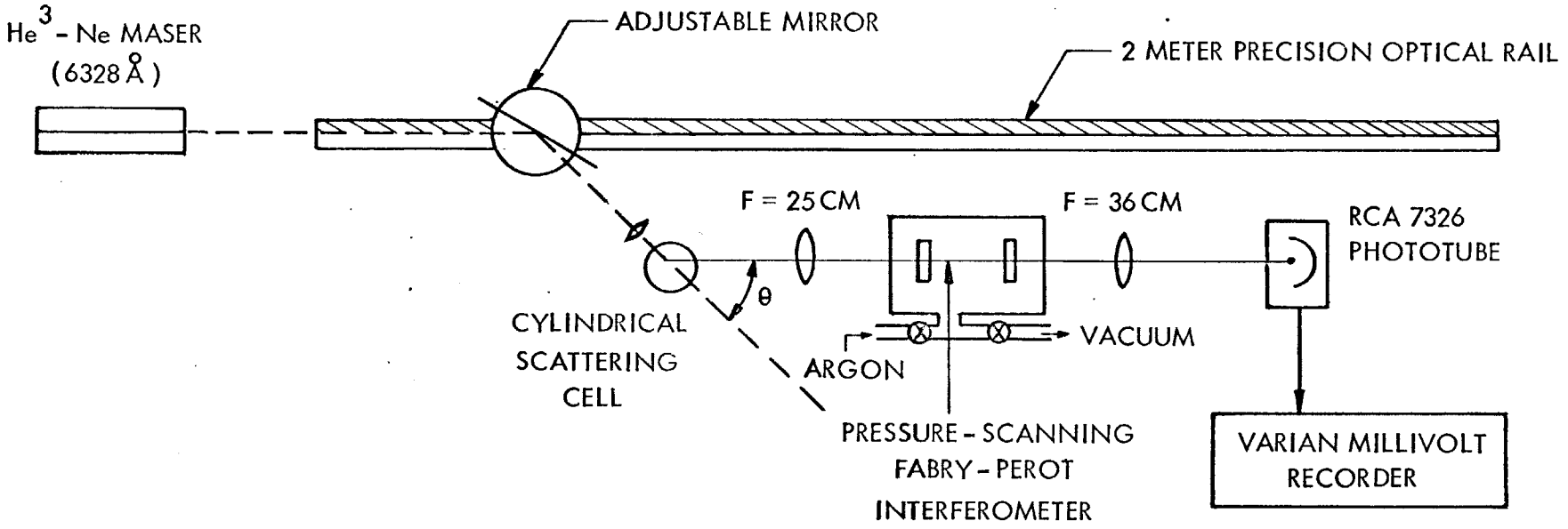
He3 - Ne MASER
(6328 Å)
ADJUSTABLE MIRROR
2 METER PRECISION OPTICAL RAIL
F = 25 CM
F = 36 CM
RCA 7326
PHOTOTUBE
θ
CYLINDRICAL
SCATTERING
CELL
VACUUM
ARGON
PRESSURE - SCANNING
FABRY - PEROT
INTERFEROMETER
VARIAN MILLIVOLT
RECORDER

fig. 22: Interferograms of Brillouin Scattering in Toluene. In (a) the scattering angle was $70.0^{o} \pm 0.3^{o}$; the temperature was $22.8\ ^{o}C$. In (b) the scattering angle was $30.0^{o} \pm 0.3^{o}$; the temperature was $22.4\ ^{o}C$. The maser power was 10 mW. The sweep rate was 316 Mc per division.

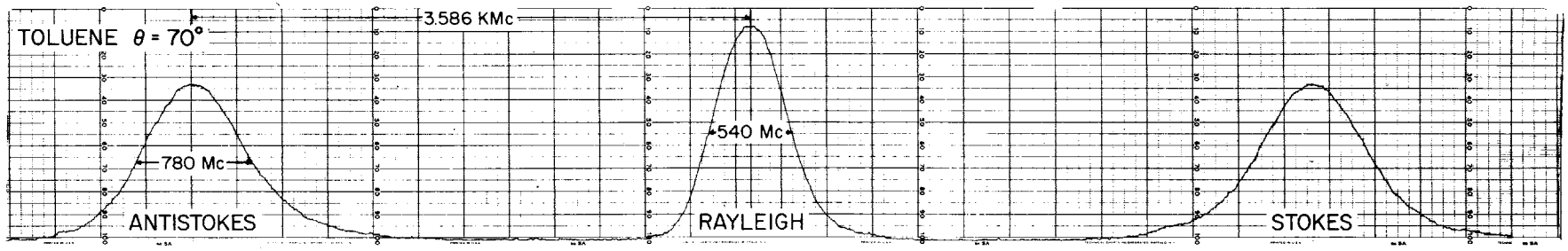

(a)

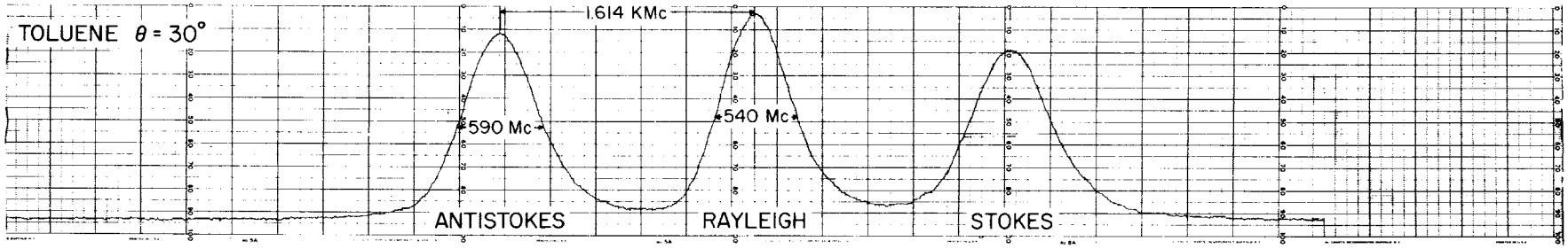

(b)

INTERFEROGRAMS OF BRILLOUIN
SCATTERING IN TOLUENE

which was obtained by using a high-gain tube in conjunction with a 94% reflectivity output mirror. Collection of the scattered radiation by a f/20 aperture lens is probably responsible for the apparent broadening of the Brillouin components at small angles, such as $\theta = 30.0^{\circ}$ shown in fig. 22 (b) since from (1.4) we see that

$$\frac{\delta \nu_A}{\nu_s} = \cot \frac{\theta}{2} \frac{\delta \theta}{2} \tag{5.37}$$

is the portion of the width of the Brillouin components due to a finite angular acceptance $\delta \theta$. For $\theta = 30.0^{\circ}$ and $\frac{\delta \theta}{2} \simeq 2 \times 10^{-2}$ rad, $\delta \nu_A \simeq 100$ Mc. However, the much greater broadening of the Brillouin components at the larger angle of $\theta = 70.0^{\circ}$ (where $\delta \nu_A \simeq 80$ Mc) apparent in fig. 22 (a), must mostly be due to the finite lifetime of the sound wave. By appropriate subtraction of linewidths, this lifetime may be measured. (Since the apparent laser lineshape is not Lorentzian, this procedure is not trivial.[85]) The frequency of the sound wave and thence its velocity from (1.4) were also measured from these spectra. In this manner the velocity and absorption/ν_s^2 of sound waves in toluene were obtained as a function of their frequency, and are plotted in fig. 23 (a) and (b) respectively. (Simple subtraction of linewidths, assuming Lorentzian lineshapes, was used to obtain fig. 23 (b).) This data is ambiguous concerning resonances.[86]

When only one measurement of velocity and absorption in the hypersonic frequency range is desired, the exact backward-scattering direction offers several distinct advantages over other observation directions. Firstly, light from the entire scattering

fig. 23: The Dispersion and Absorption of Sound Waves at Hypersonic Frequencies in Toluene.

(a)

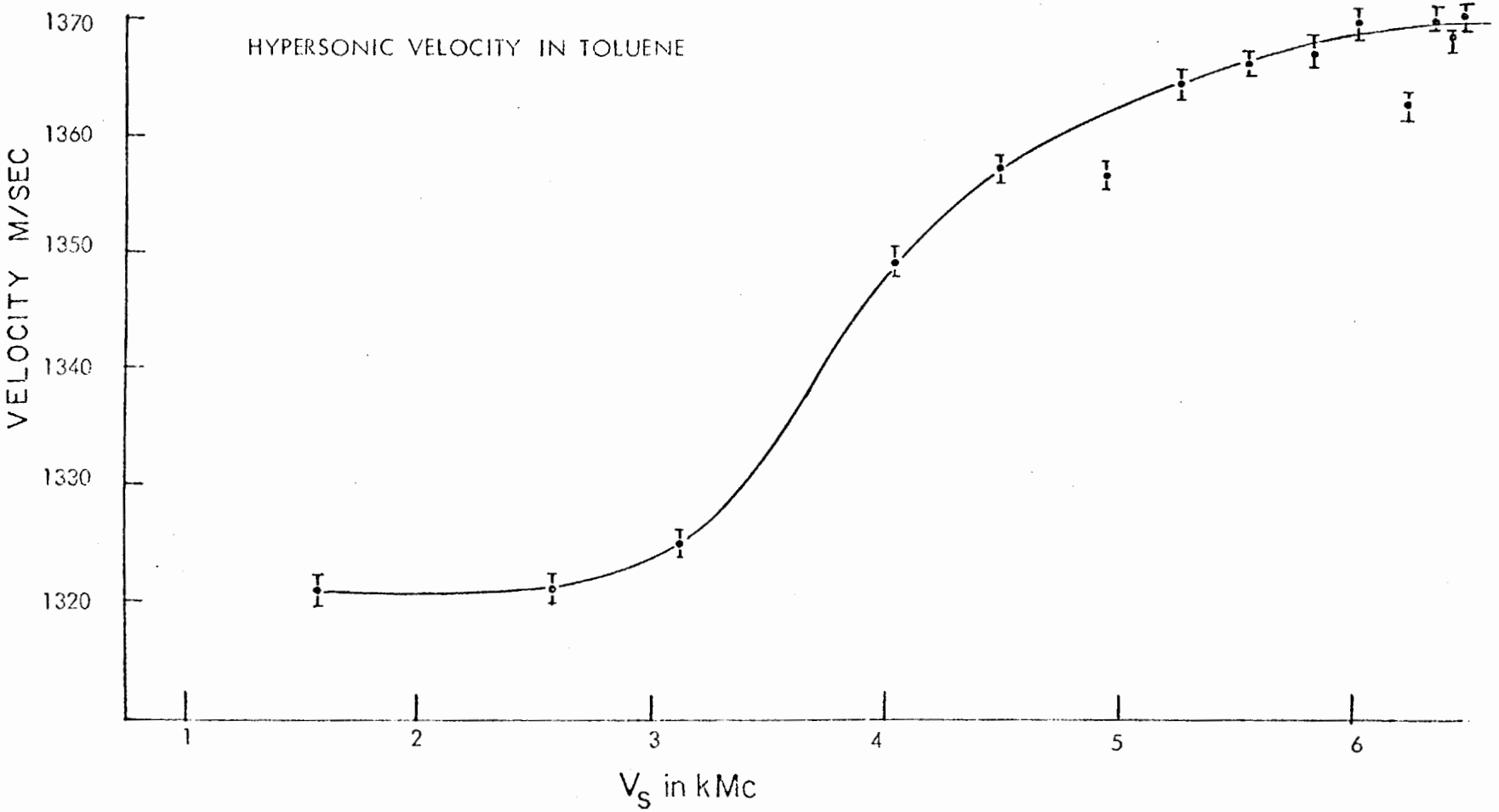
HYPERSONIC VELOCITY IN TOLUENE
VELOCITY M/SEC
1370
1360
1350
1340
1330
1320
1
2
3
4
5
6
V_S in kMc

(b)

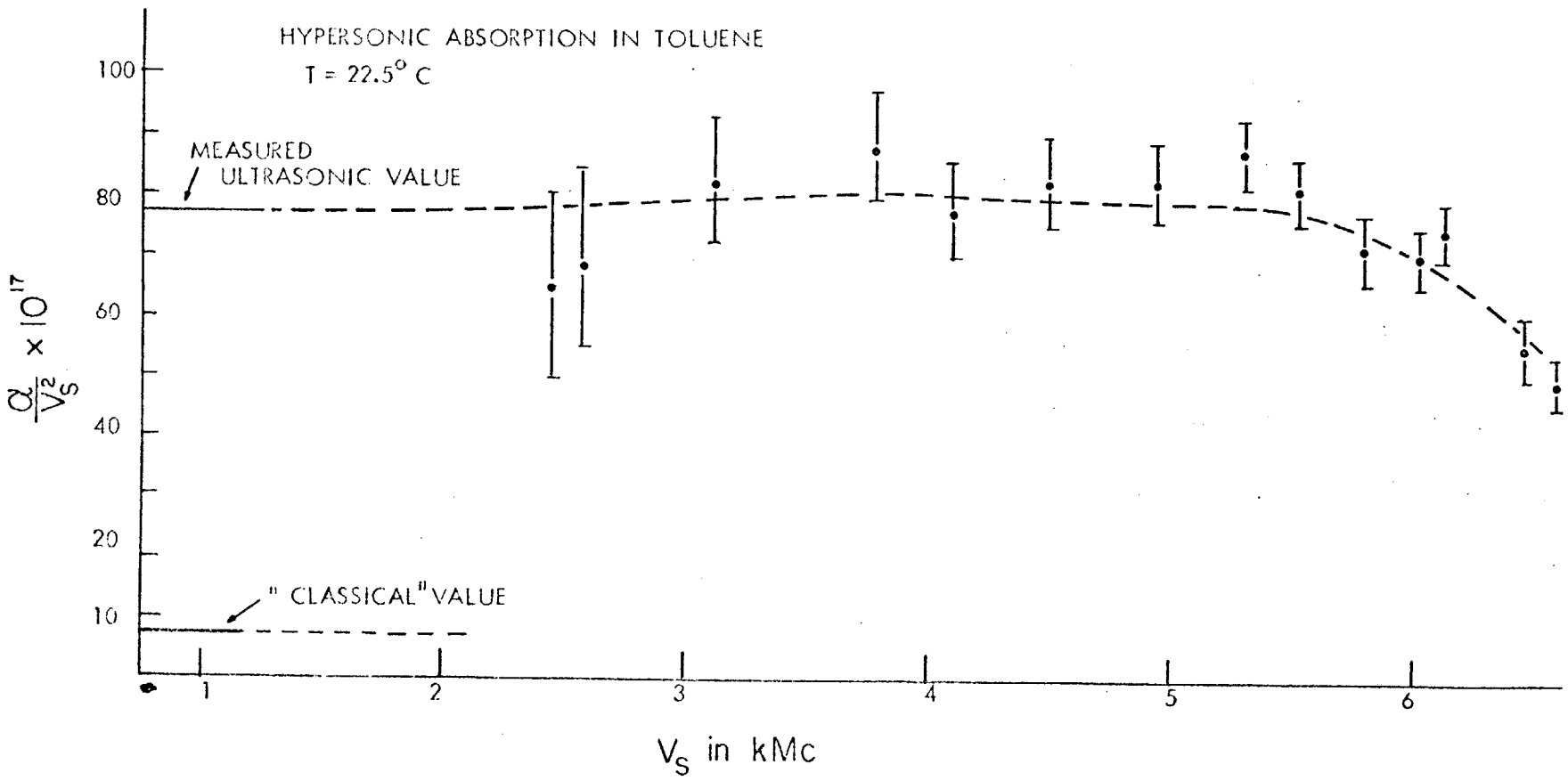
HYPERSONIC ABSORPTION IN TOLUENE
T = 22.5° C
MEASURED
ULTRASONIC VALUE
" CLASSICAL" VALUE
100
80
60
40
20
10
1
2
3
4
5
6
$\frac{\alpha}{V_s^2} \times 10^{17}$
V_s in kMc

path, the length of which is limited only by the length of the cell, is collected into the pinhole. For all other angles, the experimental arrangement shown in fig. 21 will collect light only from a scattering length of about the size of the pinhole. Thus a factor of about 10^2 increase in intensity of the Brillouin components can be obtained when a scattering cell 50 cm long is used for backward scattering. This will allow use of lasers operating in a single mode as sources. Secondly, the cell alignment is not important since the backward-travelling ray retraces the path of the incident laser ray. This allows slight reorientation of the cell to deflect the Fresnel reflections from the windows of the cell away from the collection system. Also, the changing of liquids becomes trivial since we may interchange liquid cells at will without having to worry about cell alignment. Thirdly, the orientation of the Fabry-Perot plates with respect to the incidence direction need not be overly precise, since the lens which collects the scattered light can be translated off center to deflect the backward-going radiation in such a way as to compensate for small errors. Since the exact backward direction gives much more intense scattering than even slightly off-backward directions, alignment is assured when the signal is maximized with respect to the lens translations. The experimental arrangement used[78] in detecting exact backward scattering is shown in fig. 24:

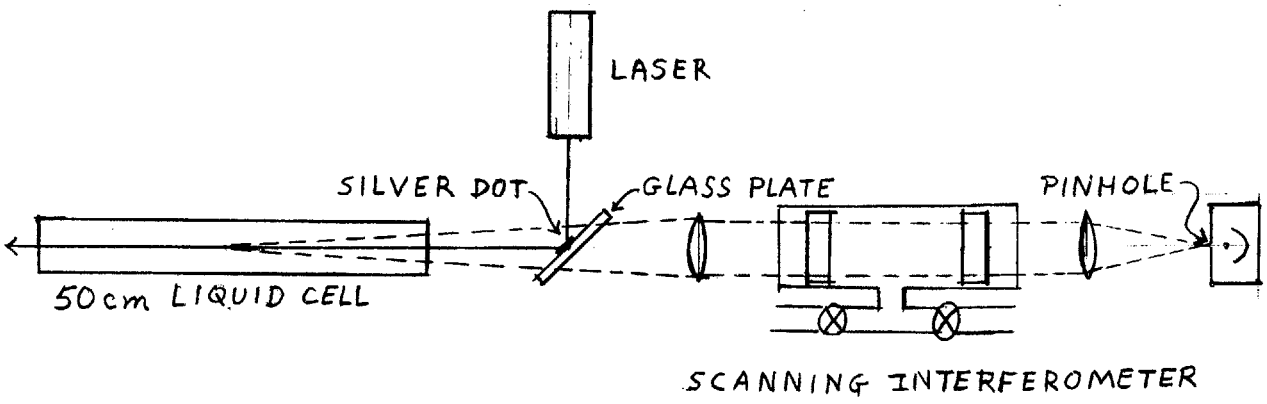

fig. 24: Exact Backward-Scattering Experiment

The technique of exact backward scattering is made feasible by the introduction of a glass plate on which is deposited a small silver dot (the diameter of the dot slightly exceeds the aperture of the laser beam) into the path of the laser beam; the glass plate is centered in such a way that the beam falls on the silver dot and is reflected into the scattering cell. All of the backward-scattered light (dashed lines in fig. 24) is collected by the collecting lens, except for a small portion blocked by the silver dot. Using this technique we have been able to observe Brillouin scattering using a 50 cm long laser (Spectra-Physics model 130) operating on a single mode with a 0.2 milliwatt output. Examples of Brillouin components thus observed are given in fig. 25. However, a severe problem arose from instability of the laser: the broader the Brillouin component, the longer it took to pass through it and the more the drift of the laser frequency tended to broaden the line spuriously. Thus the width measurements from spectra such as fig. 25 were unreliable. Also, because of the instability of the laser, the velocity measurements from such spectra varied about 5%, since the time for scanning from Rayleigh to Brillouin components is of the order of minutes, during which time the laser frequency could have drifted as much as 600 Mc. The multimode laser is much more stable since the average peak intensity is always centered on the atomic line. However, use of a stabilized single mode laser can improve very much the accuracy of Brillouin width measurements, especially since the subtraction of Lorentzian linewidths can then be performed confidently.

Another factor of about 10 increase in the intensity of the signal can be achieved by replacing the pinhole (fig. 24) by a photo-

fig. 25: Brillouin Components Observed Using the Exact Backward-Scattering Method. The asymmetry of the maser line is due to error in the centering of the pinhole. Its width is instrumental and is a measure of the resolution of the Fabry-Perot.

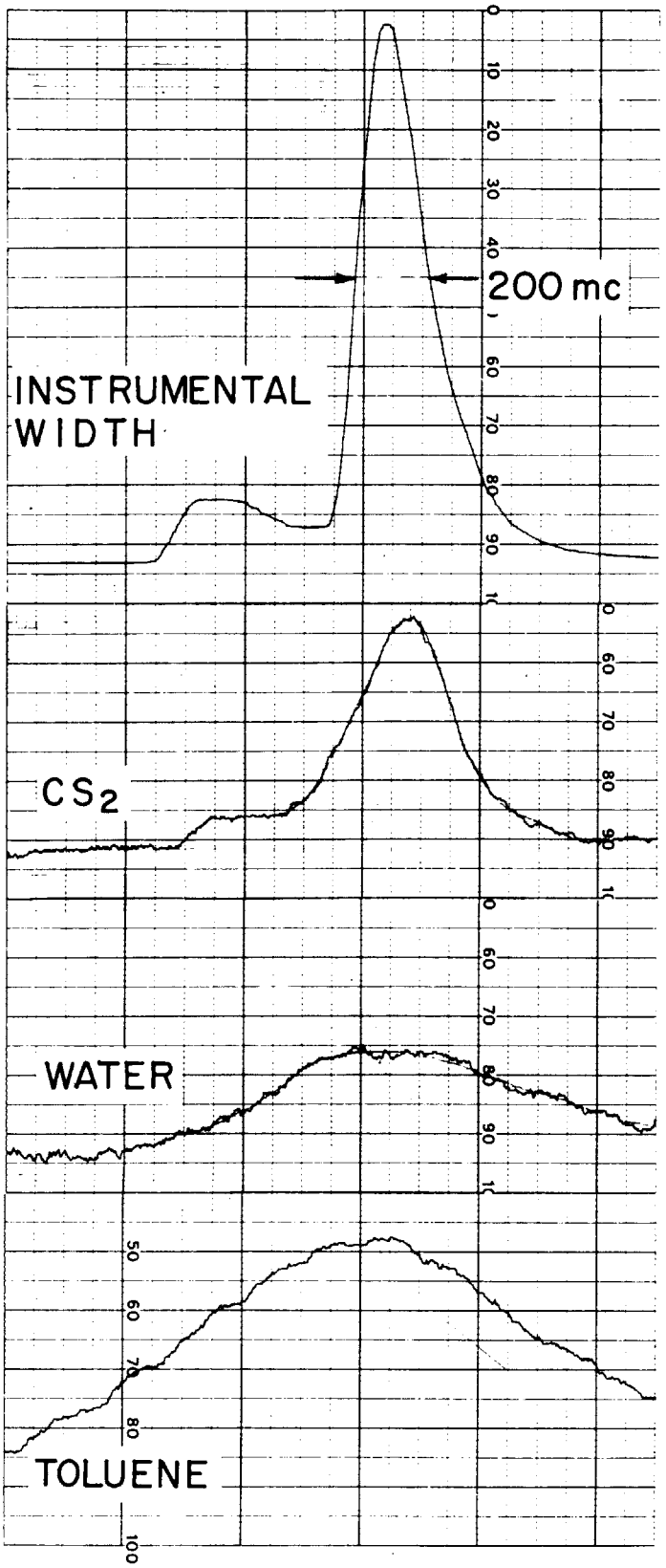

WIDTHS OF BRILLOUIN COMPONENTS

graphic mask of the Fabry-Perot rings. This mask can be produced by making a high-contrast transparent positive of the Fabry-Perot rings produced by the laser beam alone, or by photographing a master plate with the rings cut at the proper radii and widths by a lathe. When the scanning reaches a point when one of the Fabry-Perot rings is transmitted by one of the rings of the mask, by proper alignment and magnification of the rings, all of them will also be transmitted simultaneously so that there will be an enhancement of the signal by a factor equal to the number of rings on the mask. Still another useful technique for enhancing the signal, used by Benedek et al.[87], consists of using a conical lens for collection of the scattered light. Since the frequency of the Brillouin scattered light depends only on θ and is independent of ϕ, the azimuthal angle of scattering, the light collected at all values of ϕ by a properly aligned conical lens will have a very small smear in frequency, since the angular spread of the light received by the pinhole is only $\delta\theta \simeq \frac{d}{2f}$ where d is the diameter of the pinhole and f is the focal length of the lens in front of the pinhole. This small solid angle of collection is especially useful for near-forward scattering. However, since such fine angular definition is not needed for measurements of expected widths of Brillouin components of liquids at normal scattering angles, a spherical lens following the conical lens would increase the solid angle of collection and hence the signal. Thus light can again be collected from a long length of scattering path, allowing extension of the exact-backward scattering technique to other angles.

So far we have dealt with scattering from thermally excited sound waves. Another way of generating moderate amounts of sound

waves is to mix together two laser beams of slightly different frequencies[88]. An experiment utilizing this method of generation for measuring velocities and lifetimes of sound waves is described in fig. 26 (a). A similar experiment, which generates and detects Raman phonons, is described in fig. 26 (b).

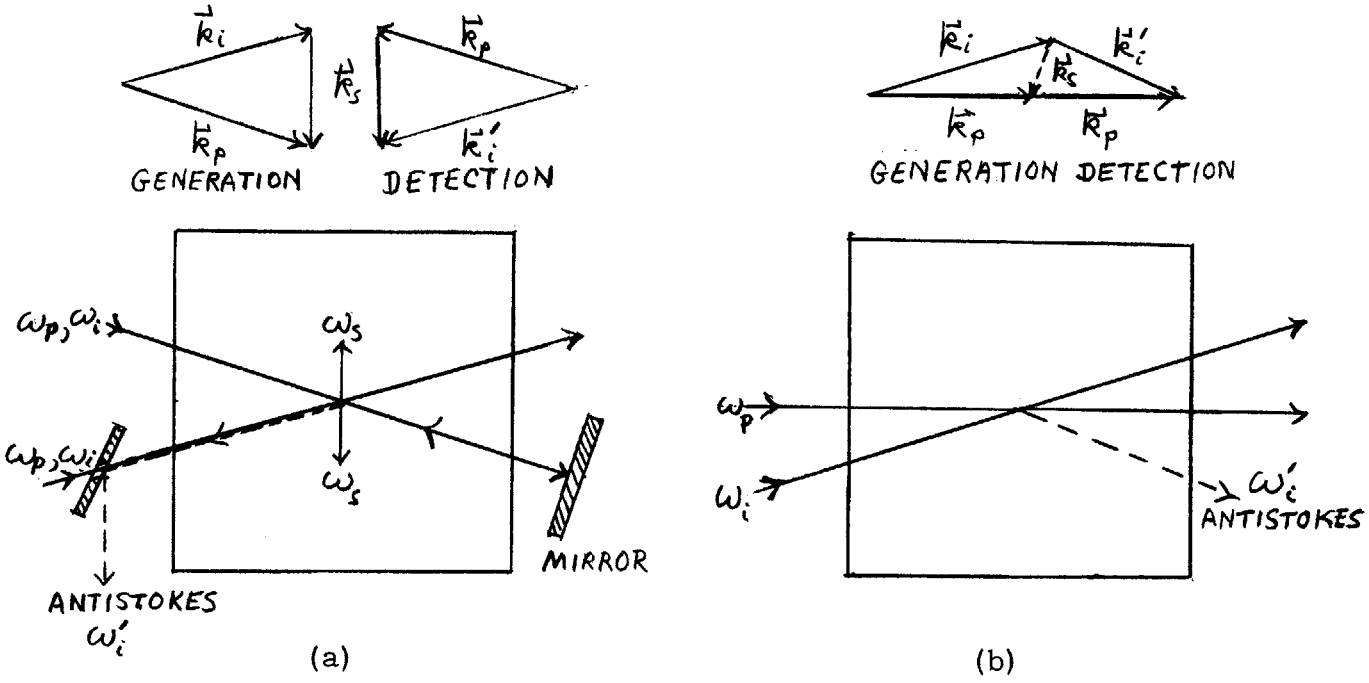

fig. 26: Experiments for Generation and Detection of Acoustical and Raman Phonons

ω_p and ω_i in fig. 26 (a) may be two cavity modes of the laser. Detection of the generated sound waves is accomplished by reflecting back on itself one of the laser beams. When the angles and frequencies are kinematically correct, anti-Stokes will be generated in the backward direction with respect to the other laser beam. For the Raman experiment described in fig. 26 (b), two different lasers must be used, but the experimental arrangement is simpler. In both these experiments, when resonance occurs, the anti-Stokes produced is

highly directional, thus allowing a small detection solid angle for enhancing the signal to noise. In the Brillouin experiment, by changing the cavity length of the laser, one can precisely vary the frequency difference of the modes, so that we can study sound waves of various frequencies. If we could vary the frequency of a laser by a sizeable amount (e. g. by changing the pressure on a semiconductor laser), then we can investigate in the Raman experiments the high-resolution structure of Raman lines in various materials. Since most of the Raman linewidths are not due to the lifetime of the Raman phonon, such spectroscopy is of limited usefulness. However, by chopping one of the lasers or utilizing the beat between two laser modes, we can determine the Raman phonon lifetime by measuring the phase shift of the anti-Stokes modulation.[89]

To calculate the power of the anti-Stokes that we would expect to be produced in these experiments, let us start with equation (5. 5) rewritten as:

$$r \equiv \left(\frac{c}{8\pi} E_{io}'^2\right) \Big/ \left(\frac{c}{8\pi} E_{po}^2\right) = \frac{(k_i' \ell)^2}{4} \left(\frac{\gamma P_{so}}{B}\right)^2 \tag{5. 38}$$

where the primed quantities refer to the generated anti-Stokes wave. In general $\frac{\gamma P_{so}}{B}$ is replaced by $\Delta \epsilon$. P_{so} is determined from the wave equation (3. 25) to be:

$$P_{so} = \frac{\gamma}{8\pi} E_{po} E_{io} \cdot \frac{\omega_s}{\alpha_s} \quad . \tag{5. 39}$$

Hence:

$$(5.40) \qquad r = \frac{1}{64}\left(\frac{\ell}{\lambda_i'}\right)^2 \gamma^4 \frac{E_{po}^2 E_{io}^2}{B^2}\left(\frac{\omega_s}{\alpha_s}\right)^2$$

$$= n_p \frac{E_{po}^2 E_{io}^2}{E_T^4}\left(\frac{\ell}{\ell_i}\right)^2$$

where E_T^2, given by (2.21), is the threshold for the stimulated Brillouin effect, with $\ell_i = \tau_i c_i$. Because of the quadratic dependence on the intensity, this experiment is only feasible when intensity in the two beams is not too many orders of magnitude from threshold (e.g. for quartz if $r = 10^{-6}$, we must have intensities of $\sim$10 Kw/cm^2 in both beams with $\ell = \ell_i$ = 100 cm.) This technique may be especially useful at low temperatures, where thermal Brillouin scattering becomes too weak to be observed and where $\omega_s \tau_s$ becomes very large. A similar calculation for the Raman effect starts with the maximum change in polarizability due to the presence of the two laser beams:[90]

$$(5.41) \qquad \Delta\alpha = \left(\frac{d\alpha}{dx}\right)^2 \frac{E_{po} E_{io}}{2 R \omega_s} = \frac{1}{k}\left(\frac{d\alpha}{dx}\right)^2 E_{po} E_{io} \frac{\omega_s}{\Delta\omega_s}$$

with $\frac{2R}{m} = \Delta\omega_s = \frac{1}{\tau_s}$, where m, R and k are respectively the mass, loss coefficient, and spring constant of a simple harmonic oscillator model for the Raman effect, x being a molecular coordinate. Since $n\Delta\alpha = \frac{1}{4\pi}\Delta\epsilon$ where n = the number of molecules per unit volume, we see that:

$$(3.42) \qquad r = 16\pi^4 \frac{n^2}{k^2}\left(\frac{d\alpha}{dx}\right)^4 E_{po}^2 E_{io}^2 \left(\frac{\omega_s}{\Delta\omega_s}\right)^2 \left(\frac{\ell}{\lambda_i}\right)^2$$

$$= \frac{E_{po}^2 E_{io}^2}{E_T^4} \left(\frac{\ell}{\ell_i}\right)^2$$

where here E_T^2 gives the stimulated Raman effect threshold and $\ell_i = 1/b$ is the loss length of the light wave. Since this threshold may be lower than that for the stimulated Brillouin effect, the power requirements for a given r may be lower. This technique may also be especially useful when infrared sources are used for Raman or Brillouin scattering, since the spontaneous Raman and normal Brillouin effect cross-section is proportional to $\frac{1}{\lambda_p^4}$, whereas (5.42) goes as $\frac{1}{\lambda_p^2}$.

Chapter VI: The Self-Trapping of Optical Beams[91]

In chapter III, we derived the equations for the stimulated Brillouin effect (3.30) and (3.31), starting with coupled wave equations (3.7) and (3.25):

$$(6.1)\qquad \frac{1}{c_i^2}\,\ddot{\vec{E}} + \frac{\alpha_i}{c_i^2}\,\dot{\vec{E}} - \nabla^2\vec{E} = \frac{\gamma}{B\epsilon_o}\left[\vec{\nabla}(\vec{\nabla}P_s\cdot\vec{E}) - \frac{1}{c_i^2}\frac{\partial^2}{\partial t^2}(P_s\vec{E})\right]$$

$$(6.2)\qquad \frac{1}{v_s^2}\,\ddot{P}_s + \frac{\alpha_s}{v_s^2}\,\dot{P}_s - \nabla^2 P_s = -\gamma\frac{\nabla^2 E^2}{8\pi}$$

and assuming slowly varying exponential solutions ($\beta \ll \omega_s \ll \omega_i$). We then saw that under certain circumstances these coupled waves can develop instabilities and grow catastrophically, i.e. exponentially, and we studied the development of such instabilities. However, such solutions tell us only how an instability begins and clearly are not valid for large t, where the nonlinear terms in the sources of (6.1) and (6.2) become large and will affect the behavior of the waves. Or, as mentioned in chapter III, there may be Van der Pol type saturation terms in α_i and α_s which would cause the oscillations to grow until they reach some sort of limit cycle, at which point they cease to grow, and the solutions take on a steady-state character. In this chapter we shall neglect such saturation effects.

Nevertheless, the coupled waves (6.1) and (6.2) do possess a steady-state solution, to which the initial instability may possibly ultimately make a transition. For if P_s becomes time independent (henceforth we assume $\alpha_i = \alpha_s = 0$), (6.2) reduces to

$$\nabla^2 P_s = v_s^2 \gamma \nabla^2 \frac{\overline{E^2}}{8\pi} . \tag{6.3}$$

Here we take only the d. c. component of E^2 since the medium cannot respond to optical frequencies. (6. 3) has a solution

$$P_s = \gamma \frac{\overline{E^2}}{8\pi} + \phi \tag{6.4}$$

where $\nabla^2 \phi = 0$. Assuming a homogeneous and unstrained medium when $E = 0$, we set $\phi \equiv 0$. Equation (6. 4) can be viewed as a statement concerning the change ~~in the change~~ in the index of refraction of the medium arising from the phenomenon of electrostriction. It states that the index of refraction of the medium is greater inside a light beam than outside. This raises the interesting possibility that a light beam will be trapped inside a dielectric waveguide of its own making. Normally a light beam with a finite aperture D will expand by diffraction with an angular divergence of:

$$\theta_D = \frac{1.22 \lambda}{n_o D} \tag{6.5}$$

where λ is the wavelength of the light and n_o is the index of refraction of the medium in the absence of stresses. However, if the index of refraction of the medium responds nonlinearly to the field strength of the light beam, i. e.

$$n = n_o + n_2 E^2 + \ldots \tag{6.6}$$

where in the case of electrostriction from (6. 4),

$$(6.7) \qquad n_2 = \frac{\gamma^2}{16\pi n_o B}$$

then the possibility of total internal reflection of diffracted rays in the beam if $\theta_D < \theta_c$ where

$$(6.8) \qquad \cos\theta_c = \frac{n_o}{n_o + n_2 E^2} \quad .$$

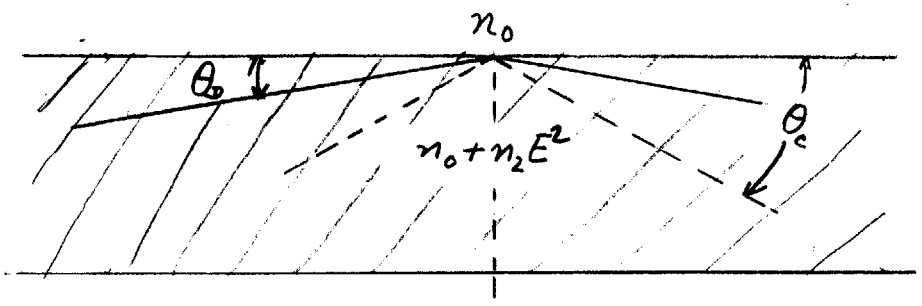

fig. 27: Critical Reflection and Self-Trapping

Assuming θ_c small the critical power at which critical reflection of diffracted rays occurs is:

$$(6.9) \qquad P_c = \frac{\pi D^2}{4} n_o \frac{c E^2}{8\pi} = (1.22\lambda)^2 \frac{c}{64 n_2} \quad .$$

Typically P_c is of the order of 10^6 watts. Note that this power is independent of the diameter of the beam. This arises physically because whereas a decrease in the beam aperture makes the diffraction angle larger, the index of refraction, due to the higher intensity of the beam increases in a compensating manner so that the beam remains trapped.

More rigorously, for there to be a steady-state solution to (6.1) and (6.4), there must be a solution of the form

$E = E_t(x,y)\cos(k_z z - \omega t)$ (i.e. a waveguide solution) which satisfies:

$$(6.10)\qquad \nabla^2 \vec{E} - \frac{\epsilon_o}{c^2}\frac{\partial^2 \vec{E}}{\partial t^2} - \frac{\epsilon_2}{c^2}\overline{E^2}\frac{\partial^2}{\partial t^2}\vec{E} = 0$$

where $\epsilon = \epsilon_o + \epsilon_2 E^2$. ϵ_2 is related to n_2 by $\epsilon_2 = 2n_o n_2$. We neglect the nontransverse source term since $\frac{|\nabla P_s|}{P_s} << k_o$ if $D >> \lambda$, which is consistent with neglecting terms $\mathcal{O}(E^4)$ in n and the source terms of (6.1) and (6.2). Therefore:

$$(6.11)\qquad \frac{\partial^2}{\partial x^2}\vec{E}_t + \frac{\partial^2}{\partial y^2}\vec{E}_t - \Gamma^2 \vec{E}_t + \frac{\epsilon_2}{2} k_o^2 E_t^2 \vec{E}_t = 0$$

where $\Gamma^2 = k_z^2 - k^2$ and $k = n_o k_o = n_o \frac{\omega}{c}$. In the case where E_t depends only on y, and assuming linear polarization:

$$(6.12)\qquad \frac{d^2}{dy^2} E_t(y) - \Gamma^2 E_t(y) + \frac{\epsilon_2}{2} k_o^2 E_t^3(y) = 0.$$

$E_t(y)$ represents a slab-shaped beam, confined in the y-directions, so that the boundary conditions are $E(y) \to 0$ as $y \to \pm\infty$ and $\frac{dE}{dy} = 0$ at $y = 0$. This excludes periodic solutions, implying $\Gamma^2 > 0$. A mechanical problem with equations identical to (6.12) is that of a particle in a one-dimensional double-well quartic potential:

$$(6.13)\qquad \ddot{x} - x + b x^3 = 0$$

where the correspondence is $x \to E_t$, $t \to \Gamma y$, $b = \frac{\epsilon_2}{2}\frac{k_o^2}{\Gamma^2}$, so

that the boundary conditions become: $x(t) \rightarrow 0$ as $t \rightarrow \pm \infty$ and $\dot{x}(0) = 0$. The potential for (6.13) is:

$$(6.14) \qquad V(x) = -\frac{1}{2} x^2 + \frac{1}{4} b x^4$$

which is drawn in fig. 28:

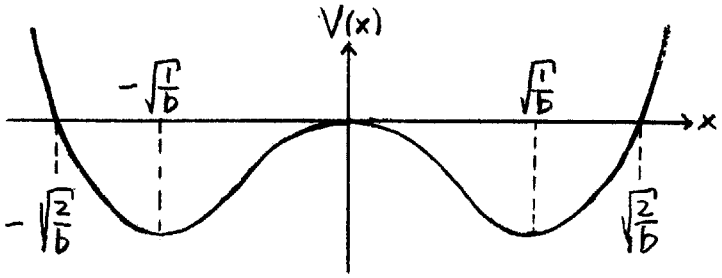

fig. 28: Potential for Mechanical Analogue to Self-Trapping

We seek solutions where $x \rightarrow 0$ as $t \rightarrow \infty$. Clearly the only possible solution is to put the particle at $\pm \sqrt{\frac{2}{b}}$ with zero initial velocity (this will satisfy the other boundary condition $\dot{x}(0) = 0$). The particle will fall into the well and reach $x = 0$ after an infinite time. Hence the only stable solution for (6.12) will have:

$$(6.15) \qquad E(0) = \sqrt{\frac{2}{b}} = 2 \frac{\Gamma}{k_o} \frac{1}{\sqrt{\epsilon_2}} .$$

We can obtain an analytical solution as follows:

$$(6.16) \qquad T + V = E = 0$$

where T = kinetic energy and V = potential energy and since $T_{initial} = V_{initial} = 0$, $E = 0$. Hence:

(6.17) $$\frac{1}{2}\dot{x}^2 = +\frac{1}{2}x^2 - \frac{1}{4}bx^4$$

(6.18) $$\dot{x} = \sqrt{x^2 - \frac{1}{2}bx^4}\ .$$

The solution is therefore:

(6.19) $$\int_{\sqrt{2/b}}^{x} \frac{dx}{\sqrt{x^2 - \frac{1}{2}bx^4}} = t = \int_{\sqrt{2/b}}^{x} \frac{dx}{x\sqrt{1 - \frac{1}{2}bx^2}}\ .$$

Clearly this integral diverges when $x = 0$, indicating an infinite period for oscillations in the well with $E = 0$ (i.e. it takes an infinite time to reach $x = 0$). For the computer solutions of the cylindrically symmetrical problem to be discussed shortly, it is useful to know the relation between the period of oscillation and an error in the initial condition $x(0)$:

(6.20) $$\int_{\sqrt{2/b}-\delta}^{0+\epsilon} \frac{dx}{x\sqrt{1 - \frac{1}{2}bx^2}} \cong \log\sqrt{\frac{b}{2}}\epsilon = -\frac{T}{2}$$

where ϵ is related to $\delta = \sqrt{\frac{2}{b}} - x(0)$ $\left(V\left(\sqrt{\frac{2}{b}} - \delta\right) = -\delta\sqrt{\frac{2}{b}}\right)$ by:

(6.21) $$\delta = \frac{1}{2}\sqrt{\frac{b}{2}}\epsilon^2\ .$$

Hence the correction to be made on the initial condition $x(0)$ is:

(6.22) $$\delta = \frac{1}{\sqrt{2b}}\ e^{-T} \cong \frac{1}{2}x(0)\ e^{-T}\ .$$

However, we can obtain the exact solution by directly evaluating (6.19):

(6.23) $$t = \cosh^{-1}\left(\sqrt{\frac{2}{b}}\ \frac{1}{x}\right).$$

So that the exact solution to (6.12) is:[92]

(6.24) $$E_t(y) = \frac{E(0)}{\cosh \Gamma y} = \frac{2}{k_o}\ \frac{1}{\sqrt{\epsilon_2}}\ \frac{\Gamma}{\cosh \Gamma y}.$$

Physically, however, most beams have a cylindrical shape. For this case, assuming circular polarization[93], (6.11) becomes:

(6.25) $$\frac{d^2 E^*(r^*)}{d r^{*2}} + \frac{1}{r^*}\ \frac{d E^*(r^*)}{d r^*} - E^*(r^*) + E^{*3}(r^*) = 0$$

where $r^* = \Gamma r$, $E^*(r^*) = \sqrt{b}\ E_t(r^*)$ and $b = \frac{\epsilon_2}{2}\left(\frac{k_o}{\Gamma}\right)^2$. This allows the steady state solutions to be scaled by the factor $\sqrt{b}$ to give any arbitrary size ($\sim \frac{1}{\Gamma}$) for the beam cross-section (with the restriction $D \gg \lambda$). Equation (6.25) appears to have no simple analytical solution: numerical methods of integration must be used. A method which is especially well adapted for this type of problem is the Manning-Millman procedure[94], with slight modification. Let $u \equiv r^*$. Equation (6.25) becomes, when we substitute $E^*(u) = \frac{1}{\sqrt{u}}\ e(u)$:

(6.26) $$e''(u) = Q_1(u)\ e(u) - Q_2(u)\ e^3(u)$$

where:

(6.27) $$Q_1(u) = 1 - \frac{1}{4u^2}$$

$$(6.28) \qquad Q_2(u) = \frac{1}{u}.$$

In general, by Taylor expansion, we see for any f(x):

$$(6.29) \qquad f(x+a) + f(x-a) = 2f(x) + a^2 f''(x) + \frac{a^2}{12}\{f''(x+a) + f''(x-a) - 2f''(x)\} + \mathcal{O}(a^4).$$

Applying this to e(u), using (6.26), we get:

$$(6.30) \qquad e(u+a) + e(u-a) = 2e(u) + a^2 Q_1(u)\, e(u) - a^2 Q_2(u)\, e^3(u) + \frac{a^2}{12}\{Q_1(u+a)\, e(u+a) - Q_2(u+a)\, e^3(u+a) + Q_1(u-a)\, E(u-a) - Q_2(u-a)\, e^3(u-a) - 2Q_1(u)\, e(u) + 2Q_2(u)\, e^3(u)\}.$$

The procedure for numerical integration is as follows: equation (6.30) tells us what e (u+a) is, if we know what e(u) and e(u-a) are. Hence, if we start from e (0) where the behavior is known, so that we can obtain e (a), if a is sufficiently small, then we can by iteration obtain e (2a), e (3a), etc. If we chose a wrong initial value e (0), we would expect oscillatory solutions, as in the one-dimensional case discussed previously; but as we approach the correct initial value, the period of these oscillations goes to infinity logarithmically (6.20), thus providing us with a correction parameter.

(6.30) is a cubic equation for e (u+a):

$$(6.31) \qquad e^3(u+a)\cdot\left(\frac{a^2}{12} Q_2(u+a)\right) + e(u+a)\cdot\left(1 - \frac{a^2}{12} Q_1(u+a)\right)$$

$$= e(u) \cdot \left(2 + \frac{10}{12} a^2 Q_1(u)\right) - e(u-a) \cdot \left(1 - \frac{1}{12} a^2 Q_1(u-a)\right)$$

$$- e^3(u) \cdot \frac{5}{6} a^2 Q_2(u) - e^3(u-a) \cdot \frac{a^2}{12} Q_2(u-a)$$

which has a solution[95]:

$$e(u+a) = w - \frac{(A/D)}{3w} \tag{6.32}$$

where

$$w^3 = \frac{H}{2D} + \sqrt{\frac{H^2}{4D^2} + \frac{A^3}{27D^3}} \tag{6.33}$$

where

$$A = 1 - \frac{a^2}{12} Q_1(u+a)$$

$$B = 2 + \frac{10}{12} a^2 Q_1(u)$$

$$C = 1 - \frac{1}{12} a^2 Q_1(u-a)$$

(6.34)

$$D = \frac{a^2}{12} Q_2(u+a)$$

$$F = \frac{a^2}{12} Q_2(u-a)$$

$$G = \frac{5}{6} a^2 Q_2(u)$$

$$H = e(u)\,B - e(u-a)\,C - e^3(u-a)\,F - e^3(u)\,G$$

To obtain the starting value e (a) let us return to equation (6.25). Either odd or even solutions are possible. The lowest mode is

even, as was the case for the one-dimensional equation (6.12). A series expansion of the even solutions near the origin gives:

$$E^*(u) = E^*(0) + E^{*''}(0)\,\frac{u^2}{2} + E^{*(4)}(0)\,\frac{u^4}{24} + E^{*(6)}(0)\,\frac{u^6}{720} + \mathcal{O}(u^8) \tag{6.35}$$

where $E^*(0)$ is known and:

$$E^{*''}(0) = \frac{1}{2}E^*(0) - \frac{1}{2}E^{*3}(0)$$

$$E^{*(4)}(0) = \frac{3}{4}E^{*''}(0)\,(1 - 3E^{*2}(0)) \tag{6.36}$$

$$E^{*(6)}(0) = \frac{5}{6}\,(E^{*(4)}(0) - 3\,(6E^*(0)\,(E^{*''}(0))^2 + (E^*(0))^2\,E^{*(4)}(0)))$$

The computer program contained three subprograms A, B, and C. A calculated the value of E (a) from (6.35) with u = a, given some initial value E (0). B calculated E (2a), E (3a), etc. (i.e. numerically integrated (6.25)) from (6.32), (6.33) and (6.34) and calculated the period T of the oscillations of E (u) thus obtained, which is a measure of the error of E (0). C calculated the correction of E (0) using (6.22) from the value of T calculated by B, and returned this corrected E (0) to A. The first value E (0) given to A was that given by (6.15) for the one-dimensional case. The program was terminated by B when the period T exceeded a certain value determined by the programmer. Fig. 29 gives the solution thus obtained for the lowest mode.

fig. 29: Calculated Radial Distribution of Electric Field in a Self-Trapped Electromagnetic Beam of Circular Cross-Section.

The values calculated by computer are:

r^*	E^*	r^*	E^*
0.0	2.20388= $E^*(0)$	4.0	3.12200×10^{-2}
0.2	2.12166	4.2	2.49881 "
0.4	1.90382	4.4	2.00236 "
0.6	1.61482	4.6	1.60633 "
0.8	1.31967	4.8	1.29005 "
1.0	1.05444	5.0	1.03791 "
1.2	0.832322	5.2	8.34838×10^{-3}
1.4	0.653324	5.4	6.72865 "
1.6	0.511935	5.6	5.43124 "
1.8	0.401312	5.8	4.39115 "
2.0	0.315071	6.0	3.55785 "
2.2	0.247862	6.2	2.89063 "
2.4	0.195417	6.4	2.35702 "
2.6	0.154404	6.6	1.93098 "
2.8	0.122253	6.8	1.59224 "
3.0	0.0969840	7.0	1.32404 "
3.2	0.0770761	7.2	1.11413 "
3.4	0.0613557	7.4	9.51994×10^{-4}
3.6	0.0489163	7.6	8.29550 "
3.8	0.0390535	7.8	7.40905 "

$$\pi \int_0^\infty E^{*2}(u)\, u\, d\, u = 5.7637$$

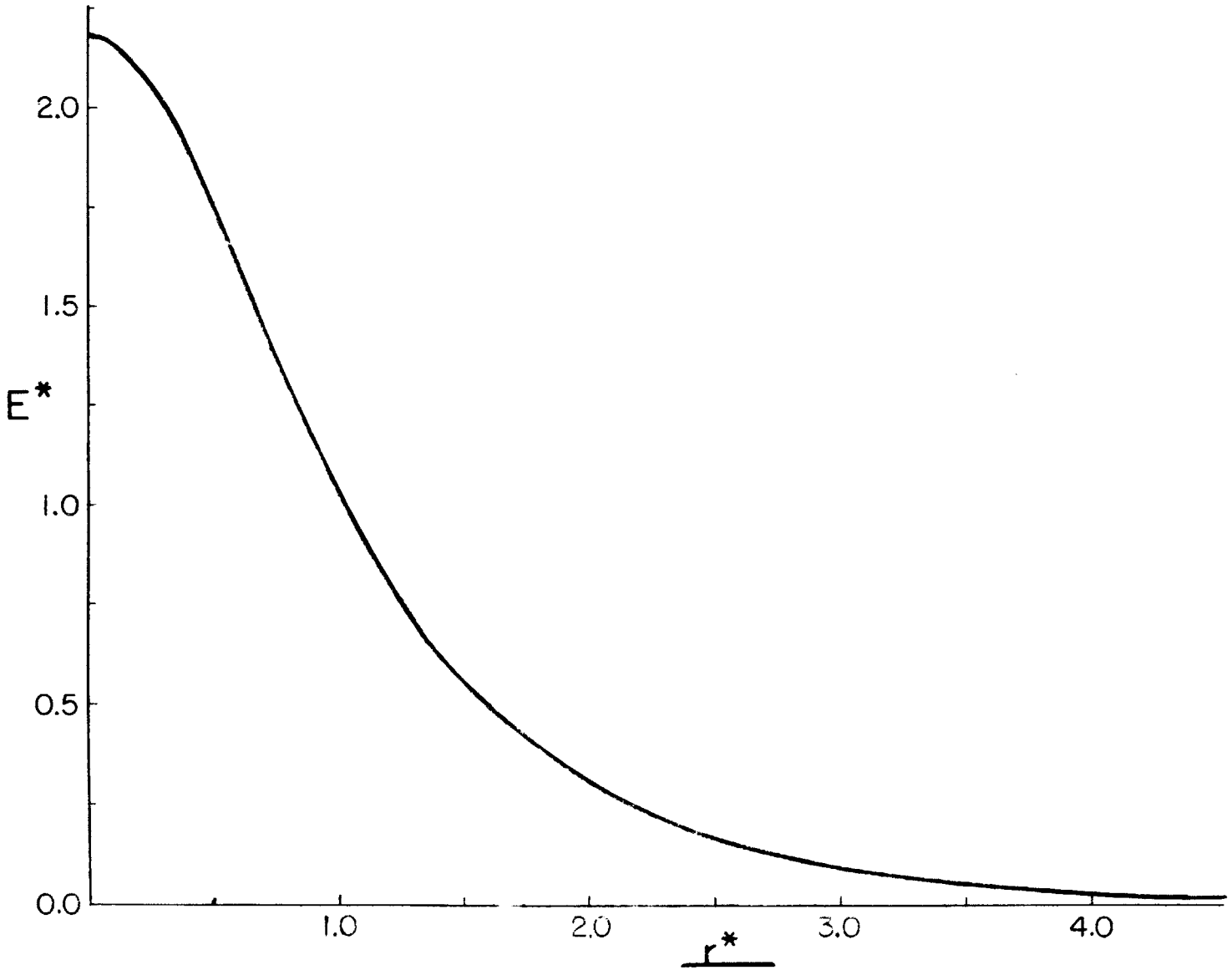
2.0
1.5
E*
1.0
0.5
0.0
1.0
2.0
3.0
4.0
r*

The critical power for the trapping of a cylindrical beam is given by:

$$P_c = \frac{c}{4\pi} n_{eff} \; 2\pi \int_0^{\infty} E^{*2}(u)\, u\, du \; \frac{1}{\Gamma^2 b} \tag{6.37}$$

where

$$n_{eff} = \frac{k_z}{k_o} = \sqrt{n_o^2 + \frac{\epsilon_2}{2b}} \,. \tag{6.38}$$

Numerical integration of (6.37) using the calculated solution gives:

$$P_c = \frac{5.7637 \cdot \lambda^2 c\, n_{eff}}{8\pi^3 n_2 n_o} \,. \tag{6.39}$$

The rough calculation (6.9) is very nearly equal to (6.39). Since $E(0) = \frac{1}{\sqrt{b}} E^*(0) = \frac{1}{\sqrt{b}} \times 2.20388$ we have:

$$n_{eff} = \frac{k_z}{k_o} = \sqrt{n_o^2 + \frac{\epsilon_2 E^2(0)}{9.71404}} \,. \tag{6.40}$$

For the one dimensional case the numerical factor multiplying $\epsilon_2 E^2(0)$ becomes $\frac{1}{4}$. The sole dependence of power on beam diameter is through n_{eff}, which is usually unimportant except for beams with diameters as small as a few wavelengths. This in conjunction with higher order non-linearities in the dielectric material will make the actual diameter of the trapped beam depend on power. It should be noted that P_c is <u>not</u> a threshold in the sense that any beam with greater power will be stably trapped. Rather it is a <u>critical</u> power at which a beam of a given diameter will be trapped. Hence if the entire power of the beam, when appreciably

above P_c, is trapped, we expect the self-trapped beam to be of a very small diameter.

The dynamics of beam formation and changes in the dielectric are not yet well understood. We do not know whether a beam whose power exceeds P_c radiates most of it away to attain P_c or whether it rather breaks up into several trapped filaments. In the case of the slab-shaped beams, the uniqueness of the solution (6.24) prevents the coëxistence of several such beams. Also, we do not know whether the steady-state solutions are stable to small arbitrary perturbations, although it is clear that once the self-trapped waveguide is established, it will serve as a waveguide for higher frequencies. For if $E' << E$, expansion of (6.10) will show that if $E' = E_t'(x,y) \cos(k_z' - \omega' t)$

$$(6.41) \qquad \frac{\partial^2}{\partial x^2} \vec{E}_t' + \frac{\partial^2}{\partial y^2} \vec{E}_t' - \Gamma'^2 \vec{E}_t' + \frac{\epsilon_2}{2} k_o^2 E_t^2 \vec{E}_t' = 0$$

where $\Gamma'^2 = k_z'^2 - k'^2$ and $k' = n_o \frac{\omega'}{c}$. This can be viewed as a time-independent Schroedinger equation with a potential $-\frac{\epsilon_2}{2} k_o^2 E_t^2(x,y)$. In order to propagate without radiation $\Gamma^2 > 0$ ($\epsilon < 0$). However, the potential well must be deep enough to allow such a bound state, which turns into a condition that $\omega' > \omega$.[96] If the frequency difference $\omega' - \omega$ is faster than the response of the medium, clearly the waveguide is undisturbed to first order. Also, it is clear that if one has two strong waves E and E' whose frequency difference is sufficiently great, then $\overline{(E + E')^2} \cong \overline{E^2} + \overline{E'^2}$, so that the presence of one wave helps cause the other to be trapped and the waveguides reinforce one another. Small perturbations in one

wave will not affect the waveguide of the other one greatly.

The self-trapping of a laser beam may be responsible for the formation of the extremely thin, long damage tracks in a piece of glass into which the beam is focussed, such as those first observed by Hersher[97]. Evidence that some sort of dielectric waveguide was being formed was obtained by Atwood et al[98]. They performed the simple experiment of placing a polaroid crossed with respect to the laser's polarization behind the glass target and found that the diffracted light emerging from the glass after track formation formed a dark Maltese cross in a light background. Since light which is totally internally reflected from a dielectric wall, like that of the waveguide, is elliptically polarized except when the electric vector is parallel or perpendicular to the plane of incidence, this is clear evidence for some form of light trapping. Furthermore, the large angle of diffraction of the light emerging from a damage track is consistent with diffraction from a very small aperture whose diameter is about equal to that of the track. However, it appears that the track travels a very slow speed ($\sim$ Mach 20), showing that the dynamics of the trapping process are playing an important role. Hence a more detailed study of the coupled equations (6. 1) and (6. 2) is required.

FOOTNOTES

Chapter I

1. Léon Brillouin, Annales de Physique, Paris, 17, 88 (22).

2. I am indebted to Dr. Francesco DeMartini for pointing out this effect. In a heterodyne experiment one expects a doublet beat note with frequency separation $\delta\nu = 2\,\nu_p\, n^2 \frac{v_s^2}{c^2} \sin^2 \frac{\theta}{2}$. One might remark that the net shift to the blue is opposite to the red-shift due to the time dilation.

3. For lowest order see R. S. Krishnan, Proc. Indian Acad. Sci., A41, 91 (55).

4. L. D. Landau and E. M. Lifshitz, Theory of Elasticity, London: Pergamon Press, 1959, p. 104. See also J. V. Atanasoff and P. J. Hart, Phys. Rev., 59, 85 (41).

Chapter II

5. We borrow the terminology of parametric amplifier theory, since one can view the stimulated process as parametric generation of a sound wave as the signal wave and the frequency-shifted light wave as the idler wave. For the case when the signal is also a light wave, see R. H. Kingston, Proc. IRE, 50, 472 (62) and N. M. Kroll, Proc. IEEE, 51, 110 (63). However, the nonlinear coupling is much smaller for this case than for the Brillouin case, and no parametric generation of two light waves has been seen experimentally.

6. By the virial theorem, the kinetic energy equals the potential energy contribution to the energy density in a sound wave; hence

$$u_s = 2\overline{\int \frac{P\,dV}{V}} = 2\,\frac{\overline{P^2}}{2B} = \frac{P_{so}^2}{2B}$$

Chapter III

7. A. Yariv, Quantum Theory for Parametric Interactions of Light and Hypersound (to be published). See also W. H. Louisell, A. Yariv and A. G. Siegman, Phys. Rev., 124, 1646 (61). The quantum mechanical treatment is identical to the classical one except for the intrinsic presence of zero-point fluctuations, which become important only at very low temperatures. Cf. Bull. Am. Phys. Soc. II, 10, 98 (64).

8. E. H. Jacobsen, Quantum Electronics, C. H. Townes, ed., New York: Columbia University Press (1960), p. 479.

9. γ is calculated from $\rho\left(\frac{\partial \epsilon}{\partial \rho}\right)_T = -\frac{1}{\alpha_T}\left(\frac{\partial \epsilon}{\partial T}\right)_p$, where α_T, the isothermal expansion coefficient and $\left(\frac{\partial \epsilon}{\partial T}\right)_p$, derived from $\left(\frac{\partial n}{\partial T}\right)_p$, is gotten from the International Critical Tables; γ must also be corrected in accordance with footnote 12.

10. The fluid motion $\vec{u}$ involved in a sound wave is adiabatic, so that B_s is the adiabatic bulk modulus, where $\frac{B_s}{B_T} = \frac{C_p}{C_V}$ is the relationship to the isothermal bulk modulus B_T. (cf. Sears, Thermodynamics, p. 155.) For a more complete discussion of the derivation of the wave equation for sound, see L. P. Landau and E. M. Lifshitz, Fluid Mechanics, London: Pergamon Press (1959), p. 245.

11. See also Panosky and Phillips, Classical Electricity and Magnetism, Addison-Wesley (1955), p. 92.

12. As mentioned in footnote 10, $\vec{u}$ describes adiabatic fluid motion. Therefore, W_{mat} is, strictly speaking, the internal energy instead of the free energy. Actually, $\epsilon = \epsilon(\rho, s)$ where s is the entropy per unit mass of fluid, so that $\frac{d\epsilon}{d\rho}$ should really be $\left.\frac{\partial \epsilon}{\partial \rho}\right|_s$ and $\gamma = \gamma_s = \rho \left.\frac{\partial \epsilon}{\partial \rho}\right|_s$. Since what is measured in most experiments

(except in Debye-Sears and Brillouin scattering) is the isothermal γ_T, we should use thermodynamics to get the relation:

$$\gamma_s = \left(\frac{C_p}{C_V}\right)\gamma_T + \left(\left(\frac{C_p}{C_V}\right) - 1\right) \cdot \frac{1}{\alpha_T} \cdot \left(\frac{\partial \epsilon}{\partial T}\right)_p$$

where $\alpha_T = \frac{1}{V}\frac{\partial V}{\partial T}\Big|_p$, C_p and C_V are the specific heat capacity at constant pressure and volume respectively. Cf. Fabelinskii, Usp. Fiz. Nauk, 63, 355 (57), p. 479 of the English translation.

13. A self-trapped light beam (cf. Chapter VI) can therefore also form a trapping waveguide for the sound waves and vice versa.

14. N. M. Kroll, J. of Appl. Phys., 16, 34 (1965).

15. The "mixed" character of the coupled waves has been pointed out by Y. R. Shen and N. Bloembergen, Phys. Rev., 137, A1787 (1965).

16. Cf. D. L. Bobroff, Technical Memorandum T-609, Raytheon Co., Research Div., Waltham, Mass, Dec. 7, 1964 and N. M. Kroll, ibid. Formula (3.57) agrees with Kroll's formula (36) and disagrees with Bobroff's formula (42).

17. For very short laser pulses, it is clear that not only must we exceed it by a sufficient amount so that the idler and sound waves can build up during the laser pulse. This means that a more meaningful threshold for the resonator case than (3.56) when t = laser pulse duration $\ll \ell_s/v_s$ is the "transient" threshold:

$$\frac{E_{po}^2}{8\pi} \geq \frac{2B\epsilon_o}{\gamma} \cdot \frac{1}{k_i k_s}\left(\frac{1}{v_s t}\right)^2 .$$

See footnote 22 for transient considerations of the backward-wave oscillator case.

18. M. Born and E. Wolf, Principles of Optics, New York: MacMillan (1959), p. 440.

19. If $L_c < \lambda_p$, the approximation of neglecting second derivatives in deriving (3.30) and (3.31) breaks down. However, this occurs only above $\sim$ 100 Gigawatts/cm^2 unfocussed laser power.

Chapter IV

20. Born and Wolf, ibid.

21. See P. M. Morse and H. Feshbach, Methods of Theoretical Physics, New York: McGraw Hill, (1953), p. 966. The general solution for (3.73) is, using our normalization convention:

$$a(k) = \oint \frac{S_+(z)}{1 - \lambda K(z)} e^{-ikz} \frac{dz}{2\pi}$$

where $\lambda = \frac{1}{E_{po}^2}$ and where $K(z) = \int_{-\infty}^{\infty} e^{ikz} c * c(k)\, dk =$

$E_{po}^2(z) = E'^2_{po} \frac{\sin^2 Kz}{(Kz)^2}$. The zeroes of the denominator of the integrand give immediately the eigenvalue condition (3.79). $S_+(z)$ is an arbitrary function which is analytic where K(z) is analytic, corresponding to arbitrary superposition of eigenfunctions.

22. N. M. Kroll, ibid. He assumes an intensity of 10^3 Mw/cm^2; hence $L_c = 3.8 \times 10^{-2}$ cm $> L_t$. To get a transient gain of e^{10} from noise, one needs an active length of 5 cm.

23. See Morse and Feshbach, ibid.

24. H. E. Bömmel and K. Dransfeld, Phys. Rev. Letters, 1, 234 (1958); E. H. Jacobsen, Phys. Rev. Letters, 2, 249 (1959); J. Acoust. Soc. Am., 32, 949 (1960); N. S. Shiren, Appl. Phys. Letters, 4, 82 (1964).

25. Stimulated Brillouin (or, more appropriately, Raman) scattering from the optical branch, which is typically 30 cm^{-1} in most materials

(see Loudon, Proc. Roy. Soc., London, A82, 393 (1963)), can cause direct generation of far-infrared radiation in piezoelectric crystals. This problem has been studied by F. DeMartini (to be published).

26. H. Takuma and D. A. Jennings, Appl. Phys. Letters, 5, 241 (1964).

27. Jenkins and White, Fundamentals of Optics, McGraw Hill (1957), p. 274; F. K. Tolansky, High-Resolution Spectroscopy, Methuen, London, 1947; K. W. Meissner, J. Opt. Soc. Am., 31, 405 (1941); J. Opt. Soc. Am., 32, 185 (1942).

28. F. J. McClung and R. W. Hellwarth, Proc. IEEE, 51, 46 (1963); R. C. Benson, R. D. Goodwin and M. R. Mirachi, NEREM Record, 4, 34 (1962).

29. J. H. Dennis and P. E. Tannenwald, Appl. Phys. Letters, 5, 58 (1964).

30. H. Takuma and D. A. Jennings, Appl. Phys. Letters, 5, 239 (1964).

31. K. E. Herzfeld and T. A. Litovitz, Absorption and Dispersion of Ultransonic Waves, New York: Academic Press (1959), p. 413.

32. Fabelinskii, loc. cit., discusses the frequency dependence of on p. 497 of the English translation.

33. R. Y. Chiao, C. H. Townes and B. P. Stoicheff, Phys. Rev. Letters, 12, 592 (1964).

34. The excellent optical quality of the ruby was confirmed by the generation of very large sparks in air ($\sim$ 1 cm long) at the focal point of a f = 5 cm focal length lens.

35. Hence we might expect a smear in the frequency of the backward-scattered stimulated Brillouin component due to the large collection angle $\delta\theta$. However, even when $\delta\theta = 0.1$, the smear in frequency will only be $\frac{\delta\nu_s}{\nu_s} = \frac{(\delta\theta)^2}{8} = 10^{-3}$. The backwards component,

after collection by the focussing lens, is very well collimated, as was demonstrated by Brewer (see footnote 49) in experiments where the target is far away from the laser.

36. A mode selector consisting of a glass plate with flat and parallel faces was placed inside the laser cavity in an attempt to limit the laser output to a single (longitudinal) mode. This technique was not reproducibly successful. However, when the laser discharged in two modes (it rarely discharged in more than two when the mode selector was used), these modes were always spaced with separation $0.53\ cm^{-1}$. A much simpler and more reproducible way to produce a single mode is to Q-switch using a saturable dye (B. H. Soffer, J. Appl. Phys., 35, 2551 (1964).)

37. We assume no amplification of the Brillouin components by the laser, as will be discussed shortly.

38. The crystal axes were identified using X-ray scattering.

39. The transverse sound waves couple much more weakly to light waves; see Mueller, Proc. Roy. Soc., London, A926, 425 (1938).

40. W. P. Mason, Piezoelectric Crystals and their Applications to Ultrasonics, New York: Van Nostrand (1950), p. 84; J. V. Atanasoff and P. J. Hart, Phys. Rev., 59, 85 (1941).

41. K. W. Meissner, J. Opt. Soc. Am., 31, 405 (1941).

42. R. S. Krishnan, Proc. Indian Acad. Sci., A41, 91 (1955).

43. R. G. Meyerand, Jr., and A. F. Haught, Phys. Rev. Letters, 11, 401 (1963).

44. J. G. Atwood, P. H. Lee and G. N. Steinberg (to be published).

45. The stimulated Brillouin radiation in the backward direction should be completely polarized in the same direction as the laser's

polarization (cf. (3.26)), just like the case of normal Brillouin scattering (see footnote 58). This has been verified experimentally in the case of glasses (footnote 44), but there seems to be some doubt in the case of liquids (footnote 49).

46. F. De Martini (to be published).

47. R. G. Brewer and K. E. Rieckhoff, Phys. Rev. Letters, 13, 334 (1964); R. G. Brewer, Appl. Phys. Letters, 5, 127 (1964).

48. E. Garmire and C. H. Townes, Appl. Phys. Letters, 5, 84 (1964).

49. R. G. Brewer and D. C. Shapero (to be published).

50. R. G. Brewer (to be published).

51. P. E. Tannenwald (to be published).

Chapter V

52. I. L. Fabelinskii, Usp. Fiz. Nauk, 63, 355 (1957); D. H. Rank, E. R. Shull and D. W. E. Axford, Nature, 164, 67 (1949); C. S. Venkateswaran, Proc. Indian Acad. Sci., A15, 362 (1942).

53. See footnotes 54-58.

54. G. B. Benedek, J. B. Lastovka, K. Fritsch and T. Greytak, J. Opt. Soc. Am., 54, 1284 (1964).

55. R. Y. Chiao and B. P. Stoicheff, J. Opt. Soc. Am., 54, 1286 (1964); O. I. Mash, V. S. Starunov and I. L. Fabelinskii, J. Exptl. Theoret. Phys. (U. S. S. R.), 47, 783 (1964).

56. C. H. Townes, Advances in Quantum Electronics, New York; Columbia University Press (1961); H. Z. Cummins, N. Knable and Y. Yeh, Phys. Rev. Letters, 12, 150 (1964); G. B. Benedek and J. B. Lastovka (private communication); see also footnote 73.

57. R. Y. Chiao and P. A. Fleury (to be published).

58. H. Z. Cummins and R. W. Gammon (to be published).

59. L. D. Landau and E. M. Lifshitz, Electrodynamics of Continuous Media, London: Pergamon Press (1960), p. 386; I. L. Fabelinskii, Usp. Fiz. Nauk., 63, 355 (1957), p. 484 of the English translation.

60. Panofsky and Phillips, loc. cit., p. 212.

61. Landau and Lifshitz, loc. cit., p. 301.

62. I am indebted to P. A. Fleury for this point.

63. Strictly speaking, we should solve the sound wave equation with a noise-driven source term to get P_s. Using the usual normal mode decomposition, this wave equation reduces to $\ddot{x} + 2\alpha_s \dot{x} + \omega_o^2 x = F(t)$, where x is the normal mode coordinate and F(t) is the noise source. Assuming "white noise", $F(t) = \sum_n C_n(t) \cos \omega_n t$ where $\overline{C_n C_m} = 0$ if $n \neq m$ and where $\overline{C_n^2}$ is independent of n, we can solve this forced harmonic oscillator problem. Forming $\overline{x^2}$ to obtain the scattering cross-section, we get the same result as starting from (5.19).

64. I. L. Fabelinskii, loc. cit., p. 540 of English translation.

65. Landau and Lifshitz, Electrodynamics of Continuous Media, p. 383.

66. I am indebted to J. B. Lastovka for pointing this out.

67. I. L. Fabelinskii, loc. cit., p. 541 of English translation.

68. See footnote 63; entropy waves are also driven by "white noise".

69. Sears, Thermodynamics, p. 155; see footnote 12.

70. Landau and Lifshitz, loc. cit., p. 391; Fabelinskii, loc, cit., p. 530.

71. Landau and Lifshitz, loc. cit., p. 392.

72. See footnote 56.

73. S. S. Alpert, Y. Yeh, and E. Lipworth (to be published); G. B. Benedek and N. Ford (to be published).

74. See footnote 55.

75. See footnote 54; also G. B. Benedek, Bull. Am. Phys. Soc. II, 10, 34 (1965); K. Kritsch and G. B. Benedek, Bull. Am. Phys. Soc. II, 10, 109 (65).

76. See footnote 55.

77. P. Jacquinot and C. Fufour, J. Recherches Centre Nat'l. Recherche Sci., Labs. Bellevue (Paris), No. 6, 91 (1948); M. A. Biondi, Rev. Sci. Instr, 27 36 (1956).

78. R. Y. Chiao, and P. A. Fleury (to be published).

79. P. A. Fleury, Ph. D. Thesis (M. I. T., 1965).

80. N. S. Shiren, Phys. Rev., 128, 2103 (1962); D. I. Bolef, Science, 136, 359 (1962).

81. J. M. Ziman, Electrons in Metals, a Short Guide to the Fermi Surface, London: Taylor and Frances (1962), pp. 77-80.

82. Cf. M. Born and K. Huang, Dynamical Theory of Crystal Lattices, Oxford University Press (1956) and Y. R. Shen and N. Bloembergen, Phys. Rev., 137, A1787 (1965).

83. If the source term of the optical branch (5. 25) is $\frac{\partial^2}{\partial t^2}$ instead of $u^2 \nabla^2 P$ then (5. 30) - (5. 35) are altered in that $\left(\frac{u}{v}\right)^2$ is replaced by 1. Also $v(\infty) = v\left(\frac{1+c_1 c_2}{2} + \frac{1}{2}\sqrt{4 c_1^2 c_2^2 + 1}\right)$.

84. Note that k_p is larger in the focal region by a small fraction $\frac{a^2}{4f^2}$ (Born and Wolf, loc. cit., p. 446) so that this will give the sound velocity (cf. (1. 4)) a slight spurious increase.

85. See the appendix of A. C. G. Mitchell and M. W. Zemansky, Resonance Radiation and Excited Atoms, Cambridge: University Press (1961).

86. Note that since the velocity of sound can be measured to better than 0. 1% accuracy whereas the absorption of sound can be measured

only to about 1%, the former is a much more sensitive means of detecting resonances, especially when a multimode maser is used; cf. (5. 36).

87. G. B. Benedek and T. Greytak (private communication).

88. A. Kastler, Comptes Rendus, 259, 4233 (1964).

89. A. Javan (private communication). From (5. 19) it can be seen that this phase shift will be $\phi = \tan^{-1}\Delta\omega\tau_s$ where $\Delta\omega$ is the modulation or chopping frequency.

90. R. Y. Chiao, E. Garmire and C. H. Townes, "Raman and Phonon Masers", Quantum Electronics and Coherent Light, Proc. International School of Physics "Enrico Fermi", (1963), P. A. Miles and C. H. Townes, eds.; E. Garmire, F. Pandarese and C. H. Townes, Phys. Rev. Letters, 11, 160 (1963).

91. R. Y. Chiao, E. Garmire and C. H. Townes, Phys. Rev. Letters, 13, 479 (1964).

92. Cf. V. I. Talanov, Izvestia V. U. Z. Radiofysika (U. S. S. R.), 7, 564 (1964). When E is pointing along the x-axis, $\vec{\nabla} P_s \cdot E = 0$ and an exact solution is possible for all orders of nonlinearity of n, by generalizing the potential V(x).

93. I am indebted to Professor C. C. Lin for pointing out that a circularly polarized beam can be a solution to (6. 25).

94. M. F. Manning and J. Millman, Phys. Rev., 49, 848 (1936).

95. G. Birkhoff and S. MacLane, A Survey of Modern Algebra, New York: Macmillan (1953), p. 112.

96. For the one dimensional case, see Gol'dman et al., Problems in Quantum Mechanics, London: Infosearch (1960).

97. M. Hersher, J. Opt. Soc. Am., 54, 563 (1964).

98. J. G. Atwood, P. H. Lee and G. N. Steinberg (to be published).